Die approbierte Originalversion dieser Diplom-/Masterarbeit ist an der Hauptbibliothek der Technischen Universität Wien aufgestellt (http://www.ub.tuwien.ac.at).

The approved original version of this diploma or master thesis is available at the main library of the Vienna University of Technology (http://www.ub.tuwien.ac.at/englweb/).

Technische Universität Wien

Diploma Thesis

Delay Times and Beam-Like Scattering States in Coherent Wave Transmission Through Resonators

ausgeführt am
Institut für Theoretische Physik
der Technischen Universität Wien

unter der Anleitung von
Prof. Dr. Stefan Rotter

durch
Philipp Ambichl BSc
Oberwinden 39
3130 Herzogenburg

Datum

Unterschrift

Contents

1. Introduction **1**

2. Multichannel scattering in wave propagation **4**
2.1. Effective Hamiltonian and the coupling matrix 6
2.1.1. One-dimensional systems 6
2.1.2. Two-dimensional systems 10
2.2. Scattering Times 14
2.2.1. The phase times and the group delay 15
2.2.2. The dwell time 18
2.2.3. Connection between group delay and dwell time 19

3. Time delay operators and particle-like scattering states **20**
3.1. The Wigner-Smith time delay operator 20
3.2. The group delay 21
3.3. The dwell time 22
3.3.1. Unitary systems 23
3.3.2. Uniform loss systems 26
3.4. Particle-like scattering states 27
3.4.1. Unitary systems 29
3.4.2. Uniform loss systems 35

4. PT-symmetric systems **39**
4.1. A 2×2 PT-matrix 40
4.2. PT-scattering 42
4.3. PT-threshold in the scattering matrix and hamiltonian 44
4.4. Particle-like scattering states in PT-symmetric systems 50
4.5. Alternative time-delay operators 53

5. Summary **60**

A. Unitary systems **62**
A.1. Derivation of Q_d 62
A.2. Equivalence of the different expressions for Q_d 65

B. Uniform loss systems **68**
B.1. Derivation of Q_d 68
B.2. Equivalence of the different expressions for Q_d 68

C. PT-symmetric systems **70**
C.1. Correspondence between the eigenvalue problem of the scattering matrix and the boundary values 70
C.2. Derivation of Q_d^{PT} 71

Acknowledgements **73**

Bibliography **74**

1. Introduction

Wave scattering through clean or disordered media is an omnipresent phenomenon in everyday life. The scattering behaviour of light and sound waves is the underlying mechanism why we can see objects and hear processes in our surrounding environment. The way acoustic waves propagate phase-coherently through 'resonators' is one of the parameters of the quality of concert hall acoustics.

Coherent wave scattering gives rise to a large variety of effects which go beyond our natural experience but which have been intensively studied in the last decades [10, 13]. Possible applications of these effects range from greatly enhanced light transmission through opaque media [5], wave focussing and object detection [6] to a significant reduction of electronic shot noise in transmission through so-called 'quantum dots' [16, 8], only to mention a few.

What most of the techniques that are used in this context have in common is that they rely on the knowledge of the scattering matrix (S-matrix) for the specific system under study. The scattering matrix contains the information about the relative phases and amplitudes of incoming and outgoing scattering channels. With the advent of spatial light modulators and coupled antenna arrays in the last few years, these amplitudes and phases have now become experimentally accessible [6, 7]. Those devices allow not only a measurement of the scattering matrix elements, but also the injection of spatially shaped wave fronts into a given system.

In the late 1940's and early 1950's, David Bohm, Leonard Eisenbud and Eugene P. Wigner were the first to point out, that another important feature of phase-coherent transport is the possibility to extract information about the duration of a scattering event from the corresponding scattering phases [27]. Following Wigner and using the concept of the S-matrix, Felix T. Smith set up his so-called 'lifetime matrix' [26]. The latter has become famous as the Wigner-Smith time delay matrix. The seemingly simple question, of how long it takes a wave to traverse a certain obstacle, turned out to be very challenging. It took about thirty years until two definitions of delay times, named group delay and dwell time, have been commonly accepted, investigated and understood [23, 24, 28].

In our earlier work [17], we showed that the Wigner-Smith time delay operator can be used in ideal, flux-conserving systems to create beam-like scattering states. These states feature beam-like propagation patterns and can be shown to follow bundles of particle trajectories which transmit a scattering region during a given time interval. Since in this way the intensity of a scattered wave is not spread over the entire scattering region but stays confined to a narrow beam, these states might find applications in secure or low-power communication.

In any real, physical system, a certain amount of flux is inevitably lost. The restriction to flux-conserving scattering processes is therefore not valid for certain experimental setups or applications. One major motivation for this thesis is to investigate the possibility of creating beam-like scattering states in systems featuring both, loss and gain, by making use of the waves' delay times. For this purpose we derive expressions for the operators measuring the group delay and the dwell time in systems with dissipating and amplifying components.

In the general expression for the operator measuring the dwell time, the so-called 'coupling matrix' is needed, which can also be used to calculate the scattering matrix. It describes the coupling of the closed system to the different scattering channels in the openings as, e.g., a resonator which is attached to wave-guides. In the literature, the matrix elements of the coupling matrix are expressed using the overlap of the incoming channel functions and the intrinsic resonances [10, 18]. Since this involves calculating infinitely many eigenfunctions of the closed system, this procedure is numerically very impractical. To resolve this impasse, we present a very compact expression for the coupling matrix, which can be directly implemented in numerical simulations and used analytically.

In this thesis, we focus on two different types of non-unitary systems. The most natural one is a uniformly absorptive system. We provide a numerical protocol to create beam-like scattering states in such systems and show that only the information about the internal dynamics of the system which is stored in the scattering matrix is needed. This fact significantly increases the number of possible experimental realizations and areas of application.

The second class of systems which we are particularly interested in features a very special distribution of both, loss and gain. These systems are invariant under the combined action of spatial reflection (P) and time inversion (T) and are, therefore, called PT-symmetric systems. The rapidly increasing interest in these systems - in theory as well as in experiment - is documented by a number of recent studies ranging from lasing [4] to the quantum brachistochrone problem [3]. Carl M. Bender was the first to realize the relevance of such systems [9] in the late 1990's. In the last few years, also first experiments realizing PT-symmetric structures were carried out successfully [1]. Below certain thresholds in the strength of loss and gain, the eigenvalues of the scattering matrix for an open PT-symmetric system are unimodular and the eigenvalues of the corresponding Hamiltonian describing the closed system are real. We present the answer to the open question how the connection between the thresholds in the eigenspectra of S-matrix and Hamiltonian looks like. In addition to this, we show that the operators for group delay and dwell time can be used to create beam-like states in PT-symmetric systems too. We also derive expressions for PT-symmetric operators that measure the generalizations of group delay and dwell time to PT-systems. In the presence of non-zero loss and gain, these scattering times are quantitatively different from their standard counterparts. We demonstrate that these PT-symmetric time delay operators can also be used for the formation of highly collimated waves and might find an interesting application in the presence of intrinsic cavity resonances.

The derivations in this thesis are formally done in the framework of the Schrödinger equation. All our results can, however, easily be transferred to equations with an equivalent structure, as e.g., the Helmholtz equation or the acoustic wave equation.

2. Multichannel scattering in wave propagation

Scattering problems in wave propagation are usually subdivided into a scattering region, where the actual, physical process of scattering takes place, and an asymptotic region, where a decomposition of the wave into asymptotic basis functions is possible. For the purposes which we are interested in, a cavity confined by hard walls forms the scattering region Ω, with two semi-infinite wave guides attached to it (Fig. 2.1(a)). The Hamiltonian of the whole system (cavity + leads) has the following form

$$\left\langle x' \right| \hat{H} \left| x \right\rangle = \frac{\left\langle x' \right| \hat{p}^2 \left| x \right\rangle}{2m} + \left\langle x' \right| \hat{V}_{pot} \left| x \right\rangle = -\frac{\hbar^2}{2m} \nabla_x^2 \delta\left(x' - x\right) + V_{pot}\left(x\right) \delta\left(x' - x\right). \quad (2.1)$$

During the scattering process the flux injected through the incoming channels gets fully redistributed into the outgoing channels, provided that the scattering process is flux-conserving. For more than one flux-carrying in- or outgoing channel, we speak of multi-channel scattering. In the case of non-flux-conserving processes additional intensity might be generated in so-called 'gain'-regions or intensity might get lost in 'loss'-regions. Such regions that lead to a violation of flux-conservation concerning the scattering channels, can be described via additional, fictitious channels [14].

A very convenient and widely used tool to describe the transition between the different open (i.e. flux-carrying) channels is the scattering matrix,

$$S = \begin{pmatrix} r & t' \\ t & r' \end{pmatrix}. \quad (2.2)$$

The unprimed quantities r and t are the reflection and transmission amplitudes for injection from the left-hand side, the primed quantities r' and t' denote the corresponding amplitudes for injection from the right-hand side. Consider as an example the complex matrix element

$$r_{mn} = \left\langle \Phi_m \right| r \left| \Phi_n \right\rangle \quad (2.3)$$

which is the amplitude for the reflection from the n-th left incoming channel into the m-th left outgoing channel.

For a strictly real potential V_{pot} in the scattering region, the Hamiltonian is hermitian and flux is conserved. This fact is expressed through the unitarity of the sacttering matrix, $S^\dagger S = \mathbb{I}$. Hamiltonians of the form (2.1), which are used throughout this thesis, are not only hermitian for $V_{pot}\left(x\right) \epsilon \mathbb{R}$, $\forall x$, but also real and transposition-symmetric. Correspondingly, whenever we refer to 'unitary' scattering systems, we adress systems not only featuring flux-conservation, but also time-reversal symmetry.

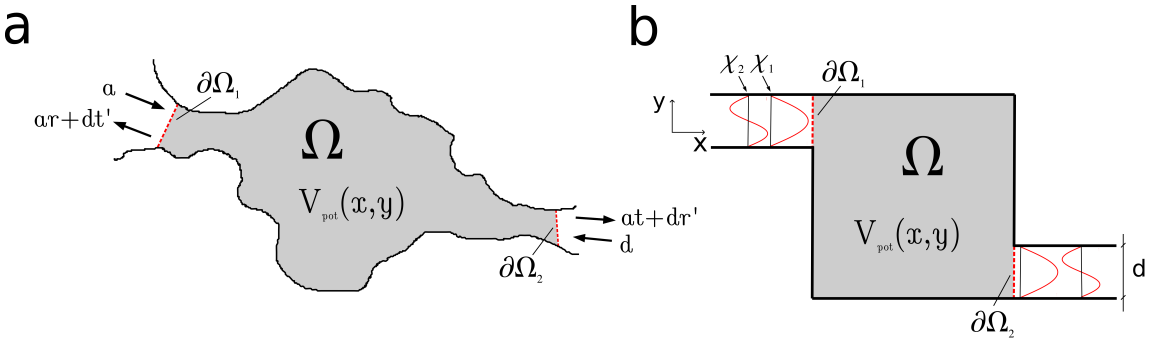

Figure 2.1.: Scattering systems featuring hard-wall boundaries consisting of the scattering region Ω (grey) and two attached leads (white). The boundaries of the cavity $\partial\Omega_1$ and $\partial\Omega_2$ are indicated by red dotted lines. (a) Arbitrarily shaped system; an incident wave, characterized by the amplitudes a and d, injected through both leads via flux-carrying channels, is scattered according to the scattering matrix S (2.2). For reasons of simplicity we assumed here, that only one channel is open in the left and right lead respectively. (b) Geometry investigated in this thesis, consisting of a quadratic cavity featuring different potentials $V_{pot}(x, y)$, and two rectangular leads. The transverse parts of the first two lead modes, χ_1 and χ_2, are displayed. The lead-width d in (b) must not be confused with the amplitude d in (a).

Since for most of the results presented in this thesis, the wave is injected into the cavity through the left lead only, we call the number of open modes in the left lead n_{in}, and the number of open modes in the right lead n_{out}. The scattering matrix then has the dimension of $(n_{in} + n_{out}) \times (n_{in} + n_{out})$. We will choose the wave guides during this work to be semi-infinite and rectangular, enclosed by hard-wall boundaries, and potential-free inside (Fig. 2.1(b)). For such structures, a very convenient choice for the channels is the so-called lead mode basis, which for the n-th incoming mode takes the following form,

$$\phi_n(x, y) = \frac{1}{\sqrt{v_n}} \chi_n(y) \, e^{ik_{x,n}x} \tag{2.4}$$

with $v_n = \frac{\hbar k_{x,n}}{m}$ being the flux carried by this mode. Since there is no potential inside the leads, the transverse part of each mode χ_n is given as

$$\chi_n(y) = \sqrt{\frac{2}{d}} \sin(k_{y,n}\, y)\,, \; k_{y,n} = \frac{n\,\pi}{d}, \tag{2.5}$$

where d is the lead-width. The wave numbers $k_{x,n}$ are calculated via the following relation using the scattering energy E,

$$k_{x,n} = \sqrt{2m\,E/\hbar^2 - k_{y,n}^2}. \tag{2.6}$$

The number of open modes n_{in}/n_{out} for the left/right lead, are determined by (2.6). For $k_{y,n}^2 \leq 2m\,E/\hbar^2$, $k_{x,n}$ is a real number and corresponds to the longitudinal part of the

wave vector for a flux-carrying mode. If $k_{y,n}^2 \geq 2m\,E/\hbar^2$, $k_{x.n} \equiv i\kappa_{n,x}$ is purely imaginary and the corresponding lead mode is an evanescent wave in x-direction, that carries no flux. For reasons of convenience, we will keep the prefactor $\left(\sqrt{v_n}\right)^{-1}$ in (2.4) also for evanescent modes and define $v_n = \frac{\hbar\kappa_{x,n}}{m}$ for $n > n_{in}$, although there is no physical flux associated to these evanescent modes.

On a basis-independent, abstract operator level the scattering matrix S can be written in terms of the system's Green's function G and the operator V describing the coupling of the closed cavity to the leads in the following manner:

$$S = -\mathbb{I} + i\hbar\, V^\dagger G V, \tag{2.7}$$

with $\mathbb{I}$ being the identity matrix. One way to calculate the Green's function G appearing in (2.7) proceeds via an effective Hamiltonian approach [13]. Following this procedure, G can be written as

$$G = \frac{1}{E - H_{\text{eff}}}. \tag{2.8}$$

The effective Hamiltonian H_{eff} and the coupling matrix V will be discussed in detail in the following section.

2.1. Effective Hamiltonian and the coupling matrix

Due to its importance for our numerical procedure, on the one hand, and for didactical reasons, on the other hand, we will start this section in the framework of a finite-differences (FD) approach which we apply to all the discussed quantities. The FD approach provides a solution of the wave equation on a finite calculation grid. At the end of each subsection we will reach the results for the continuous systems by taking the limit of vanishing grid-spacing[1] $\lim_{\Delta x_i \to 0}$.

2.1.1. One-dimensional systems

Since the Laplacian acting on a wave function ψ translates into the FD-formalism as follows

$$\nabla_x^2 \psi\,(x) \to \frac{\psi_{n-1} - 2\psi_n + \psi_{n+1}}{\Delta x^2},\ \psi_n \equiv \psi\,(x_n)\,, \tag{2.9}$$

that part of the Hamiltonian (2.1) which describes the scattering region is a $N \times N$ matrix, which has the following tri-diagonal structure

[1] All the quantities appearing in the framework of the finite-differences approach during this thesis are chosen in such a way, that grid-spacing factors are used to ensure the right dimensionality of the quantities in the continuum limit, i.e., that whenever an integration over coordinate space is performed, explicit factors of Δx and Δy are needed in the corresponding summations.

$$H_D = \Lambda_x \begin{pmatrix} -2 & 1 & & & & \\ 1 & -2 & 1 & & & \\ & \ddots & \ddots & \ddots & & \\ & & 1 & -2 & 1 & \\ & & & 1 & -2 & \end{pmatrix} + \begin{pmatrix} V_{pot}(x_1) & & & & \\ & V_{pot}(x_2) & & & \\ & & \ddots & & \\ & & & V_{pot}(x_{N-1}) & \\ & & & & V_{pot}(x_N) \end{pmatrix}. \tag{2.10}$$

$$\Lambda_x = -\frac{\hbar^2}{2m\Delta x^2}. \tag{2.11}$$

N is the number of grid points in the scattering region. Elements that are not displayed are zero. Note that we implicitly imposed Dirichlet boundary conditions (indicated by the subscript 'D') to the system

$$\psi_0 = 0 = \psi_{N+1} \tag{2.12}$$

by choosing the boundaries of the Hamilton matrix as we did. We use this Hamiltonian to set up the effective Hamiltonian for a 1D scattering region (Fig. 2.2(a)). A coupling to the leads does not affect the internal structure of the scattering region, so H_D and H_{eff} may only differ from each other in their boundary conditions. The correct Green's function in (2.8) is obtained for precisely this Hamiltonian, that describes only outgoing flux. The outgoing lead modes form just a one-dimensional basis in each lead in the case of a 1D system, more specifically a left-moving plane wave in the left lead, a right-moving one in the right lead. In other words, outside the scattering region, the wave has to follow the following propagation patterns,

$$\psi_{N+1} = \psi_N \, e^{ik\Delta x}, \tag{2.13}$$

$$\psi_0 = \psi_1 \, e^{ik\Delta x}. \tag{2.14}$$

Note that the correct FD dispersion-relation for $k(E)$ should be used [12], rather than the free particle dispersion relation. The effective Hamiltonian can then be written as a sum of H_D and a matrix B describing these boundary conditions,

$$H_{\text{eff}} = H_D + B, \; B = \Lambda_x \begin{pmatrix} e^{ik\Delta x} & 0 & & & \\ 0 & 0 & & & \\ & & \ddots & & \\ & & & 0 & 0 \\ & & & 0 & e^{ik\Delta x} \end{pmatrix}. \tag{2.15}$$

Decomposing the factor $\Lambda_x \cdot e^{ik\Delta x}$ into its real and imaginary part

$$\Lambda_x e^{ik\Delta x} = -\frac{\hbar}{2}\frac{\hbar}{m}\frac{1}{\Delta x}\left(\frac{\cos(k\Delta x)}{\Delta x} + i\frac{\sin(k\Delta x)}{\Delta x}\right) \tag{2.16}$$

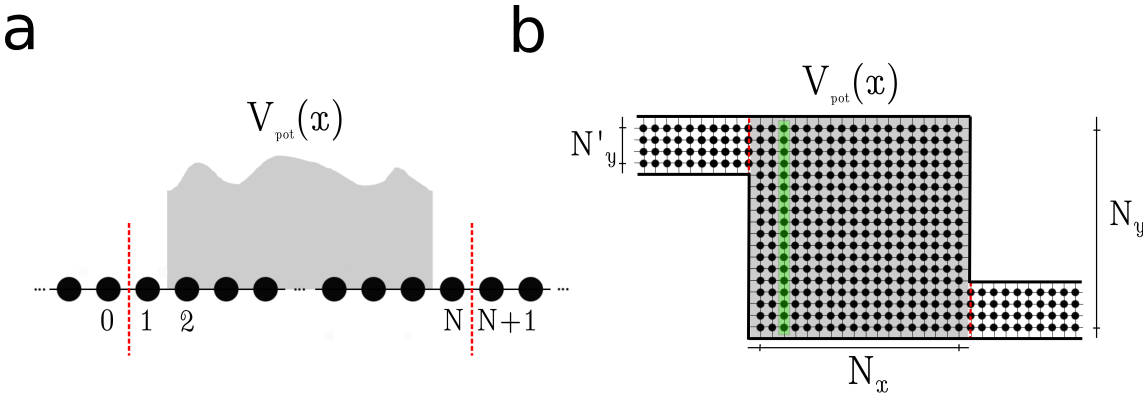

Figure 2.2.: Discretized scattering problems, the actual scattering region is marked by red dashed lines, the area with $V_{pot} \neq 0$ is highlighted grey. (a) One-dimensional system featuring an arbitrary potential $V_{pot}(x)$ inside the scattering region, containing N calculation grid points. The potential on the first and last point inside the cavity is set to 0 in order to ensure that the scattering matrix properly describes discontinous jumps of the potential at the boundaries. (b) Two-dimensional cavity containing an arbitrary potential $V_{pot}(x, y)$ attached to two leads . The total number of grid points inside the scattering region is $N_x \cdot N_y$. The problem is formulated slice by slice according to (2.32), one of the slices in transverse direction is highlighted in green.

grants better physical insight, and enables us to write H_{eff} in the following way

$$H_{\text{eff}} = H_D - \frac{\hbar}{2} W \sigma W^{\dagger} \Delta x - \frac{i\hbar}{2} V V^{\dagger} \Delta x \equiv H_h - \frac{i\hbar}{2} V V^{\dagger} \Delta x, \tag{2.17}$$

with

$$\sigma = \begin{pmatrix} \text{sign}\left[\cos\left(k\Delta x\right)\right] & 0 \\ 0 & \text{sign}\left[\cos\left(k\Delta x\right)\right] \end{pmatrix} = \text{sign}\left[\cos\left(k\Delta x\right)\right] \mathbb{I}_{2\times 2} \tag{2.18}$$

and the $N \times 2$ matrices

$$W = \frac{1}{\Delta x}\sqrt{\frac{\hbar}{m}} \begin{pmatrix} \sqrt{\frac{\cos(k\Delta x)}{\Delta x}} & 0 \\ 0 & \vdots \\ \vdots & \\ & 0 \\ 0 & \sqrt{\frac{\cos(k\Delta x)}{\Delta x}} \end{pmatrix} \tag{2.19}$$

and

$$V = \frac{1}{\Delta x}\sqrt{\frac{\hbar}{m}} \begin{pmatrix} \sqrt{\frac{\sin(k\Delta x)}{\Delta x}} & 0 \\ 0 & \vdots \\ \vdots & \\ & 0 \\ 0 & \sqrt{\frac{\sin(k\Delta x)}{\Delta x}} \end{pmatrix}. \tag{2.20}$$

Since the shortest valid wavelength λ_{min} on an FD-grid is given by twice the grid spacing, the largest possible wave-number $k_{max} = 2\pi/\lambda_{min}$ is given by

$$\lambda_{min} = 2\Delta x \Rightarrow 0 \leq k \leq k_{max} = \frac{\pi}{\Delta x}. \tag{2.21}$$

The condition (2.21) restricts $\sin(k\Delta x)$ to positive values, however, $\cos(k\Delta x)\,\epsilon\,[-1,1]$. This is why the matrix σ in (2.17) appears only in the term corresponding to W.

The matrix V given by (2.20) is exactly the desired coupling matrix used in (2.7). The reason for pulling out explicitly a factor of Δx in (2.17) is that applying an operator on the wave function ψ, formally involves an integration over the coordinate space. The physics contained in (2.17) becomes easier to understand in the continuum limit. At first consider only the term $-\frac{\hbar}{2}W\sigma W^{\dagger}\Delta x$. Since $\lim_{\Delta x\to 0}\cos(k\Delta x) = 1$, the boundary conditions become

$$\begin{aligned} \psi_{N+1} &= \psi_N \lim_{\triangle x\to 0}[\cos(k\Delta x)] && (2.22)\\ &\to \lim_{\triangle x\to 0}\frac{\psi_{N+1}-\psi_N}{\Delta x} = 0 && (2.23)\\ &\to \frac{d\psi}{dx}\,|_{x=L} = 0, && (2.24) \end{aligned}$$

analogously for $x = 0$,

$$\frac{d\psi}{dx}\,|_{x=0} = 0. \tag{2.25}$$

The conditions (2.24) and (2.25) of vanishing slope at the boundary are called Neumann boundary conditions. Note that the limit $\Delta x \to 0$ implies also $N \to \infty$. Now consider the full boundary conditions, $-\frac{\hbar}{2}\left(W\sigma W^{\dagger} + iVV^{\dagger}\right)\Delta x$. As $\lim_{\Delta x\to 0}\sin(k\Delta x)/\Delta x = k$, the boundary conditions in the continuum limit read

$$\begin{aligned} \psi_{N+1} &= \psi_N \lim_{\triangle x\to 0}[\cos(k\Delta x) + i\sin(k\Delta x)] && (2.26)\\ &\to \lim_{\triangle x\to 0}\frac{\psi_{N+1}-\psi_N}{\Delta x} = ik\psi_N && (2.27)\\ &\to \frac{d\psi}{dx}\,|_{x=L} = ik\psi(L), && (2.28) \end{aligned}$$

and for $x = 0$,

$$\frac{d\psi}{dx}\,|_{x=0} = -ik\psi(0). \tag{2.29}$$

Conditions (2.28) and (2.29) are often referred to as 'constant flux' (CF) boundary conditions in lasing theory [11]. The justification of this splitting of the boundary conditions in (2.17) is now obvious. H_{eff} can be written as the sum of a hermitian Hamiltonian H_h (since Neumann boundary conditions are hermitian) and an anti-hermitian coupling to the leads.

The expression for the coupling matrix V in the continuum limit can be written in a very compact manner

$$V(x)_n = \begin{cases} \sqrt{v}\delta(x), & n = 1 \\ \sqrt{v}\delta(x-L), & n = 2 \end{cases}, \tag{2.30}$$

with

$$v = \frac{\hbar k}{m} = \frac{1}{\hbar}\frac{\partial E}{\partial k} = \frac{\partial \omega}{\partial k}. \tag{2.31}$$

V changes over to a 1×2 matrix whose elements are functions of x, since V connects the discrete vector space, spanned by the lead modes, and the coordinate space. Note that in contrast to former formulations of the V matrix, where the lead modes were connected to the closed system eigenstates [10, 18], our expression can directly be used in transport calculations, since it does not involve the calculation of the infinitely many intrinsic resonances.

2.1.2. Two-dimensional systems

In more than one dimension, we can continue to use the above formalism, it becomes slightly more complicated though. For reasons of simplicity, we will assume in the following, that both of the leads have the same width d, which implies $n_{in} = n_{out}$. The calculations can easily be adopted to differently sized leads. The Hamilton matrix for a 2D system consisting of N_x grid points in x-direction and N_y grid points in y-direction generally has a tridiagonal block form

$$H_D = \begin{pmatrix} H_0 & H_I & & & \\ H_I^\dagger & H_0 & H_I & & \\ & H_I^\dagger & \ddots & \ddots & \\ & & \ddots & & H_I \\ & & & H_I^\dagger & H_0 \end{pmatrix} + \begin{pmatrix} V_{pot}^1 & & & & \\ & V_{pot}^2 & & & \\ & & \ddots & & \\ & & & V_{pot}^{N_x-1} & \\ & & & & V_{pot}^{N_x} \end{pmatrix}. \tag{2.32}$$

Each block has dimension $N_y \times N_y$, H_D has a total dimension of $(N_x \cdot N_y) \times (N_x \cdot N_y)$. H_0 has exactly the same structure as the first term in (2.10), the only difference is that the finite-difference derivative is taken with respect to y, since it describes the y-part of

the Laplacian for each slice (Fig. 2.2(b)),

$$H_0 = \Lambda_y \begin{pmatrix} -2 & 1 & & & & \\ & 1 & -2 & 1 & & \\ & & \ddots & \ddots & \ddots & \\ & & & 1 & -2 & 1 \\ & & & & 1 & -2 \end{pmatrix}, \tag{2.33}$$

with $\Lambda_y = -\frac{\hbar^2}{2m\Delta y^2}$. In the case of next neighbour coupling of the form (2.9), the matrix H_I is simply the identity matrix times the proper prefactor $\Lambda_x = -\frac{\hbar^2}{2m\Delta x^2}$, introducing the x-depending part of the Laplacian. The matrices V_{pot}^i are diagonal matrices, containing the potential inside the cavity for the i-th slice, respectively. Defining the Hamiltonian like (2.32), determines the FD wave function to be a vector, sequentially containing the wave functions for each slice, which gives a total dimension of the number of elements of $N_x \cdot N_y$,

$$\Psi = \begin{pmatrix} \vec{\psi}_1 \\ \vec{\psi}_2 \\ \vdots \\ \vec{\psi}_{N_x} \end{pmatrix}. \tag{2.34}$$

The ansatz for a two-dimensional wave guide shown in (2.4) leads to the following relation between the outgoing wave functions on the last slice inside the cavity and the first slice in the right-hand lead (analogously for the left lead),

$$\vec{\psi}_N = \sum_{n=1}^{\infty} c_n \chi_n, \tag{2.35}$$

$$\vec{\psi}_{N+1} = \sum_{n=1}^{N_y'} c_n' \chi_n = \sum_{n=1}^{N_y'} c_n e^{ik_{x,n}\Delta x} \chi_n. \tag{2.36}$$

Since the χ_n form an orthonormal, complete basis in transverse direction, this decomposition is possible. Note that the summation index runs over all modes, i.e., open and evanescent ones. N_y' is the number of grid points in transverse direction inside the lead, which is generally different from N_y. In an FD calculation, N_y' gives the total number of possible modes. The relation

$$c_n' = c_n e^{ik_{x,n}\Delta x} \tag{2.37}$$

is the proper generalization of (2.13) to multiple dimensions. The relation of $\vec{\psi}_N$ and $\vec{\psi}_{N+1}$ is therefore

$$\vec{\psi}_{N+1} = \chi \cdot \Gamma\left(e^{ik_x\Delta x}\right) \cdot \chi^\dagger \triangle y \cdot \vec{\psi}_N. \tag{2.38}$$

Here we introduced the notation

$$\Gamma(z) = \mathrm{diag}\left(\{z_n\}\right) \tag{2.39}$$

for a given set of numbers $\{z_n\}$. The matrix χ in (2.38) contains the transverse parts of the lead modes $\chi_n(y_i)$ in its columns

$$\chi = \begin{pmatrix} \chi_1(y_1) & \chi_2(y_1) & \cdots & \chi_{N'_y}(y_1) \\ \chi_1(y_2) & \chi_2(y_2) & \cdots & \chi_{N'_y}(y_2) \\ \vdots & \vdots & & \vdots \\ \chi_1\left(y_{N'_y}\right) & \chi_2\left(y_{N'_y}\right) & \cdots & \chi_{N'_y}\left(y_{N'_y}\right) \end{pmatrix}. \tag{2.40}$$

The matrix $\Gamma\left(e^{ik_x\Delta x}\right)$, according to (2.39), is a diagonal matrix containing the phase shifts of the coefficients c_n,

$$\Gamma\left(e^{ik_x\Delta x}\right) = \mathrm{diag}\left(\left\{e^{ik_{x,n}\Delta x}\right\}\right). \tag{2.41}$$

The matrices χ and $\Gamma\left(e^{ik_x\Delta x}\right)$ have the dimension $N'_y \times N'_y$. (2.38) makes use of the orthonormality of the χ_n, $\int_0^{W'} \chi_m^\star(y)\,\chi_n(y)\,dy = \delta_{mn}$, and $\sum_{i=1}^{N'_y} \chi_m^\star(y_i)\,\chi_n(y_i)\,\Delta y = \delta_{mn}$ in FD form respectively. Since calculating the Fourier-coefficients $c_n = \sum_{i=1}^{N'_y} \chi_n^\star(y_i)\,\psi_N(y_i)\,\Delta y$ involves an integration over the lead-width d, the additional factor Δy is needed. For the same reasons of dimensionality, the factor Δx is needed in (2.17). The boundary conditions for the effective Hamiltonian can again be written in matrix form,

$$H_{\text{eff}} = H_D + B \tag{2.42}$$

with

$$B = \Lambda_x \begin{pmatrix} A & 0 & & \\ 0 & 0 & & \\ & & \ddots & \\ & & 0 & 0 \\ & & 0 & A \end{pmatrix}, \; A := \chi \cdot \Gamma\left(e^{ik_x\Delta x}\right) \cdot \chi^\dagger \triangle y. \tag{2.43}$$

A decompositon of B leads to the following form of H_{eff},

$$H_{\text{eff}} = H_D - \frac{\hbar}{2} W\sigma W^\dagger \Delta x \Delta y + \frac{\hbar}{2}\tilde{V}\tilde{V}^\dagger \Delta x \Delta y - \frac{i\hbar}{2} V V^\dagger \Delta x \Delta y \tag{2.44}$$

$$\equiv H_h - \frac{i\hbar}{2} V V^\dagger \Delta x \Delta y \tag{2.45}$$

with

$$W=\frac{1}{\Delta x}\sqrt{\frac{\hbar}{m}}\begin{pmatrix} \chi\cdot\Gamma\left(\sqrt{\frac{\cos(k_x\Delta x)}{\Delta x}}\right) & 0 \\ 0 & \vdots \\ \vdots & 0 \\ 0 & \chi\cdot\Gamma\left(\sqrt{\frac{\cos(k_x\Delta x)}{\Delta x}}\right) \end{pmatrix},\ (N_x\cdot N_y)\times\left(2\cdot N_y'\right), \tag{2.46}$$

$$\tilde{V}=\frac{1}{\Delta x}\sqrt{\frac{\hbar}{m}}\begin{pmatrix} \chi_{eva}\cdot\Gamma\left(\sqrt{\frac{\sinh(k_x\Delta x)}{\Delta x}}\right) & 0 \\ 0 & \vdots \\ \vdots & 0 \\ 0 & \chi_{eva}\cdot\Gamma\left(\sqrt{\frac{\sinh(k_x\Delta x)}{\Delta x}}\right) \end{pmatrix},\ (N_x\cdot N_y)\times\left(2\cdot\left(N_y'-n_{in}\right)\right), \tag{2.47}$$

$$V=\frac{1}{\Delta x}\sqrt{\frac{\hbar}{m}}\begin{pmatrix} \chi_{flux}\cdot\Gamma\left(\sqrt{\frac{\sin(k_x\Delta x)}{\Delta x}}\right) & 0 \\ 0 & \vdots \\ \vdots & 0 \\ 0 & \chi_{flux}\cdot\Gamma\left(\sqrt{\frac{\sin(k_x\Delta x)}{\Delta x}}\right) \end{pmatrix},\ (N_x\cdot N_y)\times(2\cdot n_{in}). \tag{2.48}$$

Generalizing the expression (2.18) to two dimensions, we have

$$\sigma=\begin{pmatrix} \Gamma\left(\operatorname{sign}\left[\cos\left(k_x\Delta x\right)\right]\right) & 0 \\ 0 & \Gamma\left(\operatorname{sign}\left[\cos\left(k_x\Delta x\right)\right]\right) \end{pmatrix},\ \left(2\cdot N_y'\right)\times\left(2\cdot N_y'\right). \tag{2.49}$$

The decomposition (2.44) was achieved using $e^{ik_{x,n}\Delta x}=\cos\left(ik_{x,n}\Delta x\right)+i\sin\left(ik_{x,n}\Delta x\right)$ and $e^{i(i\kappa_{x,n})}=e^{-\kappa_{x,n}}=\cosh\left(\kappa_{x,n}\Delta x\right)-\sinh\left(\kappa_{x,n}\Delta x\right)=\cos\left(i\kappa_{x,n}\Delta x\right)-\sinh\left(\kappa_{x,n}\Delta x\right)$ for flux-carrying and evanescent waves, respectively. The cosine-function may be used for both, open and evanescent modes, taking into account, that the wave numbers $k_{x,n}$ become purely imaginary quantities $i\kappa_{x,n}$ for $n>n_{in}$. More caution is needed treating the sine-function, since $e^{-\kappa_{x,n}}$ involves the negative hyperbolic sine. Consequently, the term corresponding to $\tilde{V}$ in (2.44) has a positive sign.

The $N_y'\times\left(N_y'-n_{in}\right)$ matrix χ_{eva} contains the last $N_y'-n_{in}$ columns of χ corresponding to the evanescent modes, and the $N_y'\times n_{in}$ matrix χ_{flux} contains the first n_{in} columns of χ corresponding to the flux-carrying modes. The grid-spacing factors Δx and Δy in (2.44) are pulled out explicitly because of the same reasons as in the previous subsection, only that the coordinate space is now two-dimensional. The term $\frac{\hbar}{2}\tilde{V}\tilde{V}^{\dagger}\Delta x\Delta y$, that is not

appearing in the 1D case, describes scattering into evanescent modes, which translates into a hermitian boundary condition. No flux can leave the system via evanescent modes, therefore it is put into H_h. The Green's Function and the scattering matrix are obtained via (2.8) and (2.7) as follows

$$G = \frac{1}{E - H_{\text{eff}}} \frac{1}{\Delta x \Delta y} \tag{2.50}$$

and

$$S = -\mathbb{I} + i\hbar V^{\dagger} G V \, (\Delta x \Delta y)^2 \, . \tag{2.51}$$

The grid-spacing factors $\Delta x, \Delta y$ take into account the dimensionality of the Green's function, which is $\left(length^2 \cdot energy\right)^{-1}$, and the double integration over coordinate space in the inner product $V^{\dagger} G V$.

In the continuum limit the term $-\frac{\hbar}{2} W \sigma W^{\dagger} \Delta x \Delta y$ again describes Neumann boundary conditions, since $\lim_{\Delta x \to 0} \cos\left(k_{x,n} \Delta x\right) = 1$ and $\chi \chi^{\dagger}$ gives the identity matrix. The coupling matrix V also has a very similar form as in 1D,

$$V\left(x, y\right)_n = \begin{cases} \sqrt{v_n} \chi_n\left(y\right) \delta\left(x\right), & n = 1, 2, \ldots n_{in} \\ \sqrt{v_n} \chi_n\left(y\right) \delta\left(x - L\right), & n = n_{in} + 1, \ldots 2\, n_{in} \end{cases} . \tag{2.52}$$

It is a $1 \times 2\, n_{in}$ matrix with each of its elements being a function of the coordinates x and y. Inserting (2.52) into (2.7) yields the familiar form of the scattering amplitudes

$$r_{mn} = -\delta_{mn} + i\hbar \sqrt{v_m} \sqrt{v_n} \int_0^d dy \int_0^d dy' \, \chi_m\left(y\right) G\left(0, y; 0, y'; E\right) \chi_n\left(y'\right) \tag{2.53}$$

$$t_{mn} = i\hbar \sqrt{v_m} \sqrt{v_n} \int_0^d dy \int_0^d dy' \, \chi_m\left(y\right) G\left(L, y; 0, y'; E\right) \chi_n\left(y'\right), \tag{2.54}$$

as well as the corresponding expressions for r' and t'.

2.2. Scattering Times

In the following section, we will give a short overview of the commonly used expressions for observables associated to the duration of a scattering event. In particular, we will present the concepts of group delays and dwell times. The physical meaning of the group delays can be understood by investigating the so-called phase times which we will thus introduce and discuss in terms of their validity limits. For reasons of simplicity, we will restrict ourselves to a one-dimensional situation of a wave impinging on an obstacle (Fig. 2.3)). The obstacle is formed by an arbitrary scattering potential which is assumed to be different from zero between $x = 0$ and $x = L$. Note that, in principle, also a zero potential is a valid candidate for the 'obstacle'. The effect of the scattering process in this case is just a phase shift in transmission.

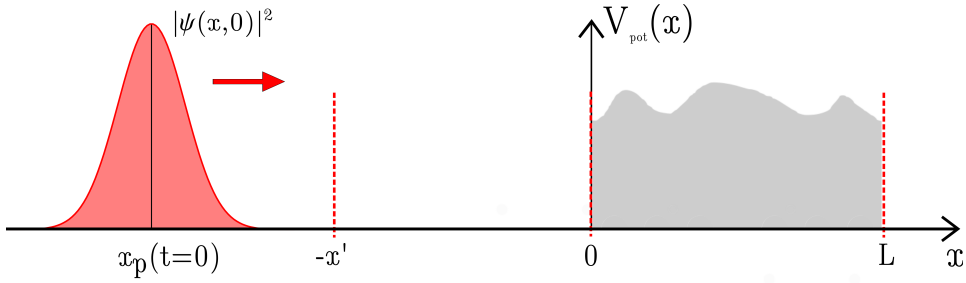

Figure 2.3.: A wave packet $\psi(x,t)$ given by (2.55) impinging on an obstacle situated between $x = 0$ and $x = L$. The packet is chosen in such a way, that it has a distinct maximum $x_p(t)$. At time $t = 0$, the packet is entirely located on the left-hand side of the obstacle. The wave is transmitted through the scattering potential V_{pot} and reflected according to the scattering amplitudes $\bar{t}(k)$ and $r(k)$. If the scattering region is chosen to be the interval $[-x', L]$, rather than $[0, L]$, the assumption of a free propagation of x_p until reaching the scattering region is valid, provided that x' is large enough (see main text).

2.2.1. The phase times and the group delay

The phase times

In the late 1940's and early 1950's, Eisenbud, Bohm [19] and Wigner [27] pointed out the possibility to extract information about the time it takes a wave to traverse a certain scattering region from the energy derivative of the corresponding scattering phases. This idea was followed by Smith [26] and lead to the formulation of the 'lifetime matrix' Q, which has become famous as the 'Wigner-Smith time delay matrix'.

Outside the scattering region, an arbitrary wave packet $\psi(x,t)$ can be decomposed into plane waves

$$\psi(x,t) = \int \frac{dk}{\sqrt{2\pi}} \phi(k)\, e^{i(kx-\omega(k)t)}, \tag{2.55}$$

where $\omega(k) = E(k)/\hbar$ and $E(k)$ is the scattering energy dependent on k via the corresponding dispersion-relation. We choose the origin of our time scale and $\phi(k)$ in such a way, that for $t = 0$, the intensity of the wave packet is entirely located on the left-hand side of the scattering region (Fig. 2.3)). Using the transmission amplitude $\bar{t}(k) = |\bar{t}(k)|\, e^{i\varphi_t(k)}$ (the bar is introduced in this subsubsection only to avoid confusion with the time t) for each Fourier component, we get for the transmitted part of the wave

$$\psi(x,t) = \int \frac{dk}{\sqrt{2\pi}} |\bar{t}(k)|\, \phi(k)\, e^{i(k(x-L)-\omega(k)t+\varphi_t(k))}. \tag{2.56}$$

In complete analogy, the reflected part of the incident packet can be calculated using the reflection amplitude $r(k) = |r(k)|\, e^{i\varphi_r(k)}$. In the asymptotic limit, i.e., for very

large t, the phase factor in (2.56) is in general rapidly fluctuating as a function of k. In this limit it is thus appropriate to apply the stationary phase approximation [27, 23], since only those Fourier components will give a considerable contribution to the wave packet (2.56) with k-values in the vicinity of a stationary point of the phase. The other Fourier components do not contribute due to destructive interference. The condition for a stationary phase reads as follows

$$\frac{\partial}{\partial k}\left(k\left(x-L\right)-\omega\left(k\right)t+\varphi_t\left(k\right)\right)=0, \tag{2.57}$$

which leads to

$$x-\frac{\partial\omega}{\partial k}t+\frac{\partial\varphi_t}{\partial k}=0\rightarrow\ x_p\left(t\right)=\frac{\partial\omega}{\partial k}t-\frac{\partial\varphi_t}{\partial k}. \tag{2.58}$$

Following the peak or any other significant instant of the wave packet $x_p\left(t\right)$, we see that it has a spatial delay of $\partial\varphi_t/\partial k$ in comparison to a packet not affected by the scattering region, which translates into a temporal delay of

$$\tau_t=\frac{m}{\hbar k}\frac{\partial\varphi_t}{\partial k}=\frac{m}{\hbar k}\frac{\partial E}{\partial k}\frac{\partial\varphi_t}{\partial E}=\hbar\frac{\partial\varphi_t}{\partial E}. \tag{2.59}$$

The last equality sign holds if a dispersion relation of the form $E\left(k\right)=\frac{\hbar^2k^2}{2m}$ is assumed. In analogy, the reflection phase time is defined as

$$\tau_r=\hbar\frac{\partial\varphi_r}{\partial E}. \tag{2.60}$$

At this point we should emphasize the validity limits of interpreting the phase times (2.59) and (2.60) as the correct, physical delay times associated to, e.g., the peak of the incident wave packet.

- The stationary phase approximation is only justified in the asymptotic regions for large x and/or for large times t.
- The delays (2.59) and (2.60) have to be understood as the relative delays of the wave packet in comparison to a wave packet that is not affected by the obstacle[2]. To this purpose, we implicitly assumed, that the peak of the wave packet x_p is moving freely until it enters the scattering region at $x=0$. This assumption might not be justified in general, since parts of the wave packet are reflected back into the negative x-direction due to the scattering process. These parts interfere with the remaining wave packet that is still approaching the scattering region. Depending on the shape and width of the wave packet, this may seriously compromise the assumption of a free propagation of the maximum x_p. This problem may be circumvented by formally defining the scattering region to be situated between $[-x',L]$ with $x'>0$ (Fig. 2.3), which is larger than the actual obstacle ($[0,L]$). If this boundary is extended far enough, the propagation of x_p up to $-x'$ can be considered free, since no parts of the packet have bridged the distance to the obstacle and back [23].

[2] In this thesis, we also consider the scattering region in the case of zero potential as an 'obstacle', since it takes the wave a finite amount of time to traverse it

- The identification of the scattering time with the time it takes the peak of a transient wave packet to reappear behind an obstacle might be problematic on its own, due to the generally strong deformation of the wave during the scattering process [21].

In the sense of the first two remarks above, the phase times only correspond to physically meaningful delay-times if they are considered as asymptotic quantities.

As was shown by Hauge et al. [22], for wave packets narrow in k-space, the expectation value of the position of the wave packet can be written as a power series of the (small) standard deviation of the wave packet in k-space σ_k. In this procedure that avoids the stationary phase approximation (but not the necessity of asymptotic scattering amplitudes!) the phase times appear as the delay of the packet's expectation value in coordinate space to leading order of the power series.

The group delay

The phase times introduced in the last subsubsection are defined for the transmitted and the reflected part of a wave packet seperately. The concept of the group delay for a wave of energy E uses both of these scattering times in the form of a weighted sum

$$\tau_g = \hbar \left(|r|^2 \frac{d\varphi_r}{dE} + |t|^2 \frac{d\varphi_t}{dE} \right). \tag{2.61}$$

The group delay can thus be viewed as the weighted sum of the times it takes the peak or any other significant instant to reappear behind the obstacle after being transmitted and to reappear after being reflected back. The weighting factors $|r|^2$ and $|t|^2$ are the reflectivity R and the transmittance T respectively. Note that the expression 'weighted sum' is more suitable here than the term 'average', because for non-unitary scattering systems, the relation $R + T = 1$ does not hold. (2.61) is the definition for the group delay, as it is used in the literature [28, 24].

We will now generalize (2.61) to multichannel scattering,

$$\tau_g = \hbar \sum_{i=1}^{n_{in}+n_{out}} |(S\vec{u})_i|^2 \frac{d\varphi_i}{dE}, \tag{2.62}$$

with S being the scattering matrix and $\vec{u}$ being a vector containing the coefficients of the incident waves for each of the $n_{in} + n_{out}$ flux-carrying channels (injected from both sides). The subscript i refers to the i-th component of the vector $S\vec{u}$, φ_i labels the phase of $(S\vec{v})_i = |(S\vec{v})_i| \, e^{i\varphi_i}$. It is easy to see that (2.62) changes over to (2.61) for a 1D system and injection only from the left side, which means $\vec{u} = (1, 0)^T$. The validity of the physical interpretation of the group delay is subject to the same restraints as discussed for the phase times above. Additional physical meaning can, however, be associated to the group delay using the concept of the dwell time, which will be discussed in the following subsections.

2.2.2. The dwell time

For a classical particle, the time it spends inside a given region $[0, L]$ during a scattering process can be written as follows

$$\tau = \int_{-\infty}^{\infty} dt \int_{0}^{L} dx\, \delta\left(x - x\left(t\right)\right), \tag{2.63}$$

where $x\left(t\right)$ describes the particle's trajectory. According to Feynman's path integral formulation of quantum mechanics, the propagation of a wave packet $\psi\left(x,t\right) = U\left(x, x_0; t, 0\right)\psi\left(x_0, 0\right)$ (with U being the time evolution operator) can be understood as an average over all possible paths and pseudopaths connecting the points $(x_0, 0)$ and (x, t). Therefore the natural generalization of (2.63) for wave packets is

$$\tau = \int_{-\infty}^{\infty} dt \int_{0}^{L} dx\, \left|\psi\left(x,t\right)\right|^2, \tag{2.64}$$

which can be seen as an average of times spent inside the interval $[0, L]$ by all different paths contributing to the wave packet. Note that the initial wave packet must be normalized to one $\int_{-\infty}^{\infty} dx\, \left|\psi\left(x,0\right)\right|^2 = 1$. It is important to emphasize, that only the initial wave packet entirely located outside the actual scattering region must be normalized, since for regions featuring complex potentials, the time evolution is not norm-conserving in general. Expanding $\psi\left(x,t\right)$ inside the scattering regions into assumingly well-known eigenfunctions with trivial time evolution $\chi\left(x;k\right)e^{-i\omega(k)t}$ yields with (2.55) for the initial wave packet

$$\tau = \int_{-\infty}^{\infty} dt \int_{0}^{L} dx \iint \frac{dk'dk}{2\pi} \phi^{\star}\left(k'\right)\chi^{\star}\left(x;k'\right)\phi\left(k\right)\chi\left(x;k\right)e^{-i(\omega(k)-\omega(k'))t}. \tag{2.65}$$

This integral can easily be simplified inserting the disperion relation of the free particle in order to evaluate $\omega\left(k\right)$, and substituting the wave numbers (k, k') with their average Q and difference q $\left(Q = 1/2\left(k + k'\right), q = k - k'\right)$ [22]. Performing the integration finally yields

$$\tau = \int \frac{dk}{\sqrt{2\pi}} \left|\phi\left(k\right)\right|^2 \frac{m}{\hbar k} \int_{0}^{L} dx\, \left|\chi\left(x;k\right)\right|^2. \tag{2.66}$$

The term

$$\tau_d \equiv \frac{m}{\hbar k} \int_{0}^{L} dx\, \left|\chi\left(x;k\right)\right|^2 = \frac{W}{j_{in}} \tag{2.67}$$

in (2.66) is the intensity stored inside the scattering region if the wave is injected at one specific wave number k divided by the incoming flux $v = \frac{\hbar k}{m}$ carried by the corresponding

plane wave $\frac{1}{\sqrt{2\pi}}e^{i(kx-\omega(k)t)}$. It can easily be understood, that (2.67) is the average time spent by the wave inside the cavity. With j_{in} being the (stationary) flux injected into the scattering region and W being the amount of intensity stored, the intensity leaves the cavity after an average time of W/j_{in}. (2.66) is therefore the average dwell time for a given wave packet, $\tau \equiv \langle \tau_d \rangle_k$. The expression (2.67) is exactly the current definition of the dwell time in the literature [23, 28, 29, 24].

The dwell time and its average respectively are the most widely accepted scattering times concerning metastable entities [22]. Starting from (2.64), the averaged dwell time undoubtedly yields what it promises: the mean time spent by a particle in a given region, averaged over all scattering channels. The latter statement includes channels described by the scattering matrix, i.e., transmission or reflection, as well as fictitious channels appearing in non-unitary systems.

2.2.3. Connection between group delay and dwell time

For unitary systems, a simple relation between the group delay and the dwell time was found by Hauge et al. [22], which was rederived by Winful for the scattering of particles obeying the Schrödinger equation [28] and generalized to electromagnetic systems [29]. It takes the appealing form

$$\tau_g = \tau_d + \tau_i. \tag{2.68}$$

The group delay consists of the dwell time and an additional term τ_i, taking into account the delay due to self-interference of the impinging wave mentioned earlier in the context of the phase times. For a one dimensional system and injection from the left exclusively, τ_i evaluates to

$$\tau_i = -\frac{Im\,(r)}{k}\frac{\partial k}{\partial E}. \tag{2.69}$$

Despite its asymptotic nature due to the phase times involved in the calculation of τ_g, from the viewpoint of (2.68) a physical meaning can be associated to the group delay for arbitrarily defined scattering regions . The group delay is the sum of the average time spent by a wave inside the actual scattering region and the additional time delay due to self-interference effects occuring when approaching the scattering region. The above expression for τ_i was actually derived first by Smith in 1960 [26], but not interpreted explicitly as a self-interference term. Smith called the sum of τ_d and τ_i 'excess dwell time'.

Note that for full transmission ($r = 0$) and for high wave numbers k, τ_i vanishes. For finite r and very small $k \to 0$, τ_i and τ_g diverge, since the wave spends most of its time in front of the scattering region being not able to traverse it.

For non-unitary scattering systems, more complicated expressions for τ_i have been found [28], also the relation between τ_g and τ_d becomes more complicated generally [24].

For both systems, unitary and non-unitary, the way the stored intensity W in (2.67) is calculated depends on the sort of waves described and on the nature of the scattering region as well.

3. Time delay operators and particle-like scattering states

In this section, we will introduce and derive operators measuring the scattering time observables described in the last section, which are the group delay and the dwell time. Making use of these operators, we will present scattering states, that follow particle-like scattering patterns during the propagation through the investigated systems.

3.1. The Wigner-Smith time delay operator

Before we present the general expression for the operators measuring the group delay and dwell time, we briefly recall the most widely used operator concerning scattering times, which is the Wigner-Smith time delay operator. Following ideas of Wigner [27], Smith [26] originally introduced an operator measuring the delay, a particle incurs due to a collision event. His derivation was performed first in one dimension and then generalized to three dimensions. Using the scattering matrix, Smith found the following form for this 'lifetime matrix'

$$Q = i\hbar \frac{dS^\dagger}{dE} S. \tag{3.1}$$

For flux-conserving processes, the scattering matrix is unitary, $S^\dagger S = \mathbb{I}$. In such systems, the Wigner-Smith time delay operator (3.1) is hermitian. Taking the energy derivative of both sides of the unitarity condition

$$\frac{d}{dE}\left(S^\dagger S\right) = \frac{dS^\dagger}{dE} S + S^\dagger \frac{dS}{dE} = 0, \tag{3.2}$$

leads directly to showing the hermiticity of Q

$$i\hbar \frac{dS^\dagger}{dE} S = -i\hbar S^\dagger \frac{dS}{dE} \tag{3.3}$$

$$\Rightarrow Q = Q^\dagger. \tag{3.4}$$

Therefore, in unitary systems, the eigenvalues of Q are real quantities and are called 'proper delay times'. In the following section, we will discuss the relation of the quantity measured by the Wigner-Smith time delay operator and the group delay.

3.2. The group delay

In what follows, we will derive the proper operator corresponding to the group delay in multi-channel scattering as we defined it in (2.62).

We make use of an identity for complex curves depending on a real parameter t, that have the general form $Z(t) = z(t)\, e^{i\varphi(t)} = a(t) + ib(t)$. For the derivative of the phase $\varphi = \arctan\left(\frac{b}{a}\right)$, one finds the following relation

$$\dot{\varphi} = \frac{1}{1+\left(\frac{b}{a}\right)^2}\left(\frac{\dot{b}}{a} - \frac{b}{a^2}\dot{a}\right) = \frac{1}{z^2}\left(a\dot{b} - \dot{a}b\right). \tag{3.5}$$

The dot indicates the derivative with respect to the parameter t. Considering the group delay (2.62), we rewrite

$$\left(S(E)\,\vec{u}\right)_n = a_n + ib_n = z_n e^{i\varphi_n}. \tag{3.6}$$

The complex numbers (3.6) are functions of the scattering energy E via the scattering matrix' energy dependence. Using the relation (3.5) and inserting (3.6) into (2.62), we can write the group delay as

$$\tau_g = \hbar \sum_n z_n^2 \dot{\varphi}_n = \hbar \sum_n \left(a_n \dot{b}_n - \dot{a}_n b_n\right). \tag{3.7}$$

Taking the expectation value of the Wigner-Smith time delay operator (3.1) for the scattering state defined by the coefficients $\vec{u}$,

$$\tau_1 = i\hbar\, \vec{u}^\dagger \dot{S}^\dagger S \vec{u} = i\hbar \frac{d}{dE}\left[(S\vec{u})^\dagger\right](S\vec{u}), \tag{3.8}$$

we find with (3.6)

$$\tau_1 = \hbar \sum_n \left(a_n \dot{b}_n - \dot{a}_n b_n\right) + i\left(\dot{a}_n a_n + \dot{b}_n b_n\right). \tag{3.9}$$

Analogously we find for the hermitian conjugate of Q, $Q^\dagger = -i\hbar S^\dagger \dot{S}$, the expectation value

$$\tau_2 = \hbar \sum_n \left(a_n \dot{b}_n - \dot{a}_n b_n\right) - i\left(\dot{a}_n a_n + \dot{b}_n b_n\right). \tag{3.10}$$

Therefore, the group delay can be written as

$$\tau_g = \frac{1}{2}\left(\tau_1 + \tau_2\right). \tag{3.11}$$

The operator measuring the group delay is then given by

$$Q_g = \frac{i\hbar}{2}\left(\dot{S}^\dagger S - S^\dagger \dot{S}\right) = \frac{1}{2}\left(Q + Q^\dagger\right), \tag{3.12}$$

which is just the hermitized version of the Wigner-Smith time delay operator Q. Note that for unitary systems, the term

$$
\begin{aligned}
i\sum_n \left(\dot{a}_n a_n + \dot{b}_n b_n\right) &= \frac{i}{2}\frac{d}{dE}\sum_n \left(a_n^2 + b_n^2\right) && (3.13)\\
&= \frac{i}{2}\frac{d}{dE}\left(\vec{u}^\dagger S^\dagger S \vec{u}\right) && (3.14)\\
&= \frac{i}{2}\frac{d}{dE}\left(u^\dagger \vec{u}\right) && (3.15)\\
&= 0 && (3.16)
\end{aligned}
$$

vanishes due to the unitarity of S and $Q_g = Q$. So we can state that for flux-conserving processes, the Wigner-Smith operator measures the group delay and its hermitized version is the proper generalization to arbitrary scattering systems.

3.3. The dwell time

We will follow the strategy we used to derive Q_g in the previous section also to identify the proper operator measuring the dwell time, which is expressing τ_d as an expectation value for the specific scattering state as we did in (3.8) and (3.12), respectively. The scattering state $\psi(\vec{x}; E)$ in a multichannel scattering system is completely defined by its expansion coefficients $\vec{u}$ in the basis of incoming channels provided that the propagation patterns for each channel are well-known. Considering the expression (2.67) for the dwell time, we require the desired operator Q_d to fulfill the following equation,

$$
\langle u| Q_d |u\rangle = \sum_{n,m} \vec{u}_n^\dagger \left(Q_d\right)_{nm} \vec{u}_m = \frac{\int_\Omega dV\ |\psi(\vec{x}; E)|^2}{j_{in}} = \frac{W}{j_{in}} = \tau_d. \tag{3.17}
$$

$|u\rangle$ denotes the incoming wave at the lead entrances, $\int_\Omega dV$ denotes the integration over the scattering region (Fig. 2.1(a)). We use the cavity's Green's function G from (2.8) and the coupling matrix V to obtain the wave inside the cavity,

$$
|\psi\rangle = i\hbar G V |u\rangle . \tag{3.18}
$$

Here, $|\psi\rangle$ denotes the wave inside the cavity. In coordinate space, inserting (2.52) for V gives

$$
\begin{aligned}
\psi(x,y) &= i\hbar \int_{\partial\Omega_1} dy'\, G\left(x, y; x' = 0, y'; E\right) \sum_{n=1}^{n_{in}} \sqrt{v_n}\chi_n(y)\, u_{1,n} && (3.19)\\
&+ i\hbar \int_{\partial\Omega_2} dy'\, G\left(x, y; x' = L, y'; E\right) \sum_{n=1}^{n_{in}} \sqrt{v_n}\chi_n(y)\, u_{2,n}. && (3.20)
\end{aligned}
$$

$\int_{\partial\Omega_i} dy'$, $i = 1, 2$ denotes integration over left and right cavity entrance respectively, the coefficients $u_{i,n} \equiv \left(\vec{u}_i\right)_n$ are the expansion coefficients corresponding to the left and right

lead, $\vec{u} = \left(\vec{u}_1^T, \vec{u}_2^T\right)^T$. The dwell time according to (3.17) can then be written as

$$\langle\psi|\,\psi\rangle = \langle i\hbar GVu|\, i\hbar GVu\rangle = (-i\hbar)\,(i\hbar)\,\langle u|\,V^\dagger G^\dagger GV\,|u\rangle = \int_\Omega dV\ |\psi\,(\vec{x};E)|^2\,. \tag{3.21}$$

Note that the flux factor j_{in} is equal to one, since we are referring to the flux-normalized basis (2.4). By comparing (3.21) to (3.17) we find the appropriate operator measuring the dwell time to be

$$Q_d = \hbar^2 V^\dagger G^\dagger GV. \tag{3.22}$$

As we will discuss in the following subsection, this expression was found earlier by Sokolov and Zelevinsky in a different context [18]. With our derivation of (3.22) and the discussion of the dwell time in the previous chapter we can, however, not only associate a physical meaning to the findings of these authors, we can also put the specific functional form of Q_d onto solid ground.

While the construction of the operator measuring the group delay Q_g (3.12) is based solely on the knowledge of the system's scattering matrix, for the construction of Q_d in its general form (3.22), far more knowledge about the internal scattering dynamics is required though. The Green's function from the entrances to every point inside the cavity has to be known, whereas in the scattering matrix only those parts of G appear, that describe propagation from the lead mouths back to the lead mouths. For special systems, such as unitary systems and systems featuring uniform loss, expressions for Q_d requiring much less internal information can be found.

3.3.1. Unitary systems

For unitary scattering systems, we can show, that Q_d can be constructed involving only the scattering amplitudes, i.e., only those parts of the Green's function connecting the lead mouths with each other are needed. In order to derive this expression, we will recall an identity which was first derived by Smith [26]. Consider the Schrödinger equation and its energy derivative for the total scattering problem

$$(H-E)\,\psi = \left(\frac{p^2}{2m} + V_{pot} - E\right)\psi = 0 \tag{3.23}$$

$$(H-E)\,\frac{\partial\psi}{\partial E} - \psi = 0. \tag{3.24}$$

Multiplying (3.24) from the left-hand side with $\psi^\star$, multiplying the conjugate of (3.23) from the left hand side with $\partial\psi/\partial E$, and subtracting the resulting equations from each other gives

$$\psi^\star\frac{p^2}{2m}\frac{\partial\psi}{\partial E} - \frac{\partial\psi}{\partial E}\frac{p^2}{2m}\psi^\star - \psi^\star\psi = 0. \tag{3.25}$$

The terms including E and V_{pot} vanish, because the scattering energy E is a real quantity anyway, and in unitary systems $V_{pot} = V_{pot}^\star$, since such systems feature real potentials only. Inserting for $\vec{p} = \frac{\hbar}{i}\vec{\nabla}$ and $\dot{\psi} \equiv \frac{\partial\psi}{\partial E}$, (3.25) can be rewritten

$$-\frac{\hbar^2}{2m}\vec{\nabla}\cdot\left[\psi^\star\vec{\nabla}\dot{\psi} - \dot{\psi}\vec{\nabla}\psi^\star\right] = \psi^\star\psi. \tag{3.26}$$

Performing an integration over the scattering region Ω (Fig. 2.1(a)), we see that we can express the stored intensity inside the cavity for an arbitrary scattering state ψ - which is equivalent to the dwell time for unit incoming flux - as a surface term

$$-\frac{\hbar^2}{2m}\int_{\partial\Omega_1+\partial\Omega_2} d\vec{A}\cdot\left[\psi^\star\vec{\nabla}\dot{\psi}-\dot{\psi}\vec{\nabla}\psi^\star\right]=\int_\Omega dV\,\psi^\star\psi=\tau_d. \tag{3.27}$$

This means, that in unitary systems, the dwell time can be calculated without actually knowing the wave function inside the cavity but just at its boundary.

We will now apply the identity (3.27) to the systems we are interested in to express τ_d as an expectation value. Inside the leads and at the entrances, the wave function can be decomposed into incoming and outgoing scattering channels

$$\psi\left(\vec{x}\right)=\begin{cases}\sum_{n=1}^{n_{in}} a_n\Phi_{1,n}\left(\vec{x}\right)+\sum_{n=1}^{\infty} b_n\Phi_{1,n}^\star\left(\vec{x}\right), & \vec{x}\epsilon\partial\Omega_1\\ \sum_{n=1}^{\infty} c_n\Phi_{2,n}\left(\vec{x}\right)+\sum_{n=1}^{n_{out}} d_n\Phi_{2,n}^\star\left(\vec{x}\right), & \vec{x}\epsilon\partial\Omega_2\end{cases}. \tag{3.28}$$

For our two-dimensional model-system featuring rectangular leads (Fig. 2.1(b)), the Φ_n are equal to the lead modes ϕ_n in (2.4) for left (1) and right (2) lead respectively. Note that, at the boundary, evanescent modes might generally give a considerable contribution to ψ, therefore, the summation concerning outgoing coefficients b_n and c_n in (3.28) formally runs up to infinity. The decomposition (3.28) together with the definition of the scattering matrix (2.2) can be used to evaluate the surface term on the left-hand side of (3.27) for our system. Inserting the scattering amplitudes for b_n and c_n gives

$$b_n=\begin{cases}\sum_{m=1}^{n_{in}} r_{nm}a_m+\sum_{m=1}^{n_{out}} t'_{nm}d_m, & n\le n_{in}\\ \sum_{m=1}^{n_{in}} \tilde{r}_{n-n_{in},m}a_m+\sum_{m=1}^{n_{out}} \tilde{t}'_{n-n_{in},m}d_m, & n>n_{in}\end{cases} \tag{3.29}$$

$$c_n=\begin{cases}\sum_{m=1}^{n_{in}} t_{nm}a_m+\sum_{m=1}^{n_{out}} r'_{nm}d_m, & n\le n_{out}\\ \sum_{m=1}^{n_{in}} \tilde{t}_{n-n_{out},m}a_m+\sum_{m=1}^{n_{out}} \tilde{r}'_{n-n_{out},m}d_m, & n>n_{out}\end{cases} \tag{3.30}$$

Here we introduced the scattering amplitudes

$$\tilde{S}=\begin{pmatrix}\tilde{r} & \tilde{t}'\\ \tilde{t} & \tilde{r}'\end{pmatrix} \tag{3.31}$$

$$\tilde{S}=i\hbar\tilde{V}^\dagger GV, \tag{3.32}$$

that describe scattering from open channels into all evanescent channels. The indices of the corresponding matrix elements are chosen in such a way, that e.g. $\tilde{t}_{3,2}$ is the amplitude for the transmission from the second flux-carrying lead mode in the left lead into the third evanescent mode in the right lead.

Inserting for the coefficients (3.29) and (3.30) into the expansion of $\psi\left(\vec{x}\right)$, we can evaluate the surface term (3.27) which finally yields for the dwell time a sum of four

terms[1]

$$\tau_d = -\, i\hbar\, \vec{u}^\dagger \left[S^\dagger \dot{S}\right] \vec{u} \tag{3.33}$$

$$+\, \frac{i}{2}\frac{m}{\hbar}\, \vec{u}^\dagger \left[S^\dagger \begin{pmatrix} \Gamma\left(k_x^{-2}\right) & 0 \\ 0 & \Gamma\left(k_x^{-2}\right) \end{pmatrix}\right] \vec{u} \tag{3.34}$$

$$-\, \frac{i}{2}\frac{m}{\hbar}\, \vec{u}^\dagger \left[\begin{pmatrix} \Gamma\left(k_x^{-2}\right) & 0 \\ 0 & \Gamma\left(k_x^{-2}\right) \end{pmatrix} S\right] \vec{u} \tag{3.35}$$

$$-\, \frac{1}{2}\frac{m}{\hbar}\, \vec{u}^\dagger \left[\tilde{S}^\dagger \begin{pmatrix} \Gamma\left(\kappa_x^{-2}\right) & 0 \\ 0 & \Gamma\left(\kappa_x^{-2}\right) \end{pmatrix} \tilde{S}\right] \vec{u}. \tag{3.36}$$

Here we again grouped the expansion coefficients a_n and d_n to the vector $\vec{u} = \left(\vec{a}^T, \vec{d}^T\right)^T$. On an abstract operator level, we can rewrite the dwell time as follows

$$\tau_d = \langle u| \left[-i\hbar S^\dagger \dot{S} + \frac{i}{2}\frac{m}{\hbar}\left(S^\dagger \left[\frac{1}{k^2}\right] - \left[\frac{1}{k^2}\right] S\right) - \frac{1}{2}\frac{m}{\hbar}\tilde{S}^\dagger \left[\frac{1}{\kappa^2}\right] \tilde{S}\right] |u\rangle\,. \tag{3.37}$$

For reasons of visibility, we introduced the simplified notation

$$\left[\frac{1}{k^2}\right] := \begin{pmatrix} \Gamma\left(k_x^{-2}\right) & 0 \\ 0 & \Gamma\left(k_x^{-2}\right) \end{pmatrix} \tag{3.38}$$

and dropped the subscript x (analogously for the operator $\frac{1}{\kappa^2}$). We can interpret the operator

$$Q_d = -i\hbar S^\dagger \dot{S} + \frac{i}{2}\frac{m}{\hbar}\left(S^\dagger \left[\frac{1}{k^2}\right] - \left[\frac{1}{k^2}\right] S\right) - \frac{1}{2}\frac{m}{\hbar}\tilde{S}^\dagger \left[\frac{1}{\kappa^2}\right] \tilde{S} \tag{3.39}$$

as the proper expression for the dwell time operator (3.22) in flux-conserving scattering systems. This operator can be decomposed into

$$Q_d = Q_g - Q_i, \tag{3.40}$$

which is in perfect agreement to the connection between group delay and dwell time given by (2.68) for the one-dimensional system, taking into account also the evanescent lead modes which are not present in the 1D case. The equivalence of (3.39) and (3.22) is shown in appendix A.2.

Rederiving previous results by Sokolov and Zelevinsky [18], we will now show that the term Q_i associated to the self-interference in (3.40) which measures the difference of group delay and dwell time in unitary systems, descends from the energy dependence of the system's coupling to the outside region. Starting from the Wigner-Smith time delay operator $Q = -i\hbar S^\dagger \dot{S}$, which is equivalent to the group delay operator Q_g for flux-conserving scattering, inserting

$$S = -\mathbb{I} + i\hbar V^\dagger G V \tag{3.41}$$

[1] A detailed derivation of this result can be found in appendix A.1.

for the scattering matrix, we find

$$Q_g = -i\hbar \left(-\mathbb{I} - i\hbar V^\dagger G^\dagger V\right) (-\mathbb{I} + i\dot{\hbar} V^\dagger G V). \tag{3.42}$$

Taking into account only the resonant energy dependance via $G = (E - H_{\text{eff}})^{-1}$ gives for the derivative of G (see also appendix A.2)

$$\dot{G} = -G^2. \tag{3.43}$$

Neglecting also the engergy dependence of V, we get

$$\begin{aligned} Q_g^{res} &= \hbar^2 V^\dagger G G V + i\hbar^3 V^\dagger G^\dagger V V^\dagger G G V && (3.44)\\ &= \hbar^2 V^\dagger G G V + \hbar^2 V^\dagger \left(G^\dagger - G\right) G V && (3.45)\\ &= \hbar^2 V^\dagger G^\dagger G V. && (3.46) \end{aligned}$$

Here we have used the identity $i\hbar G^\dagger V V^\dagger G = \left(G^\dagger - G\right)$, which we derive in (A.63). What we find is, that Q_g^{res} is equal to Q_d. The derivation of (3.44) shows that the dwell time τ_d is indeed the fraction of delay time due to intrinsic resonances. Sokolov and Zelevinsky found the same expression for Q_g^{res} but did not interpret it correctly as the operator measuring τ_d rather than τ_g.

3.3.2. Uniform loss systems

Absorption in scattering systems leads to an additional decay of the wave's intensity. This loss can either be included into calculations through an imaginary shift in the scattering energy $E' = E + i\gamma$ or through an imaginary part of the scattering potential $V'_{pot} = V_{pot} - i\gamma$, since all necessary scattering quantities such as, e.g., the scattering matrix S, derive from the Green's function $G = 1/\left(E - H_{\text{eff}}\right)$, where only the difference of E and H_{eff} appears. In this thesis we will follow the latter procedure by adding a spatially uniformly distributed imaginary part to the system's Hamiltonian.

Starting again from the Schrödinger equation

$$\left(\frac{p^2}{2m} + V_{pot} - E\right)\psi = 0, \tag{3.47}$$

we consider the difference of (3.47) multiplied with $\psi^\star$ from the left-hand side and (3.47) multiplied with ψ from the right-hand side,

$$\psi^\star \frac{p^2}{2m}\psi - \psi \frac{p^2}{2m}\psi^\star + \psi^\star\psi \left(V_{pot} - V_{pot}^\star\right) = 0. \tag{3.48}$$

An integration over the scattering region Ω gives with $p = \frac{\hbar}{i}\vec{\nabla}$ gives

$$-\frac{\hbar^2}{2m}\int_{\partial\Omega_1+\partial\Omega_2} d\vec{A}\,\left(\psi^\star\vec{\nabla}\psi - \psi^\star\vec{\nabla}\psi\right) = -2i\,\mathrm{Im}\left(V_{pot}\right)\int_\Omega dV\,\psi^\star\psi. \tag{3.49}$$

The imaginary part of the potential $\mathrm{Im}\,(V_{pot}) = -\gamma$ can be put in front of the integral since we assumed it to be constant. Using the decomposition of the wave at the lead entrances (3.28) in order to evaluate the left-hand side of (3.49) we find (appendix B.1)

$$\tau_d = \int_\Omega dV\, \psi^\star \psi = \frac{\hbar}{2\gamma}\, \vec{u}^\dagger \left[\mathbb{I} - S^\dagger S\right] \vec{u}. \tag{3.50}$$

The operator measuring the dwell time in systems featuring uniform loss is then given by

$$Q_d = \frac{\hbar}{2\gamma} \left(\mathbb{I} - S^\dagger S\right), \tag{3.51}$$

using the sub-unitary scattering matrix. The expression (3.51) yields a very intuitive relation between the scattering matrix and the dwell time: The higher the dwell times for a given system are, the higher is the deviation of the scattering matrix from unitarity. Our result agrees with the findings of Savin and Sommers [25], but with the above derivation, we can put the results of these authors on solid ground and provide the proper physical interpretation.

In extension of this result, we also demonstrate in appendix B.2 the equivalence of the general expression for the dwell time operator (3.22) (which is also valid for non-uniform absorption) and its special form in uniformly absorptive systems (3.51).

3.4. Particle-like scattering states[2]

A specific, unambigous runtime can be associated to a classical particle traversing a cavity or an obstacle. In section 2.2 we discussed the difficulties assigning a runtime to a wave or wave packet respectively. We say a wave has a 'well-defined' scattering time if it is an eigenstate of one of the time delay operators defined in the previous sections. In an earlier work [17], we showed that within the set of the eigenvectors of the Wigner-Smith time delay matrix, very special scattering states featuring unique, particle-like propagation patterns can be found in unitary systems. Only particle trajectories of very similar runtimes that lie in narrow bundles in phase space contribute to those waves. This leads to highly collimated wave fronts and a beam-like shape of the propagating waves. When we refer to 'beam-like' or 'particle-like' scattering states in the following, states featuring scattering patterns known from classical particles are addressed. This behaviour particularly involves

- A reflection or transmission probability of either one or zero in the case of flux-conserving scattering
- Beam-like propagation through the cavity in contrast to a spreading of the wave's intensity over the entire scattering region

[2] In this section we will switch to atomic units, i.e., we set $\hbar \equiv 1$ and $m \equiv 1$, for the sake of a better readability.

- Well-defined delay times, i.e., the states are eigenstates of one of the time delay operators

Since a classical particle cannot be injected simultaneously from both sides, we are clearly interested in states that have incoming flux through one of the leads only. The first point in the above enumeration has to be understood in this sense of single-port injection.

The third point seems to contradict the necessity of being injected only from one side, since all the presented operators have the dimension of the scattering matrix, that is $(n_{in} + n_{out}) \times (n_{in} + n_{out})$. A state defined by its expansion coefficients $\vec{u} = \left(\vec{a}^T, 0\right)^T$ that enters the cavity through the left lead exclusively has only n_{in} non-zero components though. Decomposing the particular time delay operator Q_α $(\alpha = g, d)$ into its block-structure, we express the action of Q_α in matrix notation as follows

$$Q_\alpha \vec{u} = \begin{pmatrix} Q_{11} & Q_{12} \\ Q_{21} & Q_{22} \end{pmatrix} \begin{pmatrix} \vec{a} \\ 0 \end{pmatrix} = \begin{pmatrix} Q_{11}\vec{a} \\ Q_{21}\vec{a} \end{pmatrix}. \tag{3.52}$$

The blocks are chosen in such a way, that Q_{11} has the dimension $n_{in} \times n_{in}$, the block Q_{21} the dimension $n_{out} \times n_{in}$. We demand, that $\vec{u}$ is an eigenvector of Q_α, so the eigenvalue problem reads

$$Q_\alpha \vec{u} = \begin{pmatrix} Q_{11}\vec{a} \\ Q_{21}\vec{a} \end{pmatrix} = q \begin{pmatrix} \vec{a} \\ 0 \end{pmatrix} = q\vec{u}, \tag{3.53}$$

with q being the eigenvalue. From (3.53) we see, that the desired vector $\vec{a}$ has to fulfill the two conditions of being an eigenstate of Q_{11} and of lying in the kernel of Q_{21},

$$Q_{11}\vec{a} = q\vec{a} \tag{3.54}$$

$$Q_{21}\vec{a} = 0, \tag{3.55}$$

in order that $\vec{u}$ be an eigenstate of Q_α. Previously, we could show for unitary systems, that if the state $\vec{a}$ satisfies both conditions (3.54) and (3.55), the wave is either fully reflected or transmitted [17]. This property lead us to name these states 'NOTEs'. This acronym stands for Noiseless Time Delay Eigenstates. The term 'noiseless' generally refers to states with full transmission (or reflection), since for such states, the quantum shot-noise in electronic transport vanishes.

The procedure followed during this thesis to find such NOTEs works in two steps:

1. We diagonalize Q_{11}
2. and identify those states in the eigenspace of Q_{11} that lie simultaneously in the nullspace of Q_{21}.

Note that the time delay operators Q_g (3.12) and Q_d (3.22) are per construction hermitian matrices. Therefore, the block Q_{11} is a hermitian matrix as well and its eigenstates form a complete and orthogonal basis for states injected from the left-hand side. To verify condition (2.) we introduce a measure χ which is the norm of the n_{out} dimensional vector resulting from the action of Q_{21} on $\vec{a}$,

$$\chi = \|Q_{21}\vec{a}\|. \tag{3.56}$$

χ determines the degree to which the (normalized) vector $\vec{a}$ lies in the kernel of Q_{21}. The quality of a NOTE is better, the closer $\chi \epsilon [0, \infty]$ is to zero. As we will see in the following, investigating non-unitary systems, a small nullspace-norm χ is not sufficient to determine whether a state is a NOTE. For that reason, we will use the transmission

$$T = \vec{a}^\dagger t^\dagger t \vec{a} = \|t\vec{a}\|^2 , \tag{3.57}$$

and the reflection

$$R = \vec{a}^\dagger r^\dagger r \vec{a} = \|r\vec{a}\|^2 \tag{3.58}$$

additionally to identify NOTEs in the eigenspace of Q_{11}.

3.4.1. Unitary systems[3]

In this subsection, we apply the procedure to find beam-like scattering states presented in the previous subsection to flux-conserving systems featuring different potentials inside the scattering region. The investigated geometry is of the simple shape displayed in Fig. 2.1(b), the wave injection is performed at a total wave number of $k = \sqrt{k_x^2 + k_y^2} = 30.5\pi/d$, such that 30 modes are open. For a unitary scattering matrix, one expects the NOTEs to have full or zero transmission $T \approx 0, 1$ and low null-space norms χ. Fig. 3.1 shows (χ, T, R) for all the 30 eigenstates of the Q_{11} blocks of Q_d (green balls) and Q_g (blue crosses). Since the relation $R + T = 1$ is valid, all points come to lie on the line defined by $R = 1 - T$. We stick to this three-dimensional display for reasons of uniformity, also when the unitarity relation is not valid in flux non-conserving sytems. NOTEs can only exist in the 'corners' of the plot where either $T = 1$ or $R = 1$ (red circles). Among these states, those with a small null-space-norm χ can be identified as beam-like. For the states numbered in Fig. 3.1 (marked by the red arrows) we show the wave function intensities $|\psi(x, y)|^2$ and scattering characteristics in Table 3.1 for Q_d. The smaller inset in Fig. 3.1 shows (q, T, R) with q being the corresponding Q_{11} eigenvalue. From this plot and from Table 3.1 one sees that the NOTE states not only correspond to small nullspace-norms, but also to rather short dwell times. An example of a Q_{11} eigenstate that doesn't feature the desired properties of a beam-like scattering state is shown in Table 3.1 as well.

A remarkable detail of Fig. 3.1 is, that there is only a slight difference between the data corresponding to the group delay and the dwell time. As a measure of the difference of Q_d and Q_g we will introduce the quantity

$$\omega = \sqrt{\frac{\left\langle (Q_g - Q_d)^2 \right\rangle}{\langle Q_g^2 \rangle}}. \tag{3.59}$$

The notation $\langle A \rangle$ means taking the average of the eigenvalues of the matrix A. This average 'smears out' the influence of single possibly very large eigenvalues in the case

[3] A detailed investigation and statistical analysis of beam-like shaped scattering states in unitary clean and disordered systems using $Q_g \equiv Q$ can be found in our earlier work [17].

of cavity resonances. Note that in unitary systems $Q_g - Q_d$ is exactly the operator measuring the self-interference Q_i. For the clean cavity featuring zero potential we find $\omega \approx 0.0021$, so the influence of the self-interference on the overall delay time can be considered very small. This fact seems to arise rather from the chosen geometry than from any (hermitian) potential inside the cavity at the chosen scattering energy.

To substantiate this statement, we investigated the same geometry featuring a short-range disorder, a long range disorder and a Sinai-type obstacle, the corresponding (χ, T, R)-plots are displayed in Fig. 3.2(a), (b), (c). The smaller insets show the specific potentials; the numbered states and the corresponding scattering data for Q_g are shown in Table 3.2. We find that indeed also in these systems the influence of the self-interference is very small. The ω values are approximately 0.0013, 0.0009 and 0.0013 for the short-range disorder, the long-range disorder and the Sinai potential, respectively; so in these special cases we even find a decrease of ω in comparison to the system with no external potential. The average reflectivities of the former three systems

$$\bar{R} = \frac{\sum_{i=1}^{n_{in}} R_i}{n_{in}} \tag{3.60}$$

are given by 0.67, 0.86 and 0.62 in comparison to 0.36 for the system with zero potential. According to the functional form of the self-interference time for a 1D system (2.69), a stronger reflectivity should rather favour a stronger influence of τ_i, which is obviously not the case for our geometry. Keeping in mind that the operator Q_i arises from the energy dependence of the coupling between scattering region and leads according to subsection 3.3.1, we may conclude that for the investigated geometry, this energy dependence is negligible from the viewpoint of scattering times.

Selected states marked by red arrows in Fig. 3.2 for the three different systems are displayed in Table 3.2. For the long-range disorder and for the Sinai billiard we even find NOTE states (#3 and #5), whereas all beam-like states are destroyed in the case of the short-range disorder. State #1 in Fig. 3.2(a) is perfectly reflected and has a very small null-space norm which would normally indicate a NOTE state. Investigating its runtime q, we find that this state is immediately backscattered at the entrance and does not even enter the cavity. States that do not enter the scattering region are clearly eigenstates of Q_d with a very small eigenvalue - which also explains the small value of χ. The states #2, #4 and #6 having large values of χ are generic scattering states that do not show beam-like propagation patterns.

Choosing a different geometry, the self-interference delay might not be negligible at all. The cavity displayed in Fig. 3.2(d) consists of a thin aperture connected to two leads. The actual scattering region is just the space inside the aperture, and is, therefore, very small. In this case, self-interference has a major contribution to the group delay, since the dwell time is very short due to the small extension of the scattering region. The ω-value for this system evaluates to 0.4508, such that on average, nearly half of the delay a wave suffers traversing the aperture is due to self-interference. Note, that unlike Fig. 3.2(a)-(c), Fig. 3.2(d) does not show (χ, T, R) for all 30 eigenstates of the Q_{11} blocks of Q_d and Q_g, respectively, but a zoom on the highly transmitted states for the sake of better visibility. The data and intensity of one eigenstate of each block (states #7 and

#8) are shown in Table 3.2. Investigating $|\psi(x,y)|^2$ and (χ, T, R) for the example states, we find that for this system featuring high self-interference delays relative to dwell times, Q_d is more likely to deliver NOTEs than Q_g. From Fig. 3.2 we see, that the eigenvalues of the corresponding Q_{11} blocks of states #7 and #8 are very similar. One shall not be misled by this similarity in the eigenvalues; the group delay for the Q_d eigenstate #7, which is calculated taking the expectation value of Q_g, is very different from its dwell time and amounts only to about 4.5% of the dwell time.

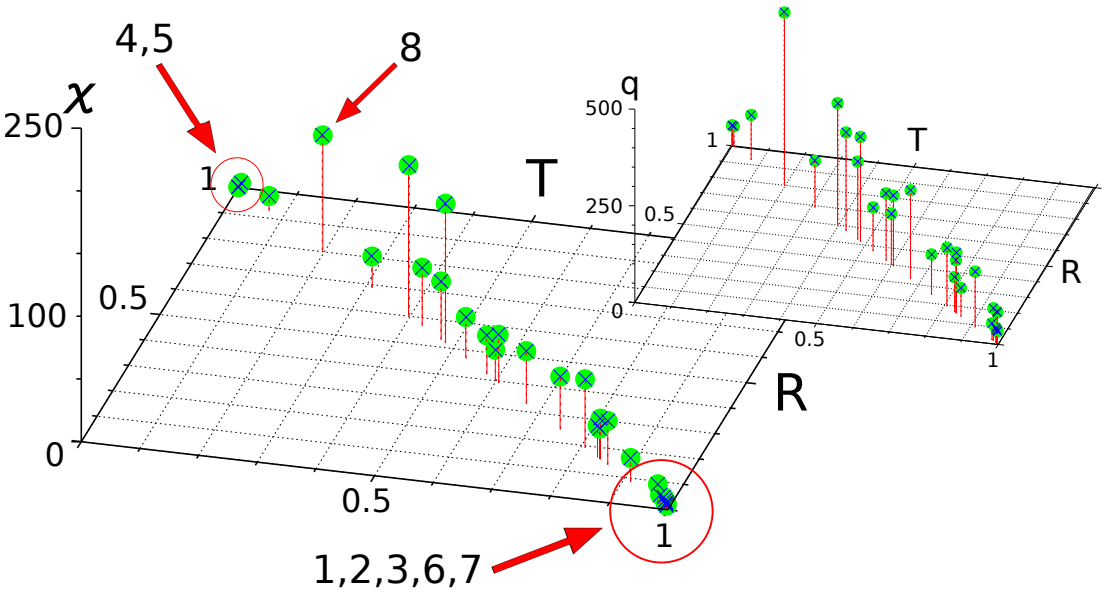

Figure 3.1.: (χ, T, R) for all 30 eigenstates of $[Q_d]_{11}$ (green balls) and $[Q_g]_{11}$ (blue crosses) for the scattering geometry depicted in Fig. 2.1(b) at a wave number $k = 30.5\,\pi/d$ with $V_{pot}(x,y) = 0$. NOTEs lying in the corners of the plot at $T \approx 1$ or $R \approx 1$ are marked by the red circles. The scattering data of the numbered states can be found in Table 3.1. The smaller inset shows (q, T, R) for the given states, NOTEs correspond to rather small delay times, since small delay times enable the wave to stay highly collimated during the transit through the cavity. As an example of a state that is not shaped beam-like, the state with the highest delay time is also shown in Table 3.1.

#	$\lvert\psi(x,y)\rvert^2$	#	$\lvert\psi(x,y)\rvert^2$
1	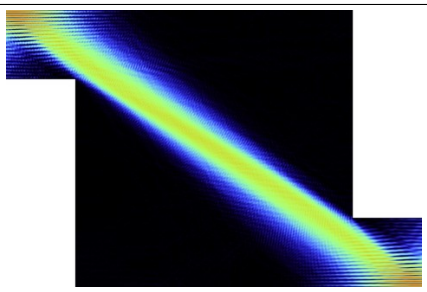	5	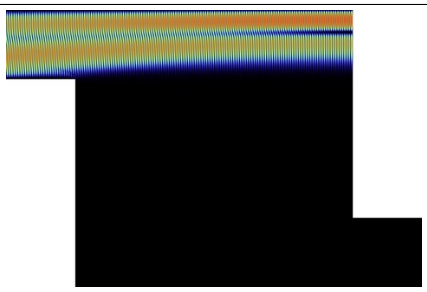
2	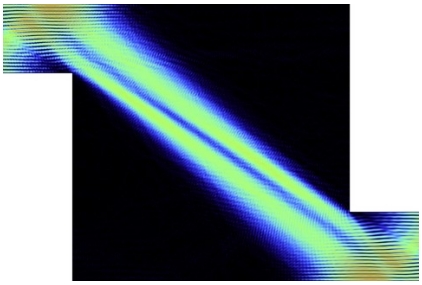	6	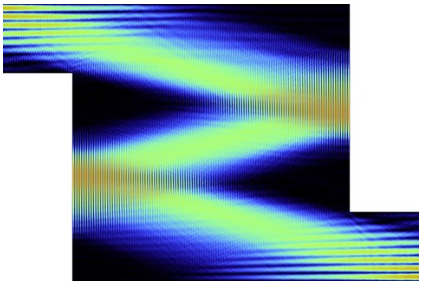
3	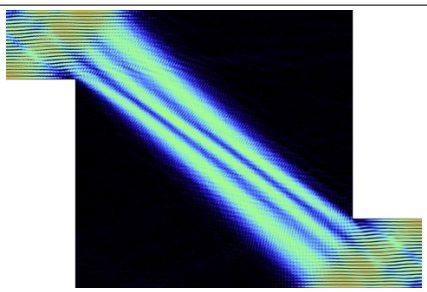	7	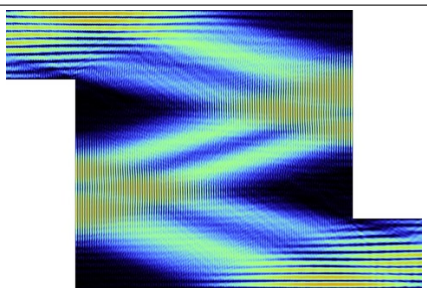
4	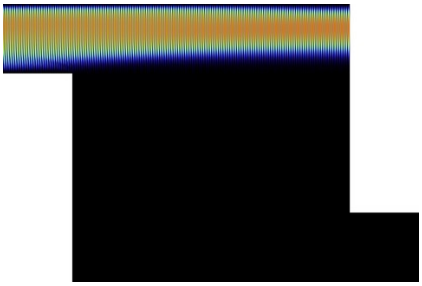	8	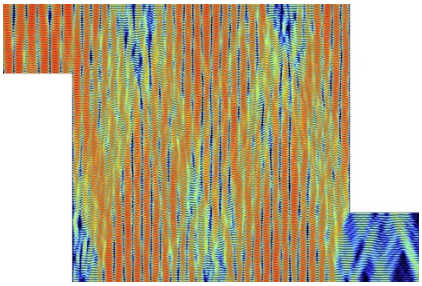

#	T	R	χ	q	#	T	R	χ	q
1	0.9976	0.0024	4.3912	32.6705	5	0.0001	0.9999	0.6481	52.7574
2	0.9965	0.0035	5.2922	34.6569	6	0.9970	0.0030	2.7363	81.7509
3	0.9943	0.0057	6.5023	36.5932	7	0.9946	0.0054	3.6552	83.0514
4	0.0000	1.0000	0.3693	52.4879	8	0.1966	0.8034	92.1776	445.3424

Table 3.1.: Intensity and scattering data for the states marked in Fig. 3.1. The data for all displayed states is taken from the $[Q_d]_{11}$ eigenstates. The corresponding data for the $[Q_g]_{11}$ eigenstates is very similar (not shown).

#	$\lvert\psi(x,y)\rvert^2$	#	$\lvert\psi(x,y)\rvert^2$
1		5	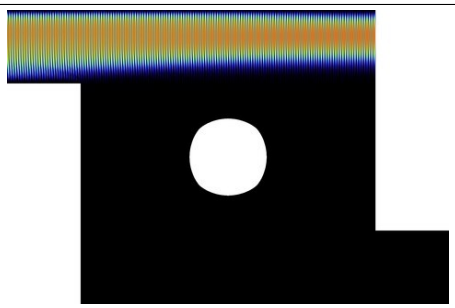
2	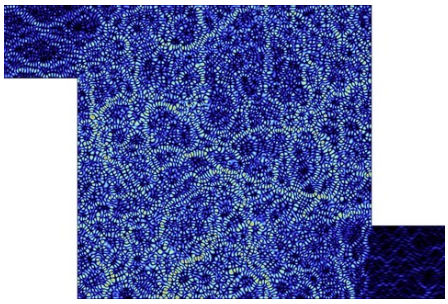	6	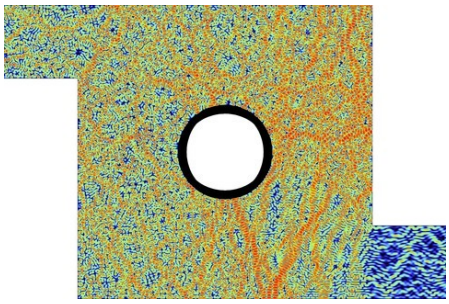
3	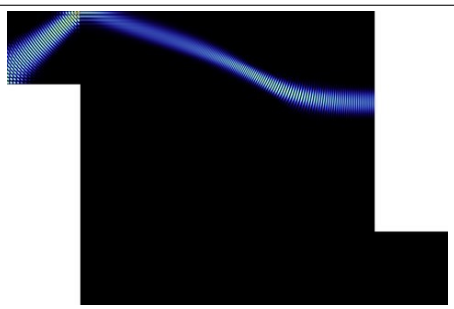	7	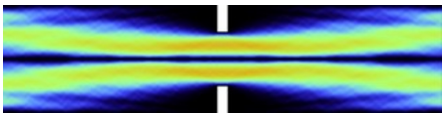
4	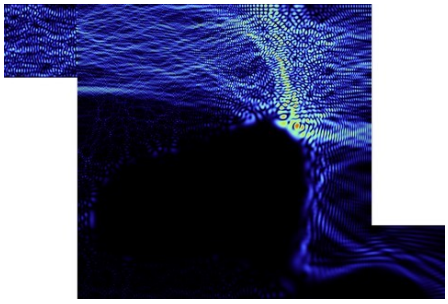	8	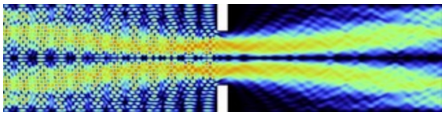

#	Q	T	R	χ	q	#	Q	T	R	χ	q
1	d	0.000	0.9991	4.3814	1.6903	5	d	0.0000	1.0000	0.2821	52.486
2	d	0.3793	0.6207	239.09	425.13	6	d	0.4733	0.5267	169.59	322.61
3	d	0.0000	1.0000	0.0926	25.152	7	d	1.0000	0.0000	0.0057	0.6499
4	d	0.3581	0.6419	128.45	156.59	8	g	0.9575	0.0425	0.0598	0.6656

Table 3.2.: Intensity and scattering data for the states marked in Fig. 3.2. The letters 'd' and 'g' indicate of which operator, $[Q_d]_{11}$ or $[Q_g]_{11}$, the displayed state is an eigenstate.

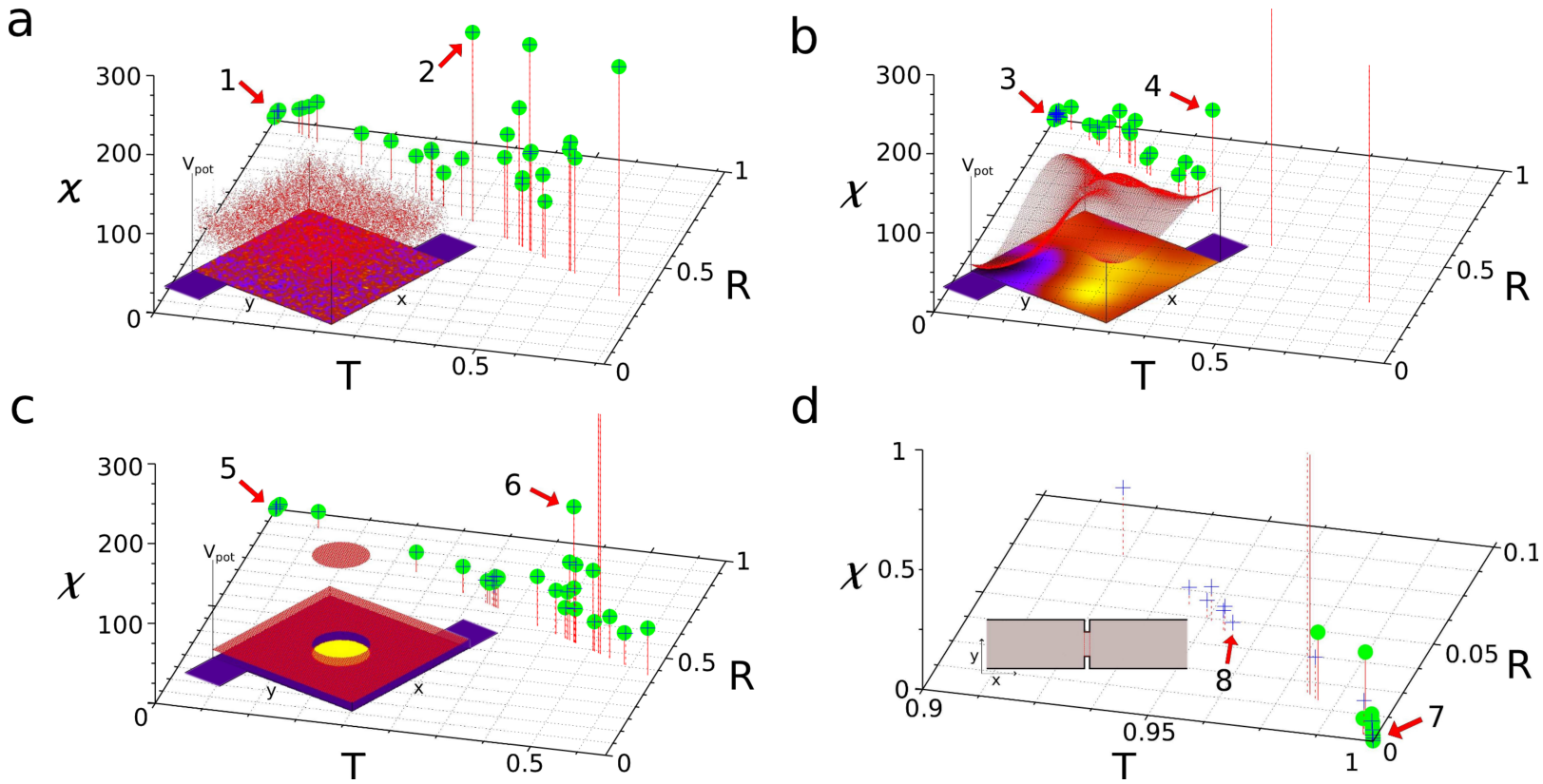

Figure 3.2.: (χ, T, R) for the eigenstates of $[Q_d]_{11}$ (green balls) and $[Q_g]_{11}$ (blue crosses) at a wave number $k = 30.5\,\pi/d$ for the scattering geometry depicted in Fig. 2.1(b) featuring different potentials V_{pot} shown in the insets (a, b, c) and for a thin aperture as shown in the corresponding inset (d). Black means high negative potential, purple zero and yellow high positive potential. (a) Short-range disorder with correlation-length $\xi_c = 0.5\,\lambda$ with $\lambda = 2\pi/k$ being the wave-length and an amplitude of the height of the scattering energy $A_{pot} = k^2/2 = E$. (b) Long-range disorder with $\xi_c = 15\,\lambda$ and $A_{pot} = E$. For reasons of visibility, the χ-range is set to $[0, 300]$, for states with higher χ-values than 300, only their position in the (T, R)-plane is shown. The highest appearing χ-value for this scattering setup is given by 1311. (c) Sinai-type billiard with a circular hard-wall obstacle of radius $r = 1/6\,L$, L is the side-length of the cavity. Only χ-values < 300 are shown, the highest appearing χ-value is 369. (d) The actual scattering region is the area inside the aperture (red dashed lines) of width $w = 0.5\,d$ and length $L = 0.1\,d$. The plot is a zoom onto the highly transmitted states only. For states with $\chi > 1$, only T and R are plotted. The scattering data and wave intensity-plots for all numbered states indicated by the red arrows can be found in Table 3.2.

3.4.2. Uniform loss systems

In systems featuring a non-unitary scattering matrix, such as uniform loss systems, where S is a sub-unitary matrix, the relation $R + T = 1$ is clearly not valid (Fig. 2.1(b), $V_{pot} = -i\,\gamma$). Flux is inevitably lost, therefore any scattering state cannot be expected to have either a full transmission or reflection of 1. The concepts for finding NOTEs introduced in the previous subsections stay mostly the same though. Also in these absorptive systems, we search for states with a maximum transmission (or reflection) and small null-space-norms χ. Fig. 3.3 shows (χ, T, R) for the eigenstates of $[Q_d]_{11}$ (green balls) and $[Q_g]_{11}$ (blue crosses), the injection energy is again $E = (30.5\pi/d)^2/2$. We chose quite a strong absorption in order to demonstrate that our concepts still work also under such extreme conditions; the most highly transmitted state only has a T-value of 0.145. The smaller inset shows (q, T, R). We see that in contrast to the unitary systems, there is quite a big difference between the two time delay operators measuring group delay and dwell time, respectively. The intensity-plots for the states numbered in Fig. 3.3 and the corresponding scattering data can be found in Table 3.3. Again we find that states lying in the 'corners' of high transmission or reflection of the plot feature small χ-values and have a beam-like shape. The family of directly transmitted NOTEs (represented in our selection by state #1) can be found using both of the operators. In the case of the family of directly reflected states, Q_g finds only one member properly (#5 in comparison to #6 and #7), whereas Q_d gives three (#5,#2,#3). What cannot be found via optical inspection of Fig. 3.3 but by investigating closely the scattering data is the family of z-shaped NOTEs (represented by #4). They separate from their 'neighbour'-states (in terms of their runtime) through their relatively higher (but small) transmission in the case of states that are completely absorbed (#8), on the one hand, and through their reflection of zero and their smaller χ from spreaded states that are not completely absorbed, on the other hand. For states of the same shape (#1,#4,#5) contained in both of the eigenspaces of Q_d and Q_g only the data for the $[Q_d]_{11}$ eigenstates is shown in Table 3.3.

From the insets in Fig. 3.3 showing (T, R, q), we see that like in the case of unitary systems, the beam-like states correspond to short dwell times, but in contrast, to the highest group delays. As discussed in the previous chapter, the dwell time gives an average for the time spent by a wave inside the scattering region. This average includes *all* channels through which flux leaves the system. The physical interpretation of the dwell time is thus reasonable also in flux non-conserving systems. The interpretation of the group delay is, however, more difficult. Recalling the expression for τ_g,

$$\tau_g = \hbar \sum_{i=1}^{n_{in}+n_{out}} |(S\vec{u})_i|^2 \, \frac{d\varphi_i}{dE}, \tag{3.61}$$

we see that the terms in the sum consist of two competing factors. Although the beam-like states correspond to the smallest phase-derivatives $d\varphi_i/dE$, their prefactors $|(S\vec{u})_i|^2$ are much larger compared to states that are strongly absorbed (for which $S\vec{u} \approx 0$). This explains why the beam-like states correspond to the highest group delays, since these states are least absorbed.

Summarizing, we state that in uniformly absorptive systems, both operators, Q_g and Q_d can be used to create beam-like scattering states. However, we conclude from the results presented in Fig. 3.3 and Table 3.3, that Q_d is preferable, since it contains more NOTEs in its eigenspace than Q_g. From numerical as well as experimental points of view, also the construction of Q_d is advantageous, since according to (3.51), only the scattering matrix at a single energy is needed, whereas Q_g involves its energy derivative. A question that is still open is the behavior of the group delays in the limit of vanishing absorption. In unitary systems, NOTEs correspond to small $[Q_g]_{11}$ eigenvalues (which are equal to the expectation value of Q_g because these states are only injected from the left), but in the investigated strongly absorbing system, they correspond to comparatively large eigenvalues, though.

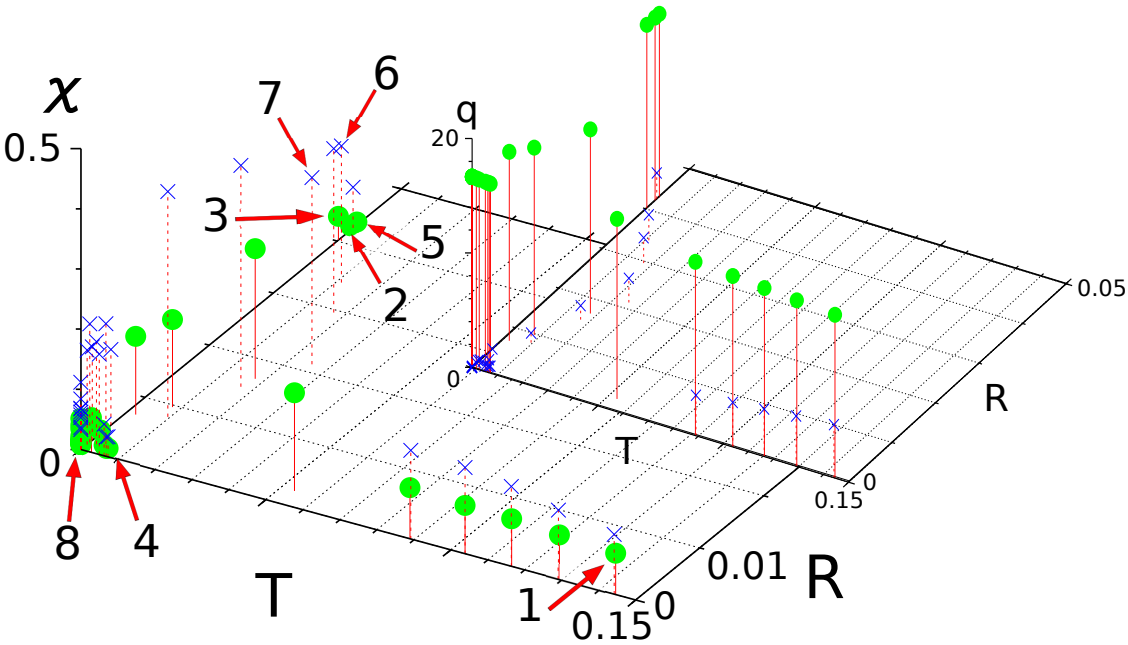

Figure 3.3.: (χ, T, R) for all 30 eigenstates of $[Q_d]_{11}$ (green balls) and $[Q_g]_{11}$ (blue crosses) for the scattering geometry consisting of two leads attached to a quadratic cavity depicted in Fig. 2.1(b) featuring an absorptive potential inside the scattering region $V_{pot}(x, y) = -i\,\gamma$. The scattering energy is again $E = (30.5\,\pi/d)^2/2$. $\gamma \approx 0.004\,E$ corresponding to an absorption length of $\xi_a \approx 1.28\,L$, where L denotes the length of the cavity. Like in unitary systems, NOTEs are lying at high transmission and zero reflection and vice versa. The scattering data of the numbered states marked by red arrows can be found in Table 3.1. If the intensities of the eigenstates of the two operators $[Q_g]_{11}$ and $[Q_d]_{11}$ have a very similiar shape, which is the case for states #1,#4 and #5, only the data for the Q_d-states is shown in Table 3.1. The smaller inset shows (q, T, R) for the given states. NOTEs correspond to small dwell times, but in contrast to unitary systems, to high group delays. An example of a state that is completely absorbed (#8) is also shown in Table 3.1.

#	$\lvert\psi(x,y)\rvert^2$	#	$\lvert\psi(x,y)\rvert^2$
1	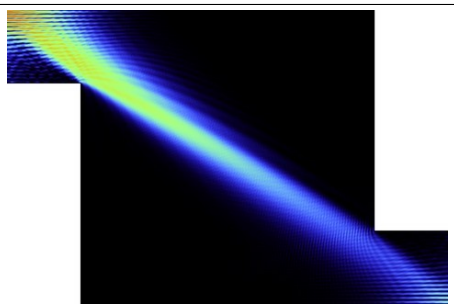	5	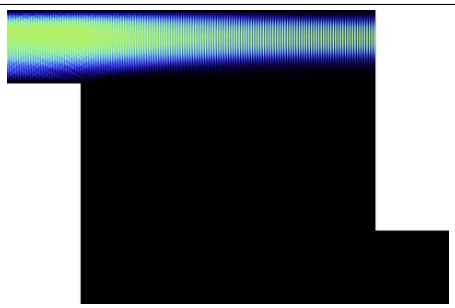
2	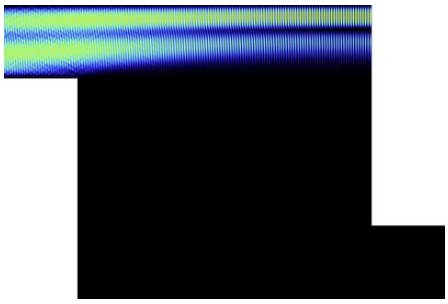	6	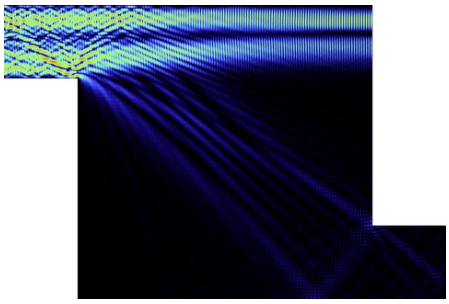
3	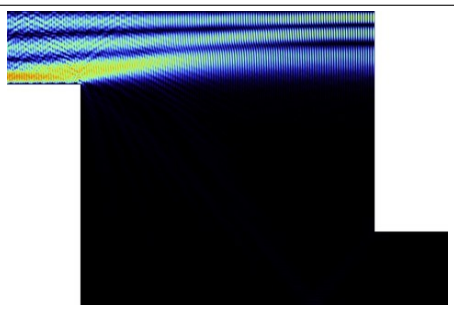	7	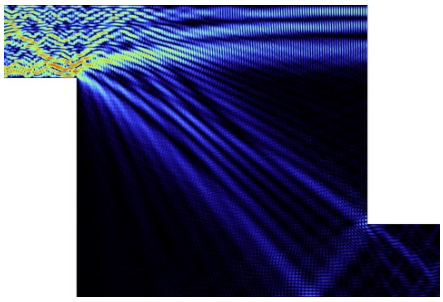
4	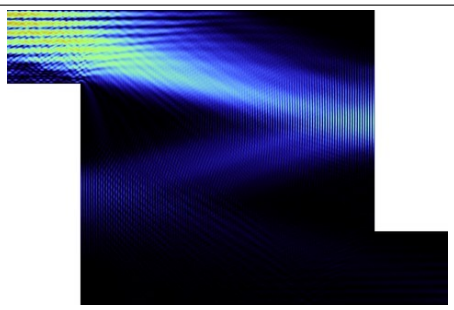	8	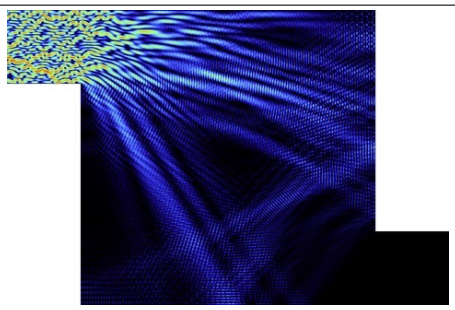

#	Q	T	R	χ	q	#	Q	T	R	χ	q
1	d	0.1446	0.0000	0.0691	14.254	5	d	0.0000	0.0431	0.0050	15.948
2	d	0.0000	0.0421	0.0071	15.964	6	g	0.0112	0.0342	0.2270	2.2312
3	d	0.0000	0.0402	0.0393	15.987	7	g	0.0256	0.0213	0.3102	2.1143
4	d	0.0074	0.0000	0.0144	16.543	8	d	0.0000	0.0000	0.0344	16.654

Table 3.3.: Intensity and scattering data for the states marked in Fig. 3.3. The letters 'd' and 'g' indicate of which operator, $[Q_d]_{11}$ or $[Q_g]_{11}$, the displayed state is an eigenstate. For the states #1, #4 and #5, the scattering data is provided only for the Q_d eigenstates as the intensity distribution of the corresponding Q_g eigenstates is very similar.

4. PT-symmetric systems

PT-symmetric systems are systems that remain invariant under a combined reflection of both space and time. In quantum mechanics and complex wave propagation, the effect of the time-reversal operator T involves a complex conjugation. The action of the parity operator P is flipping the spatial coordinates. If the center of reflection is the origin, this effect reads $x_i \to -x_i$. In 1D a Hamiltonian of the general structure

$$H = -\frac{\hbar^2}{2m}\nabla_x^2 + V_{pot}(x)\,, \tag{4.1}$$

is thus PT-symmetric if the potential V_{pot} satisfies the following two conditions,

$$\mathrm{Re}\left(V_{pot}(x)\right) = \mathrm{Re}\left(V_{pot}(-x)\right) \tag{4.2}$$

and

$$\mathrm{Im}\left(V_{pot}(x)\right) = -\mathrm{Im}\left(V_{pot}(-x)\right). \tag{4.3}$$

The Laplacian is not affected by the PT-transformation since it is real, on the one hand, and the spatial derivative appears only quadratically, on the other hand. One of the simplest Hamiltonians obeying these conditions, which was intensively studied by Bender et al. [9], is given by

$$H = -\frac{\hbar^2}{2m}\nabla_x^2 + ix^3. \tag{4.4}$$

Note that every *hermitian* Hamiltonian of the form (4.1) with P-symmetry, is PT-symmetric as well, since $\mathrm{Im}\left(V_{pot}(x)\right) \equiv 0$. PT-symmetric operators have the remarkable feature of possessing real eigenvalues below a certain threshold, above which the eigenvalues form complex conjugate pairs. These thresholds are generally different for every pair of eigenvalues and depend on the strength and shape of $\mathrm{Im}\left(V_{pot}\right)$.

The eigenvectors $|\phi_i\rangle$ of such generally non-hermitian operators do not form an orthogonal set in the convential sense, however, an orthogonality relation exists, if the inner product is redefined. Instead of taking the ordinary rule of making a ket a bra, which is hermitian conjugation, Bender introduced a new inner product,

$$\langle P\phi_i|\,\phi_j\rangle = \langle\phi_i|\,P\,|\phi_j\rangle\,. \tag{4.5}$$

In the sense of this PT-inner product, the eigenvectors are orthogonal. They can also be normalized with respect to (4.5), but with the drawback, that this norm is indefinite and vanishes if the corresponding eigenvalue becomes complex above threshold. Below threshold, the problem of definiteness can be fixed by introducing an operator, which

Bender called C, due to its formal similarity to the charge-conjugation operator in Dirac-theory. C can be explicitely constructed using the $|\phi_i\rangle$,

$$C = \sum_i |\phi_i\rangle \langle P\phi_i| \,. \tag{4.6}$$

The action of C applied to one of the Hamiltonian eigenstates is then reproducing the state with the proper sign of its PT-norm. The metric defined by the inner product

$$\langle PC\phi_i| \, \phi_j\rangle = \langle \phi_i| \, C^\dagger P \, |\phi_j\rangle \tag{4.7}$$

is therefore positive definite. Note that $P^\dagger = P$. The operators P and C are distinct square roots of the unity operator,

$$P^2 = \mathbb{I} = C^2. \tag{4.8}$$

In the limit of a P-symmetric, hermitian Hamiltonian, however, C becomes equal to P. The TPC-inner procuct (4.7) then reduces to the ordinary inner product of quantum mechanics, since $P^2 = \mathbb{I}$.

The Hamiltonian (4.1) is in fact not only PT-symmetric but also transposition-symmetric. The property of being PT-symmetric,

$$H = PH^\dagger P, \tag{4.9}$$

can therefore be written as

$$H = PH^\star P. \tag{4.10}$$

The eigenvectors of matrices fulfilling (4.10) are simultaneously eigenvectors of the operator PT too, given their eigenvalue is below PT-threshold. One speaks of an unbroken PT-symmetry if all eigenvectors of a given operator are eigenvectors of PT as well, otherwise the PT-symmetry is broken. One result of this property is, that in the unbroken phase, i.e., below the lowest threshold, C commutes with PT. The eigenvectors of non-symmetric matrices, for which only (4.9) is valid, do not share this feature. For the latter matrices, symmetry is broken in a way that is independent of the strength of loss and gain, since their eigenvectors are not simultaneously PT-eigenvectors also below the thresholds in the eigenvalue spectrum. For that reason, $[C, PT] \neq 0$. To the best of our knowledge, such operators have not been discussed by other authors.

In the following subsection, we will give a simple, illustrative example of a matrix obeying $A = PA^\dagger P$, showing all the remarkable features of PT-symmetric matrices.

4.1. A 2×2 PT-matrix

In what follows, we will show all the special consequences resulting from PT-symmetry for a 2×2 matrix satisfying (4.9). With this simple but illustrative example we can demonstrate that the eigenvalues are real below the threshold and find the formation of a complex conjugate pair above. We demonstrate the explicit construction of the C operator and show that (4.7) indeed defines a positive-definite inner product.

The simplest possible, valid parity operator is given by

$$P = \begin{pmatrix} 0 & 1 \\ 1 & 0 \end{pmatrix}. \tag{4.11}$$

This gives the restrictions $A_{11} = A_{22}^\star$, $A_{12} = A_{12}^\star$ and $A_{21} = A_{21}^\star$ on the matrix A fulfilling (4.9). Such a matrix generally has the form

$$A = \begin{pmatrix} r\,e^{i\theta} & s \\ t & r\,e^{-i\theta} \end{pmatrix}, \tag{4.12}$$

where the four parameters r, s, t and θ are real. The eigenvalues of A calculate to

$$\lambda_{1,2} = r\,\cos(\theta) \pm \sqrt{s\,t - r^2 \sin^2(\theta)}. \tag{4.13}$$

If $s\,t \geq r^2 \sin^2(\theta)$, the eigenvalues are real, if $s\,t \leq r^2 \sin^2(\theta)$ they form a complex conjugate pair, therefore, the PT-threshold for this matrix is given by $s\,t = r^2 \sin^2(\theta)$. The first inequation implies, that below the threshold, s and t must have the same sign, since $r^2 \sin^2(\theta)$ is larger or equal than zero. The corresponding eigenvectors evaluate to

$$\vec{v}_1 = \frac{1}{\sqrt{N}} \begin{pmatrix} \sqrt{s} e^{i\alpha/2} \\ \sqrt{t} e^{-i\alpha/2} \end{pmatrix} \tag{4.14}$$

and

$$\vec{v}_2 = \frac{i}{\sqrt{N}} \begin{pmatrix} \sqrt{s} e^{-i\alpha/2} \\ -\sqrt{t} e^{i\alpha/2} \end{pmatrix}, \tag{4.15}$$

where we set $\sin(\alpha) := \frac{r}{\sqrt{s\,t}} \sin(\theta)$. The normalization constant $N = 2\cos(\alpha)\sqrt{s\,t}$ is chosen here in such a way, that the $\vec{v}_i$ are normalized corresponding to the PT-inner product (4.5). It is checked very easily, that these vectors are generally not eigenstates of PT (in fact for $s = t$ they are, though) but they are orthonormal with respect to the PT-metric. Note that s and t are real quantities but do not need to be positive, therefore the factors $\sqrt{s}$ and $\sqrt{t}$ might be imaginary and are affected by T as well. The operator C can be explicitly constructed and gives

$$C = \sum_{i=1}^{2} \vec{v}_i \otimes \vec{v}_i^\dagger P = \frac{1}{\cos(\alpha)} \begin{pmatrix} i\,\sin(\alpha) & \sqrt{\frac{s}{t}} \\ \sqrt{\frac{t}{s}} & -i\,\sin(\alpha) \end{pmatrix}. \tag{4.16}$$

The commutator $[PT, C]$ gives

$$[PT, C] = PTC - CPT = \frac{1}{\cos(\alpha)} \begin{pmatrix} \sqrt{\frac{t}{s}} - \sqrt{\frac{s}{t}} & 0 \\ 0 & \sqrt{\frac{s}{t}} - \sqrt{\frac{t}{s}} \end{pmatrix},$$

which vanishes only in the case of $s = t$. From this we conclude that the operator ordering in the TPC-inner product (4.7) is crucial, because only T and P commute. At last we will show, that this norm indeed leads to a positive definite inner product. Let

$\vec{\psi} = (a, b)^T$ be an arbitrary state vector with $a = x + i\,y$ and $b = u + i\,v$ and $x, y, u, v \in \mathbb{R}$. The norm of this vector is

$$\langle PC\psi|\,\psi\rangle = \frac{1}{\cos(\alpha)}\left(x^2\sqrt{\frac{t}{s}} + v^2\sqrt{\frac{s}{t}} + 2x\,v\sin(\alpha) + y^2\sqrt{\frac{t}{s}} + u^2\sqrt{\frac{s}{t}} - 2y\,u\sin(\alpha)\right). \tag{4.17}$$

Since below threshold $s\,t \geq r^2\sin^2(\theta) \rightarrow \left|\frac{r}{\sqrt{s\,t}}\sin(\theta)\right| \leq 1$ which defines $\alpha = \arcsin\left(\frac{r}{\sqrt{s\,t}}\sin(\theta)\right)$ to be real, and the range from which the values of α are taken to be $\left[-\frac{\pi}{2}, \frac{\pi}{2}\right]$. For this reason, $\cos(\alpha) \geq 0$. Since s and t need to have the same sign below the PT-threshold, the factors $\left(\sqrt{s/t}\right)^{\pm 1}$ are real and positive. For the first three terms in the round brackets in (4.17) the following inequality is valid

$$\begin{aligned} x^2\sqrt{\frac{t}{s}} + v^2\sqrt{\frac{s}{t}} + 2x\,v\sin(\alpha) &\geq x^2\sqrt{\frac{t}{s}} + v^2\sqrt{\frac{s}{t}} - 2\,|x\,v| && (4.18)\\ &= \left(|x|\left(\frac{t}{s}\right)^{1/4} - |v|\left(\frac{s}{t}\right)^{1/4}\right)^2 && (4.19)\\ &\geq 0 && (4.20) \end{aligned}$$

An analogous inequality is valid for the remaining three terms, and the inner product is therefore proven to be greater or equal zero, and vanishes only for $x = y = u = v = 0$.

4.2. PT-scattering

Unitary scattering systems owe their name to the unitarity of the scattering matrix $S^\dagger = S^{-1}$. This condition implies flux conservation, since the norm of any vector containing incoming coefficients remains unchanged under the action of the scattering matrix. The unitarity of S is a direct consequence of the hermiticity of the Hamiltonian H of the closed system. In the case of a non-hermitian PT-symmetric Hamiltonian, this unitarity relation does not hold and needs modifications. The proper expression was found by Chong, Ge and Stone [2] and reads

$$PS^\dagger P = S^{-1}. \tag{4.21}$$

If the scattering system (cavity + leads) exhibits a certain symmetry in its Hamiltonian, represented by the operator Ξ,

$$\Xi H \Xi^{-1} = H, \tag{4.22}$$

and if $|\psi\rangle$ is a solution of the corresponding Schrödinger equation

$$(H - E)\,|\psi\rangle = 0, \tag{4.23}$$

then $\Xi\,|\psi\rangle$ is also a solution,

$$\Xi\,(H - E)\,\Xi^{-1}\Xi\,|\psi\rangle = (H - E)\,\Xi\,|\psi\rangle = 0. \tag{4.24}$$

In the following, we will give Chong's, Ge's and Stone's very instructive derivation of (4.21) making use of (4.24).

The solution $\psi(x,y)$ in the asymptotic region can be decomposed into different channels, e.g., in our case into the lead modes in the left and right lead

$$\psi(\vec{x}) = \sum_n \left[a_n \phi_n^{in}(\vec{x}) + b_n \phi_n^{out}(\vec{x})\right] = \sum_n \left[a_n \phi_n^{in}(\vec{x}) + \sum_m (S_{nm} a_m)\, \phi_n^{out}(\vec{x})\right]. \quad (4.25)$$

Note, that here the expansion coefficients for *all* incoming and outgoing channels (i.e., for our systems the modes in both of the leads) are contained in the vectors $\vec{a}$ and $\vec{b}$, respectively. In the following we will set $\Xi = PT$. The action of T on $\phi_n^{in/out}$ is

$$T\phi_n^{in/out} = \phi_n^{\star in/out} = \phi_n^{out/in}. \quad (4.26)$$

We will not specify the action of P in this subsection in detail, since not only parity, but also π rotations and inversions satisfying $P^2 = \mathbb{I}$ are valid candidates for P. We write for a matrix representation of P

$$P\phi_n^{out/in} = \sum_m P_{mn} \phi_m^{out/in} \quad (4.27)$$

$$\Rightarrow P \sum_n c_n \phi_n^{out/in} = \sum_m \left(\sum_n P_{mn} c_n\right) \phi_m^{out/in}. \quad (4.28)$$

With (4.26) and (4.28) we get

$$PT\psi(\vec{x}) = \sum_n \left[(PT\vec{a})_n\, \phi_n^{out}(\vec{x}) + (PT\, S\vec{a})_n\, \phi_n^{in}(\vec{x})\right]. \quad (4.29)$$

Since we know from (4.24) with $\Xi \equiv PT$ that $PT\psi$ is also a solution of the Schrödinger equation, it follows from (4.29) with $(PT)^2 = \mathbb{I}$, that

$$PT\vec{a} = S\, PT\, S\vec{a} = S\, PT\, S\, PT\, PT\vec{a}, \quad (4.30)$$

and therefore

$$S\, PT\, S\, PT = S\, PS^\star P = \mathbb{I}, \quad (4.31)$$

which is the desired result (4.21), since $S = S^T$. Taking into account also complex scattering energies E, the derivation gives

$$PS^\dagger(E^\star)\, P = S^{-1}(E). \quad (4.32)$$

From (4.32) Chong, Ge and Stone drew the important conclusion, that for a PT-system, the eigenvalues of S are either unimodular (below certain thresholds) like in a unitary scattering system, or form pairs of reciprocal moduli (above threshold) [2]. These authors also stated, that in a general PT-symmetric system, the poles and zeros are related by complex conjugation, just as they are in unitary systems.

Interpreting $\langle P\psi|$ as another valid way for PT-systems to transform a ket-state into a bra-state rather than by hermitian conjugation, (4.21) can easily be interpreted as a unitarity relation for S according to the PT-inner product (4.5).

4.3. PT-threshold in the scattering matrix and hamiltonian

The aim of this subsection is to establish a relation between the PT-thresholds in the scattering matrix and the thresholds in the eigenvalues of the corresponding Hamiltonians. As we discussed in the previous subsections, the thresholds in S separate the phase of unimodular eigenvalues, from the phase of eigenvalues with reciprocal moduli that are different from 1, the thresholds in H decide between real and pairs of complex conjugate eigenvalues.

We will restrict ourselves to one-dimensional systems, where the scattering matrix possesses only two eigenvalues. Consider the geometry displayed in Fig. 4.1(a), which consists of two layers of loss and gain of the same length (blue and red balls, the real part of the potential is set to zero). The calculation grid features only ten grid points for reasons of simplicity. Just as in section 2.1, we will start in the framework of finite-differences, executing the continuum limit at the end of the subsection.

The PT-threshold in S is a function, on the one hand, of the loss/gain parameter γ, which is for our calculations just the imaginary part of the potential $V_{pot} = \pm i\gamma$, and the scattering energy E, on the other hand. In Fig. 4.2, the phase of unimodular eigenvalues of the scattering matrix $\sigma(E, \gamma)$ is marked white, the phase of broken symmetry is marked in grey, the boundary between these phases is the exceptional line. Since the closed system is independent of the scattering energy, the eigenvalues of the corresponding Hamiltonians are just functions of γ. The green and blue lines in Fig. 4.2(a) show the real parts of all the ten eigenvalues of the Hamiltonians H_D and H_N featuring Dirichlet ($\psi(0) = 0 = \psi(L)$) and Neumann ($\partial_x\psi(0) = 0 = \partial_x\psi(L)$) boundary conditions, respectively. The eigenvalue curves form parabolas in a pairwise fashion; at the vertices where the real parts meet, the PT-thresholds are located where the eigenvalues become complex conjugate pairs. These thresholds mostly lie near to the exceptional line, but for the eigenvalues marked by the red arrows in Fig. 4.2(a), it can clearly be seen, that the phase transitions in H_D or H_N and S do, in general, not coincide.

Note, that the effective Hamiltonian (2.17) $H_{\text{eff}} = H_h - i\hbar/2\, VV^\dagger$ appearing in the scattering matrix is not a PT-matrix due to the anti-hermitian coupling. Therefore, it features no PT-thresholds at all.

A scattering state is a solution to the Schrödinger equation with E being an eigenvalue of the Hamiltonian describing the whole system. We will now construct a special Hamiltonian H_λ, that while describing not the entire system but only the scattering region, contains E in its spectrum as well. The Schrödinger equation for H_λ and its eigenstate ψ reads

$$H_\lambda \psi = E\psi. \tag{4.33}$$

Since H_λ describes just the scattering region, it can only differ from the Dirichlet Hamiltonian H_D through the boundary conditions. We choose both boundary elements in the corresponding FD representation of H_λ to have the same value. This can easily be written as

$$H_\lambda = H_D + \lambda B \tag{4.34}$$

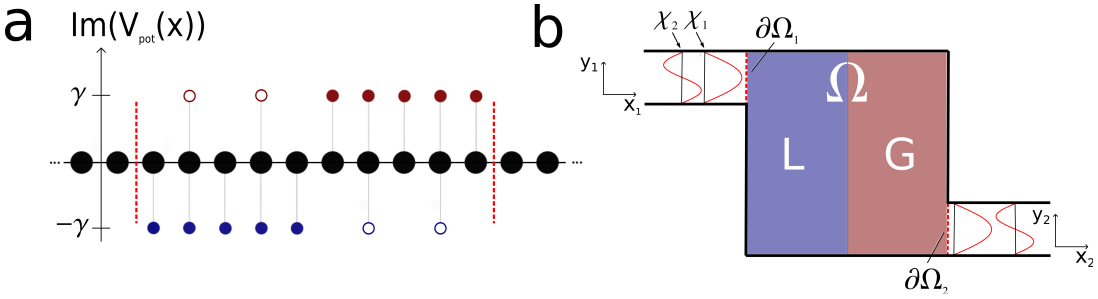

Figure 4.1.: PT-symmetric scattering systems in 1D (a) and 2D (b). (a) One dimensional system consisting of 10 grid points. The imaginary part of the potential is displayed by the blue and red balls. The filled balls describe a system consisting of 2 layers of loss and gain. The empty balls show a system featuring 10 layers, the sign of $\mathrm{Im}\,(V_{pot})$ alternates at every grid point. If the potentials of the 2 layers and the 10 layers coincide, only filled balls are drawn. (b) Two dimensional system Ω featuring 2 layers of loss (blue) and gain (red) attached to two leads.

with

$$B = \begin{pmatrix} -\frac{\hbar^2}{2m\Delta x^2} & & & & \\ & 0 & & & \\ & & \ddots & & \\ & & & 0 & \\ & & & & -\frac{\hbar^2}{2m\Delta x^2} \end{pmatrix} \tag{4.35}$$

and the generally complex number λ. Equation (4.34) translates into the boundary conditions

$$\psi_0 \quad = \quad \lambda\psi_1 \tag{4.36}$$

and

$$\psi_{N+1} = \lambda\psi_N \tag{4.37}$$

for the first and the last grid point respectively. With this ansatz at hand, we can rewrite (4.33) as a generalized eigenvalue problem where the eigenvalue E is known and the boundary condition λ is unknown. Since the matrix $(E - H_D)$ is invertible, also a reformulation as an ordinary eigenvalue problem can be carried out,

$$(E - H_D)^{-1} B\psi = \frac{1}{\lambda}\psi. \tag{4.38}$$

Here the matrices H_D and B are PT-matrices, satisfying (4.10), so the matrix $A \equiv (E - H_D)^{-1} B$ is a PT-matrix as well. However, because B contains only two entries different from zero, A is highly singular and possesses only two finite eigenvalues $(\lambda_{1,2})^{-1}$. As a consequence, there exist two different Hamiltonians H_{λ_i} for each combination of

(E,γ), that satisfy (4.33). Below the threshold in $A(E,\gamma)$, both λ_i are real numbers, leading to hermitian boundary conditions. In this regime, the H_{λ_i} are PT-matrices with one of their real eigenvalues being the scattering energy E in each case. Above the threshold in A, there exists still a real eigenvalue E in the (complex) spectra of both H_{λ_i}, but the H_{λ_i} are not PT-matrices due to the complexity of the λ_i.

The exceptional line in the boundary conditons determined by $A(E,\gamma)$ is exactly the same as for the scattering matrix $S(E,\gamma)$ which we will show in the following. An eigenstate of the scattering matrix is defined by

$$S\vec{u} = \sigma\vec{u}, \qquad \vec{u} = \begin{pmatrix} a \\ d \end{pmatrix}, \tag{4.39}$$

with a and d being the incoming coefficents, corresponding to the waves on both sides of the scattering region. The conditions for a and d read

$$ra + t'd = \sigma a \equiv b \tag{4.40}$$

$$ta + r'd = \sigma d \equiv c. \tag{4.41}$$

Using a plane-wave basis $\frac{1}{\sqrt{v}}e^{\pm ikx}$ for the waves outside the scattering region, we find in the finite difference formalism with $\psi_1 \equiv \psi(x=0)$, $\psi_0 \equiv \psi(x=-\Delta x)$

$$\psi_1 = \frac{1}{\sqrt{v}}(a+b) \tag{4.42}$$

$$= \frac{1}{\sqrt{v}}a(1+\sigma) \tag{4.43}$$

$$\psi_0 = \frac{1}{\sqrt{v}}\left(ae^{-ik\triangle x} + be^{ik\Delta x}\right) \tag{4.44}$$

$$= \frac{1}{\sqrt{v}}a\left(e^{-ik\triangle x} + \sigma e^{ik\Delta x}\right) \tag{4.45}$$

with v being the phase-velocity of the plane waves that is equal to the carried flux in 1D. Inserting (4.43) and (4.45) into the relation (4.36) for ψ_0 and ψ_1 given by the boundary condition, we find

$$\sigma = \frac{e^{-ik\Delta x} - \lambda}{\lambda - e^{ik\Delta x}}. \tag{4.46}$$

We see that the eigenvalue of the scattering matrix σ is unimodular if and only if λ is real. Equation (4.46) shows the direct correspondence between hermitian boundary conditions for H_λ and unimodular eigenvalues of S: Since the connection of the unimodularity of σ and the property of λ being real is an equivalence relation, the PT-threshold in A defines exactly the phase transition boundary for S. The same connection between σ and λ can be found performing the above derivation with $\psi_{N+1} \equiv \psi(x = L + \Delta x)$ and $\psi_N \equiv \psi(x = L)$ rather than with ψ_1 and ψ_0 (appendix C.1). This is possible because of the ansatz (4.34) we chose for the boundary elements using the same λ at both boundaries of the scattering region. Note that the relation (4.46) is valid below and above the exceptional line. Furthermore, the eigenstates of the H_{λ_i} corresponding

to the eigenvalue E are exactly the eigenstates of the scattering matrix. It is imperative to choose the basis outside the scattering region in such a way, that all the four plane waves have zero phase at the left and right entrances, respectively (appendix C.1).

Another way of showing the equivalence of the phase transitions in the open and the closed system is choosing an arbitrary real λ rather than solving (4.33), and investigating the eigenvalues and their PT-transitions of the resulting Hamiltonian H_λ. A conclusion drawn from (4.38) and (4.46) is that for every point (E, γ) that lies in the PT-symmetric phase of S, there exist two real λ_i, such that E is an eigenvalue of each of the corresponding two H_{λ_i}. This means, in turn, that when scanning the real axis for λ each point in the PT-symmetric phase is 'hit' by two eigenvalue curves (parameterized by γ) of two different H_{λ_i}. Fig. 4.2(b) shows the eigenvalues of each H_{λ_i} with λ_i evenly spaced in the interval $[-5, 5]$. Indeed we find that the PT-symmetric phase is exactly reproduced. The expectional line in S is given by the envelope of all eigenvalue-parabolas. It turns out, that it is in fact necessary to scan λ along the entire real axis from $-\infty$ to $+\infty$.

If the system features a more complicated PT-symmetric potential rather than consisting of only two layers of loss and gain, the PT-boundary takes on a more complicated form, and does not form a single line in general. To substantiate our above statements, we applied our concepts to a structure consisting of ten layers in total (Fig. 4.1(a)). Fig. 4.3(a) shows the PT-symmetric and PT-broken phase for the corresponding S-matrix and the real parts of the eigenvalues of H_D and H_N. The plots for the H_{λ_i} are shown in Fig. 4.3(b). Also for this complicated system, we find that no curve corresponding to a real eigenvalue of any H_{λ_i} crosses the PT-broken phase of S. The sum of all these curves reproduces the unbroken phase and its envelope coincides exactly with the PT-phase boundaries.

Using the boundary condition (4.36) we can establish the following relation

$$\lim_{\Delta x \to 0} \frac{\psi_1 - \psi_0}{\Delta x} = \lim_{\Delta x \to 0} \frac{1-\lambda}{1+\lambda} \frac{2}{\Delta x} \psi_{1/2} \equiv \Lambda \lim_{\Delta x \to 0} \psi_{1/2} \tag{4.47}$$

with $\psi_{1/2} = (\psi_1 + \psi_0)/2$. An analogous relation can be found for the right-hand side of the scattering region. The desired boundary conditions therefore read

$$\partial_x \psi(x)|_{x=0} = \Lambda \psi(0) \tag{4.48}$$

and

$$\partial_x \psi(x)|_{x=L} = -\Lambda \psi(L) \tag{4.49}$$

in the continuum limit.

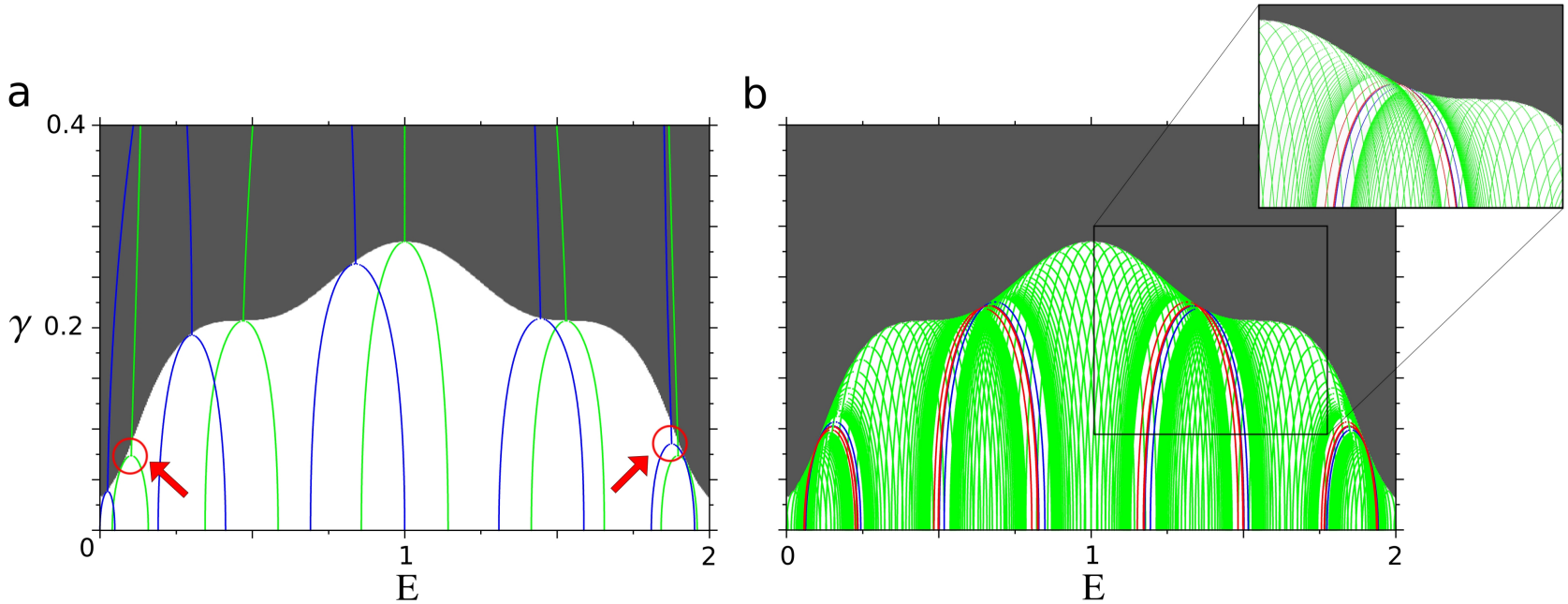

Figure 4.2.: PT-symmetric (white) and PT-broken phase (grey) for the scattering matrix $S(E,\gamma)$ for the system displayed in Fig. 4.1(a). (a) shows the real-parts of the 10 eigenvalues of H_D (green lines) and H_N (blue lines). The thresholds in the eigenvalues of the Hamiltonians do not exactly coincide with the exceptional line in S (red arrows). (b) shows all 10 eigenvalues of each H_{λ_i} with $\lambda_i \epsilon [-5,5]$ evenly spaced with $\Delta\lambda = 0.2$ (green). For reasons of visibility, the eigenvalues are only drawn below threshold. The set of the eigenvalue curves of *all* possible hermitian boundary conditions defined by a real λ reproduces the region where the eigenvalues of S are unimodular, its boundary is exactly the exceptional line. The red and blue lines show the eigenvalues for $\lambda_i = +10^i$ (red) and $\lambda_i = -10^i$ (blue), with $i = 1,2,3$, underlining the necessity to scan the entire real axis in order to reproduce the whole PT-symmetric phase in $S(E,\gamma)$. At each point (E,γ) in the PT-symmetric phase, two eigenvalue curves cross.

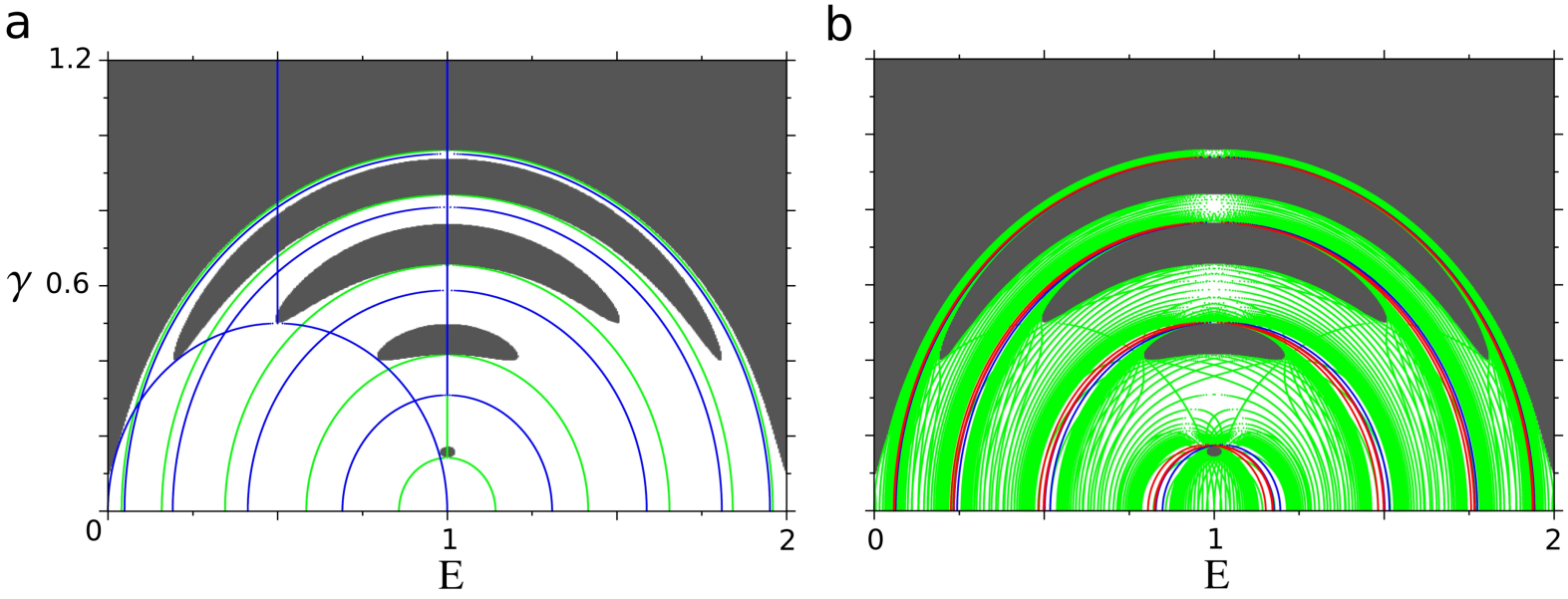

Figure 4.3.: PT-symmetric (white) and PT-broken phase (grey) for the scattering matrix $S(E,\gamma)$ for the system consisting of ten layers displayed in Fig. 4.1(a). (a) shows the real-parts of the 10 eigenvalues of H_D (green lines) and H_N (blue lines). For this geometry, the thresholds in the eigenvalues of H_D lie at the phase transition boundaries, however, this is due to the symmetry of the system and not a general feature. (b) shows all 10 eigenvalues of each H_{λ_i} with $\lambda_i \epsilon [-5,5]$ evenly spaced with $\Delta\lambda = 0.2$ (green). For reasons of visibility, the eigenvalues are only drawn below threshold. The red and blue lines show the eigenvalues for $\lambda_i = +10^i$ (red) and $\lambda_i = -10^i$ (blue), with $i = 1,2,3$.

4.4. Particle-like scattering states in PT-symmetric systems

The time-delay operators Q_g and Q_d can also be used in PT-symmetric systems to generate beam-like states traversing the cavity.

Consider the cavity in Fig. 4.1(b) featuring a PT-symmetric potential consisting of two broad layers of loss and gain at a given wave number of $k = 30.5\,\pi/W$. The (χ, T, R) and (q, T, R) plots for all 30 eigenstates of both operators, $[Q_g]_{11}$ and $[Q_d]_{11}$, can be found in Fig. 4.4. The scattering data and the intensity plots for the states marked and numbered in Fig. 4.4 are given in Table 4.1. Most of the states lie very near to the line defined by the unitarity relation $R + T = 1$. Although the system is PT-symmetric and features a rather high $\gamma = \pm\mathrm{Im}\,(V_{pot})$ of about $0.004\,E$, where E is the scattering energy, these states suffer no net loss or gain. This is possible if the waves' intensities are distributed symmetrically in the loss and gain regions. State #4 marked by a red arrow in Fig. 4.4, which is an eigenstate of $[Q_d]_{11}$, is an example. As a counterexample, a state lying far away from the 'unitarity line' is also shown, #8 which is a $[Q_g]_{11}$ eigenstate. The intensity of the latter state is located more on the loss-side, such that, this state lies beneath the unitarity line in the (T, R)-plane.

Very similar to the corresponding unitary system, the NOTEs that can be found in the investigated PT-symmetric system lie at high values of transmission or reflection in the 'corners' of the plot, and possess rather short scattering times (both group delays and dwell times). The families of directly reflected and z-shaped NOTEs can be found in equal quality with both operators (states #3 and #7 in Fig. 4.4 and Table 4.1), the wave is not spread inside the cavity but stays a collimated beam during its propagation. The familiy of directly transmitted states, however, are much 'cleaner' for Q_d than for Q_g. As can be seen investigating $|\psi\,(x, y)|^2$ in Table 4.1, the $[Q_g]_{11}$ eigenstates (#5, #6) are reflected at the boundary between the loss and gain region which leads to a spreading of the waves' intensity, whereas the $[Q_d]_{11}$ eigenstates (#1, #2) are not. Despite this spreading at the loss/gain-boundary, the transmission of states #5 and #6 is very high and their null-space norms χ as well as their eigenvalues q are low, so the scattering data $\{T, \chi, q\}$ does not mirror this reflection, unfortunately. We assume that the explanation for both the lack of evidence for the reflection in the scattering data of the $[Q_g]_{11}$ eigenstates, and the better quality of the $[Q_d]_{11}$ eigenstates, is given by the amount of information stored in the time-delay operators. Q_g (3.12) is constructed solely based on the scattering matrix, containing information connecting the leads only. The Q_d operator (3.22) contains also information about the wave inside the cavity, not only about its asymptotic scattering behaviour. Those parts of the system's Green's function are stored in Q_d, that connect the leads with *every* point (x, y) in the cavity, since Q_d measures the stored intensity inside the scattering region. The scattered intensity at the loss/gain-boundary, which does not leave the cavity through either lead, therefore, remains 'unrecognized' by Q_g, but not by Q_d.

We can conclude, that concerning the formation of NOTEs, Q_d is generally preferable to Q_g also in PT-symmetric systems. A major drawback is, however, that the construction of Q_d in these systems requires a lot more information about the internal scattering dynamics than the construction of Q_g does. In the following section, we will present

two alternative operators that can also be used to create beam-like scattering states in PT-symmetric systems, whose matrix elements depend only on the scattering amplitudes.

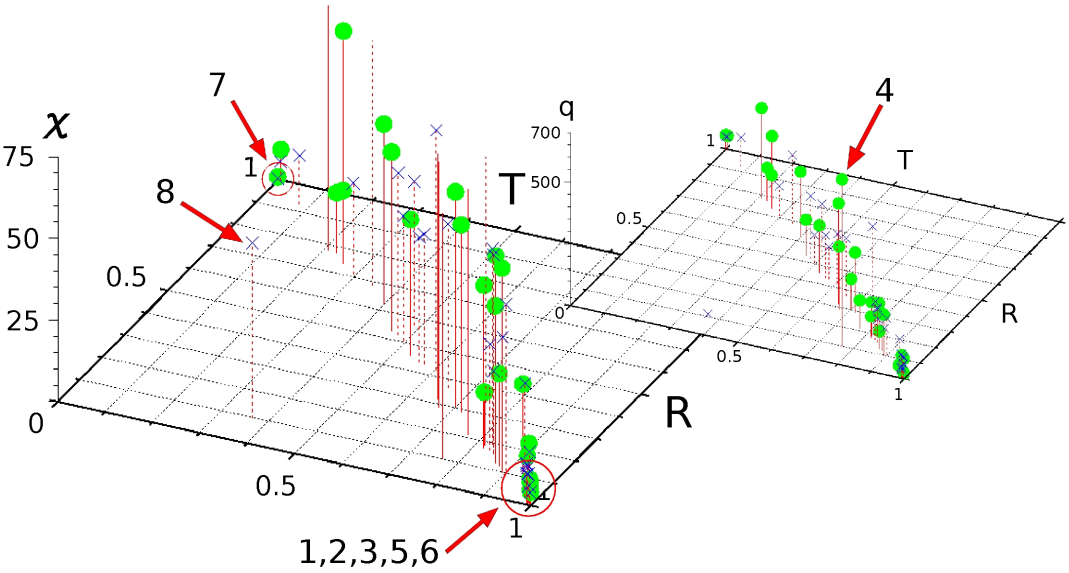

Figure 4.4.: (χ, T, R) for all 30 eigenstates of $[Q_d]_{11}$ (green balls) and $[Q_g]_{11}$ (blue crosses) at a scattering energy $E = (30.5\,\pi/d)^2/2$ for the scattering geometry depicted in Fig. 4.1(b) featuring a PT-symmetric potential consisting of two broad layers with $\mathrm{Im}\,(V_{pot}) = \gamma \approx \pm 0.004\,E$. NOTEs lie in the corners of the plot at $T \approx 1$ or $R \approx 1$. The scattering data of the numbered states can be found in Table 4.1. The smaller inset shows (q, T, R) for the given states. Just as for unitary sytems, NOTEs correspond to rather small scattering times. Most of the states lie very close to the line defined by $R + T = 1$, however, there exist also states that clearly violate this relation. For an example of this kind of states (#8), the scattering data is also shown in Table 4.1.

#	$\lvert\psi(x,y)\rvert^2$	#	$\lvert\psi(x,y)\rvert^2$
1	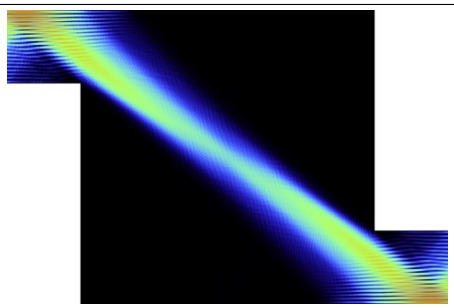	5	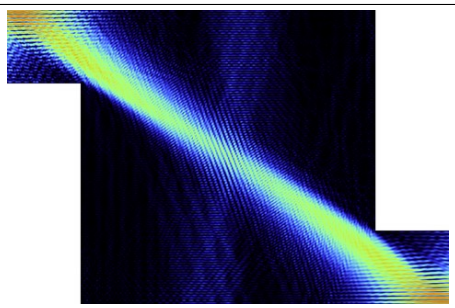
2	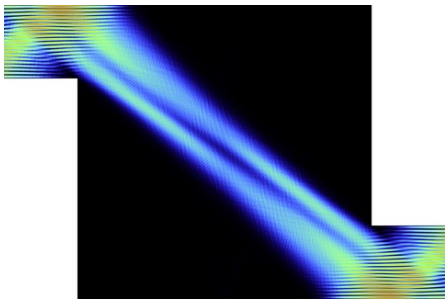	6	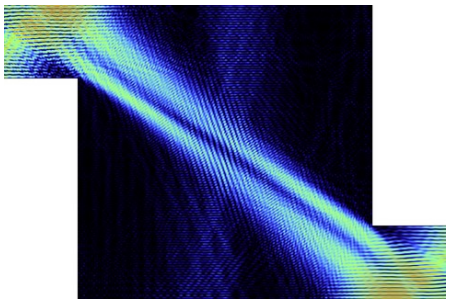
3	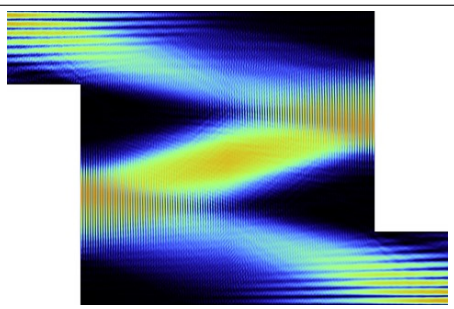	7	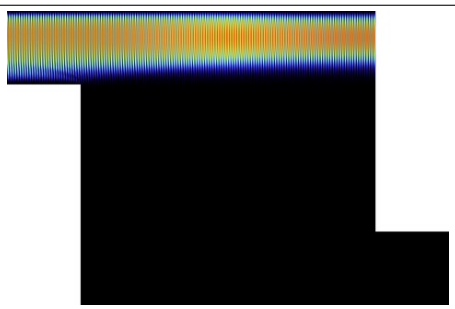
4	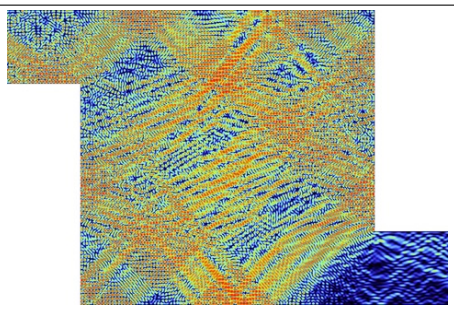	8	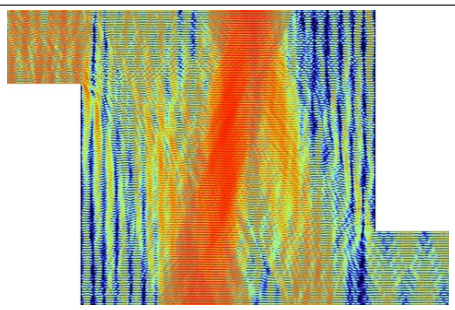

#	Q	T	R	χ	q	#	Q	T	R	χ	q
1	d	0.9996	0.0000	4.0691	20.962	5	g	0.9928	0.0036	9.2512	32.789
2	d	0.9995	0.0000	4.8673	21.751	6	g	0.9899	0.0056	10.785	34.783
3	d	0.9982	0.0018	4.8398	79.519	7	d	0.0000	0.9979	0.9875	57.954
4	d	0.2584	0.7410	71.168	292.73	8	g	0.3670	0.0964	53.623	14.611

Table 4.1.: Intensity and scattering data for the states marked in Fig. 4.4. The letters 'd' and 'g' indicate of which operator, $[Q_d]_{11}$ or $[Q_g]_{11}$, the displayed state is an eigenstate. For NOTEs that can be found in the eigenspaces of both operators (states #3,#7) the data is only shown for the $[Q_d]_{11}$-eigenstates.

4.5. Alternative time-delay operators

In PT-symmetric systems, also other time delay operators rather than Q_d and Q_g can be defined. The following derivation works to a large extent in analogy to the calculation done in subsection 3.3.1 and appendix A.1 for unitary scattering systems featuring time-reversal symmetry.

We will again start from the Schrödinger equation and its energy derivative

$$(H - E)\,\psi = \left(\frac{p^2}{2m} + V_{pot} - E\right)\psi = 0 \tag{4.50}$$

$$(H - E)\,\frac{\partial\psi}{\partial E} - \psi = 0, \tag{4.51}$$

in order to derive certain quantities which we will identify as scattering times. We will express these times as expectation values of two operators, that, in a last step, we will define as the desired time delay matrices.

The potential V_{pot} in (4.50) satisfies

$$\mathrm{Re}\left(V_{pot}\left(x,y\right)\right) = \mathrm{Re}\left(V_{pot}\left(-x,-y\right)\right) \tag{4.52}$$

and

$$\mathrm{Im}\left(V_{pot}\left(x,y\right)\right) = -\mathrm{Im}\left(V_{pot}\left(-x,-y\right)\right), \tag{4.53}$$

so the Hamiltonian is a transposition-symmetric matrix featuring PT-symmetry. Instead of taking advantage of the time-reversal symmetry as we did in subsection 3.3.1, we use the PT-symmetry of the geometry. In complete analogy to (3.25), it follows from (4.50) and (4.51) that

$$\left[PT\psi\right]\frac{p^2}{2m}\frac{\partial\psi}{\partial E} - \frac{\partial\psi}{\partial E}\frac{p^2}{2m}\left[PT\psi\right] - \left[PT\psi\right]\psi = 0, \tag{4.54}$$

since $V_{pot}^{\star}\left(-x,-y\right) = V_{pot}\left(x,y\right)$. Reformulating (4.54) as a surface term and performing an integration over the scattering region denoted by Ω gives

$$-\frac{\hbar^2}{2m}\int_{\partial\Omega_1+\partial\Omega_2} d\vec{A}\cdot\left[\left[PT\psi\right]\vec{\nabla}\dot{\psi} - \dot{\psi}\vec{\nabla}\left[PT\psi\right]\right] = \int_{\Omega} dV\ \left[PT\psi\right]\psi \equiv \tau_d^{PT}. \tag{4.55}$$

The dot denotes the energy derivative. $\partial\Omega_1$ and $\partial\Omega_2$ mean the boundary of the scattering region at the left and right lead respectively. Here we introduced the quantity $\int_\Omega dV\ \left[PT\psi\right]\psi$; the naming τ_d^{PT} underlines its similarity to the dwell time τ_d. Note that this resemblance has to be understood qualitatively in the sense of its functional form, not quantitatively. We assume that ψ is normalized to unit incoming flux. Additionaly we have

$$P\psi\left(x,y\right) = \psi\left(P\left(x,y\right)\right), \tag{4.56}$$

since $P^{-1} = P$, such that for the parity operator, passive and active transformations correspond to the same operator.

While (4.55) is generally valid for any scattering system possessing PT-symmetry, we will specialize again on the 2D model-system displayed in Fig. 2.1(b) in the next step. At

the boundaries of the cavity, the wave function ψ shall be decomposed into lead modes according to (3.28) with

$$\Phi_{1,n}(\vec{x}_1) = \frac{1}{\sqrt{v_n}} e^{ik_{n,x}x_1} \sin\left(\frac{n\pi}{d} y_1\right) \tag{4.57}$$

and

$$\Phi_{2,n}(\vec{x}_2) = \frac{1}{\sqrt{v_n}} e^{ik_{n,x}x_2} \sin\left(\frac{n\pi}{d} y_2\right). \tag{4.58}$$

The numbering 1 and 2, as in the previous chapters, stands for left and right lead respectively. In order to keep notation simple, we introduced the coordinate systems (x_1, y_1) and (x_2, y_2), whose origins are chosen in such a way, that the lead entrances are addressed with $x_i = 0$ and the lower boundary of each lead with $y_i = 0$. The origin of the overall coordinate system (x, y) is located at the center of the cavity. The parity operator affects the coordinates according to $[(x, y)]_1 \to [(-x, d-y)]_2$, analogously for the right lead. $[(a, b)]_i$ denotes a point referring to the i-th coordinate system. The action of P on the lead modes maps incoming (outgoing) waves on the left-hand side onto incoming (outgoing) waves on the right-hand side and vice versa

$$P\Phi_{1,n}([x, y]_1) = \Phi^\star_{2,n}([-x, d-y]_2) = (-1)^{n-1}\, \Phi^\star_{2,n}([-x, y]_2). \tag{4.59}$$

The alternating sign in (4.59) takes into account the internal parity of the sine-waves. From (4.59) it follows, that the representation of the P-operator in the lead-mode basis is

$$P = \begin{pmatrix} 0 & U \\ U & 0 \end{pmatrix} \tag{4.60}$$

with the $n_{in} \times n_{in}$ matrix

$$U_{ij} = (-1)^{i-1}\, \delta_{ij}. \tag{4.61}$$

δ_{ij} denotes the Kronecker-delta. For the surface term on the left-hand side of (4.55) we find (appendix C.2),

$$\begin{aligned}
\tau_d^{PT} = & - i\hbar\, \vec{u}^\dagger P \left[P S^\dagger P \dot{S} \right] \vec{u} && (4.62)\\
& + \frac{i}{2}\frac{m}{\hbar}\, \vec{u}^\dagger P \left[P S^\dagger P \begin{pmatrix} \Gamma\left(k_x^{-2}\right) & 0 \\ 0 & \Gamma\left(k_x^{-2}\right) \end{pmatrix} \right] \vec{u} && (4.63)\\
& - \frac{i}{2}\frac{m}{\hbar}\, \vec{u}^\dagger P \left[\begin{pmatrix} \Gamma\left(k_x^{-2}\right) & 0 \\ 0 & \Gamma\left(k_x^{-2}\right) \end{pmatrix} S \right] \vec{u} && (4.64)\\
& - \frac{1}{2}\frac{m}{\hbar}\, \vec{u}^\dagger P \left[P \tilde{S}^\dagger \tilde{P} \begin{pmatrix} \Gamma\left(\kappa_x^{-2}\right) & 0 \\ 0 & \Gamma\left(\kappa_x^{-2}\right) \end{pmatrix} \tilde{S} \right] \vec{u}, && (4.65)
\end{aligned}$$

with $\vec{u}$ containing the expansion coefficients for injection from the left and from the right and using (2.39) for the function Γ. In (4.65) we introduced the matrix $\tilde{P} = \begin{pmatrix} 0 & \tilde{U} \\ \tilde{U} & 0 \end{pmatrix}$

with $\tilde{U} = (-1)^{i-1}\delta_{ij},\ i,j = n_{in}+1\ldots\infty$. The sum (4.62) - (4.65) can be rewritten in a very compact fashion,

$$\tau_d^{PT} = \langle Pu| \left[-i\hbar PS^\dagger P\dot{S} + \frac{i}{2}\frac{m}{\hbar}\left(PS^\dagger P\left[\frac{1}{k^2}\right] - \left[\frac{1}{k^2}\right] S\right) - \frac{1}{2}\frac{m}{\hbar} P\tilde{S}^\dagger \tilde{P}\left[\frac{1}{\kappa^2}\right]\tilde{S}\right] |u\rangle\,, \tag{4.66}$$

where we simplified the notation for the matrices involving the wave numbers in the same way we did in subsection 3.3.1 and dropped the subscript x. We define the operator

$$Q_d^{PT} := -i\hbar PS^\dagger P\dot{S} + \frac{i}{2}\frac{m}{\hbar}\left(PS^\dagger P\left[\frac{1}{k^2}\right] - \left[\frac{1}{k^2}\right] S\right) - \frac{1}{2}\frac{m}{\hbar} P\tilde{S}^\dagger \tilde{P}\left[\frac{1}{\kappa^2}\right]\tilde{S} \tag{4.67}$$

and find that it measures τ_d^{PT} in its PT-expectation value,

$$\tau_d^{PT} = \langle Pu|\, Q_d^{PT}\, |u\rangle\,. \tag{4.68}$$

Q_d^{PT} has the same formal structure as Q_d in unitary systems, but taking the PT-conjugate $PS^\dagger P$ instead of the hermitian conjugate $S^\dagger$ of the matrices S and $\tilde{S}$. In section 3.1 we showed the hermiticity of the Wigner-Smith time delay operator in unitary scattering systems starting from $S^\dagger S = \mathbb{I}$. Using the corresponding relation for S in PT-symmetric systems, $PS^\dagger P = \mathbb{I}$, it can be shown analogously, that

$$Q_g^{PT} := -i\hbar PS^\dagger P\dot{S} \tag{4.69}$$

and Q_d^{PT} are PT-matrices satisfying (4.9), since for the matrices $[k]$ and $[\kappa]$ the following relations hold, $[PT,[k]] = 0 = [PT,[\kappa]]$.

Below the PT-threshold, all eigenvectors of Q_i^{PT}, $i = g,d$ have non-vanishing PT-norms, but these norms have alternating signs, since the PT-inner product is indefinite. In this regime of very weak gain and loss, however, the C operator can be established according to (4.6). Note that the Q_i^{PT} are not transposition-symmetric matrices, such that C does not commute with PT. The PT-expectation value of the Q_i^{PT} for an eigenstate may differ from the corresponding eigenvalue in a sign due to its indefiniteness. Taking the TPC-expectation value of Q_i^{PT}, however, cancels possible sign differences between the eigenvalues and the τ_i^{PT} (which are the PT-expectation values) for the eigenstates. For all other states different from the eigenstates, the action of C is more than just a sign. Therefore, we call the TPC-expectation value

$$\langle PCu|\, Q_i^{PT}\, |u\rangle := \tau_i^{TPC} \tag{4.70}$$

which is quantitatively different from τ_i^{PT} in general. In the limit of vanishing loss/gain-strength, the PT-time delay operators smoothly change over into the corresponding operators for unitary systems,

$$\lim_{\gamma\to 0} Q_i^{PT} = Q_i. \tag{4.71}$$

Since in this limit, the C operator becomes equal to the parity operator P, also the TPC-expectation values of the Q_i^{PT} become the τ_i,

$$\lim_{\gamma\to 0} \tau_i^{TPC} = \lim_{\gamma\to 0} \langle PCu|\, Q_i^{PT}\, |u\rangle = \langle u|\, Q_i\, |u\rangle = \tau_i. \tag{4.72}$$

The real quantities τ_i^{TPC}, $i = g, d$, which are TPC-expectation values of the operators Q_g^{PT} and Q_d^{PT}, may therefore be viewed as the proper generalization of group delay and dwell time to PT-symmetric systems.

These operators can also be used to create beam-like scattering states. For the (high) value of the loss/gain parameter of $\gamma \approx 0.004\,E$ used in the previous section (Fig. 4.4 and Table 4.1), these operators find NOTEs of good quality, but not of a better quality than Q_g (Fig. 4.5(a)), i.e., the waves are also scattered at the loss/gain boundary.

The operators Q_d^{PT} and Q_g^{PT} might, however, find an interesting application for lower values of γ in the case of cavity resonances. Such a resonance can be identified investigating the scattering times. Fig. 4.5(b) shows the mean of the absolute values of the eigenvalues of Q_g and Q_g^{PT} in the interval $\gamma \epsilon [0.002\,E, 0.003\,E]$. We see that a sharp peak is located in this interval for both operators, which indicates a resonance. Fig. 4.6 shows (χ, T, R) for the $\left[Q_g^{PT}\right]_{11}$ and $\left[Q_d^{PT}\right]_{11}$ eigenstates at $\gamma = 0.00245\,E$, which is in the vicinity of the resonant peak.[1] Table 4.2 shows a comparison of the intensity plots of some selected $[Q_g]_{11}$, $[Q_d]_{11}$ and $\left[Q_g^{PT}\right]_{11}$ eigenstates. Very similar to the discussion in subsection 3.4.1 for the unitary case ($\gamma = 0$) and the operators Q_g and Q_d, we find that there is no significant difference between Q_g^{PT} and Q_d^{PT} in the investigated PT-symmetric system. For that reason, only results for Q_g^{PT} are shown in Table 4.2. We see that the states found by Q_g are heavily affected by their coupling to the intrinsic resonance, whereas the beam-like states found by Q_d and Q_g^{PT} are of excellent quality. The peak in Fig. 4.5(b) in the curve corresponding to Q_g^{PT} is smaller than the peak for Q_g, such that the effect of the resonance on the former operator seems to be smaller. This might explain the significantly better quality of the NOTEs found by Q_g^{PT} (and Q_d^{PT}) as compared to the ones found by Q_g.

We conclude that, if the loss/gain parameter is not too high, the PT-symmetric time-delay operators Q_g^{PT} and Q_d^{PT} can be used to find beam-like scattering states. In the case of cavity resonances, the NOTEs found by Q_g seem to be much more likely to couple to the resonance than the ones found by Q_d, Q_g^{PT} and Q_d^{PT}. The Q_i^{PT}, $i = g, d$ rather than Q_d form a true alternative to Q_g in the sense of finding NOTEs, since their construction requires much less information about the internal scattering dynamics than the construction of Q_d in PT-symmetric systems.

[1] Unfortunately, it is not possible to show the τ_i^{TPC}, because for the presented value of $\gamma = 0.00245\,E$, the matrices Q_i^{PT} are already above the lowest threshold, so the C operator cannot be constructed due to the vanishing PT-norm of at least one pair of eigenstates. This threshold for Q_g^{PT} is located between the very low loss/gain levels of $\gamma = 0.0001\,E$ and $0.0002\,E$, the threshold for Q_d^{PT} between $\gamma = 0.0002\,E$ and $0.0003\,E$.

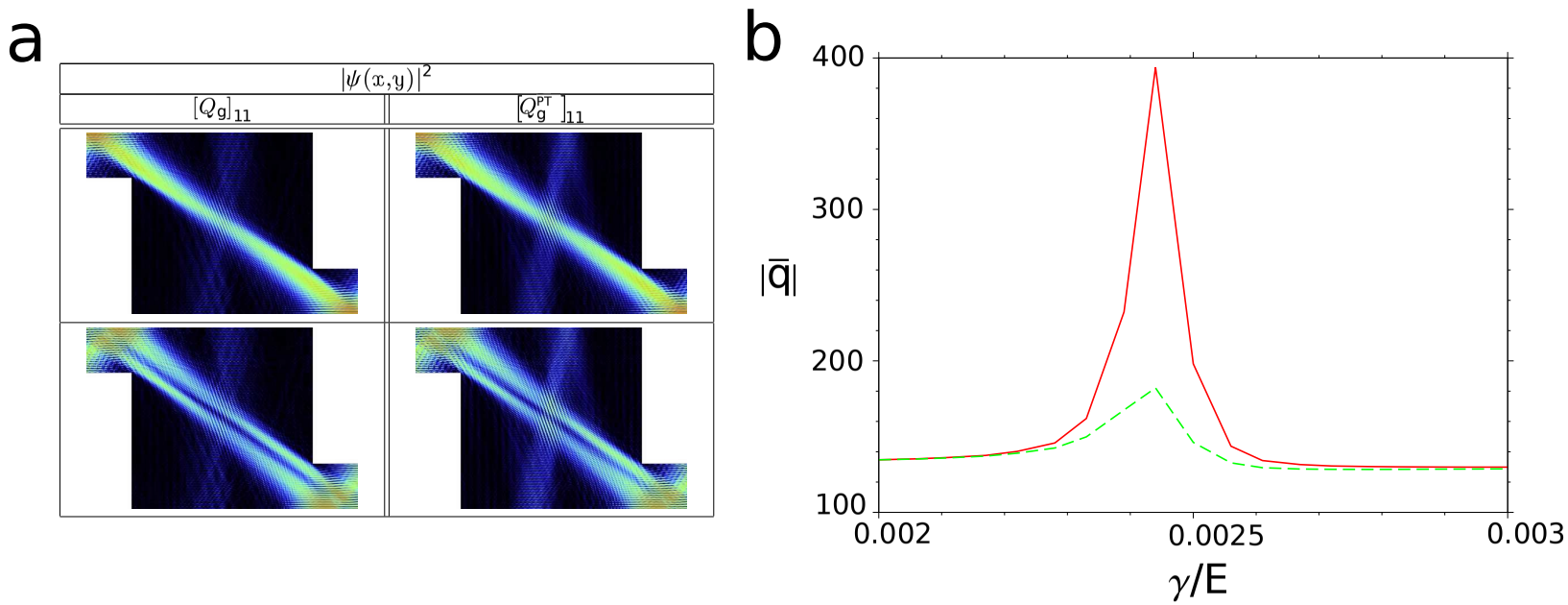

Figure 4.5.: (a) shows intensity plots of NOTEs found by Q_g and Q_g^{PT} at $\gamma \approx 0.004\,E$. The families of directly reflected and z-shaped NOTEs exist in good quality in the eigenspaces of $[Q_g]_{11}$ and $\left[Q_g^{PT}\right]_{11}$, but the family of directly transmitted states is scattered at the boundary between the loss and gain regions at such high γ-values. (b) shows the mean of the absolute values of the eigenvalues of Q_g (red line) and Q_g^{PT} (green line) for $\gamma \epsilon\ [0.002\,E, 0.003\,E]$. Both of these curves have a sharp peak at $\gamma \approx 0.00245\,E$, which indicates an intrinsic cavity resonance. The resonant peak in the curve for Q_g^{PT}, however, is much smaller than the peak for Q_g. The curves are shown for Q_g and Q_g^{PT}, since the construction of these two operators requires the same amount of information about the internal scattering dynamics.

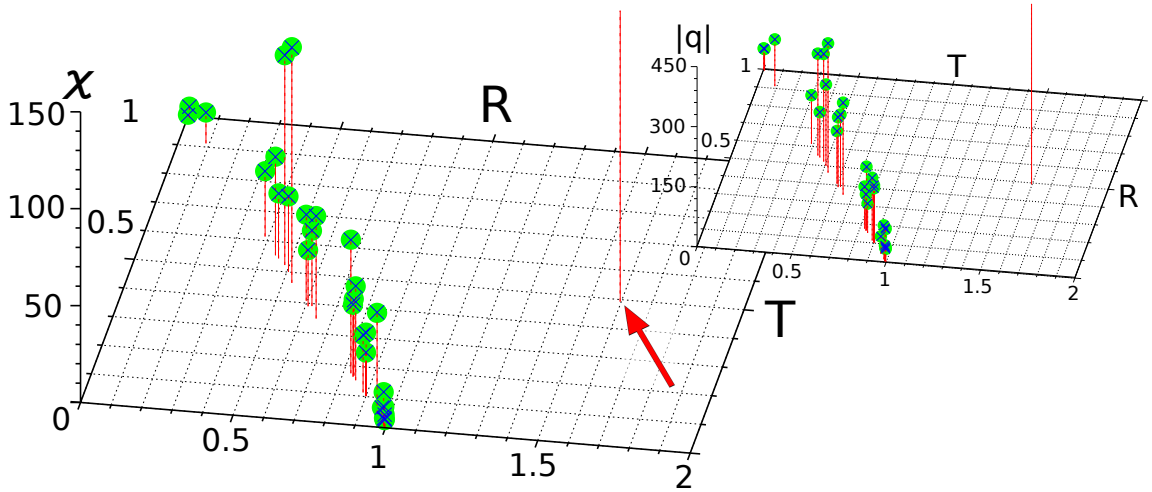

Figure 4.6.: (χ, T, R) for all 30 eigenstates of $\left[Q_d^{PT}\right]_{11}$ (green balls) and $\left[Q_g^{PT}\right]_{11}$ (blue crosses) at a scattering energy $E = (30.5\,\pi/d)^2/2$ for the scattering geometry depicted in Fig. 4.1(b). The loss/gain strength is $\gamma = 0.00245\,E$ which is in the vicinity of a resonance. The NOTEs correspond to small null-space-norms χ also for the PT-symmetric operators. The smaller inset shows $(|q|, T, R)$ for the given states. Unlike in the case of Q_g and Q_d, which are hermitian matrices, the eigenvalues of $\left[Q_d^{PT}\right]_{11}$ and $\left[Q_g^{PT}\right]_{11}$ are not real quantities. However, for the investigated system, the imaginary part is for most of the eigenvalues at least three orders of magnitude smaller than the real part. Only for the state with the largest value of $|q| \approx 2230$, that couples most to the resonance (red arrow), the imaginary part and the real part are of comparable size. For this state, only its position in the (T, R)-plane is shown. The intensities for selected beam-like scattering states for Q_g^{PT} in comparison to states found by Q_g and Q_d are shown in Table 4.2.

$\lvert\psi(x,y)\rvert^2$		
$[Q_g]_{11}$	$[Q_d]_{11}$	$[Q_g^{PT}]_{11}$
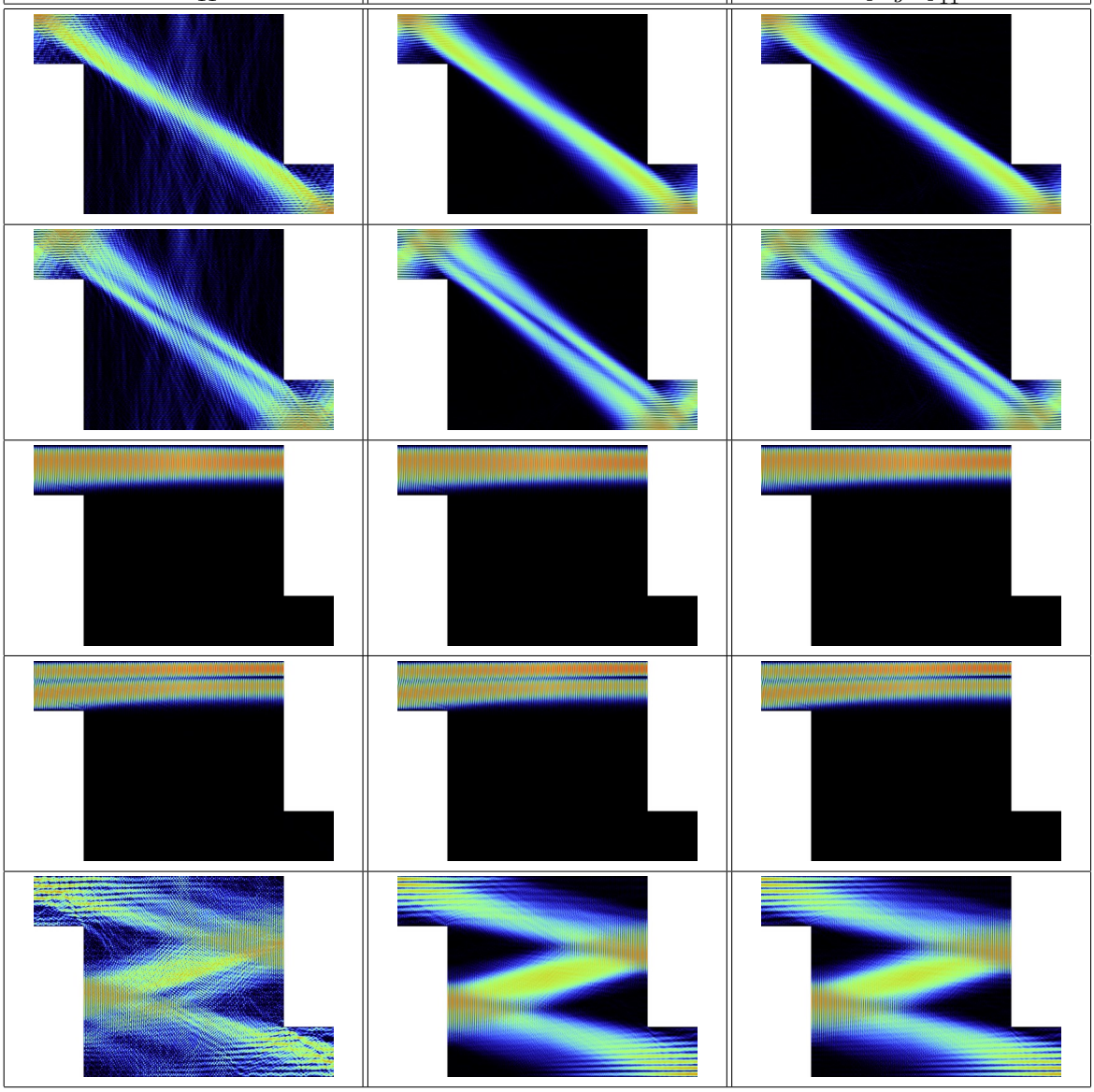		

Table 4.2.: $[Q]_{11}$ eigenstates for Q_g, Q_d and Q_g^{PT} at $\gamma = 0.00245\,E$ which is in the vicinity of the cavity resonance. Since the eigenstates for Q_d^{PT} look very similar to those for Q_g^{PT}, results are only shown for the latter operator. Most of the beam-like scattering states in Q_g are heavily affected by the intrinsic resonance, however, Q_d and Q_g^{PT} produce NOTEs of satisfying quality.

5. Summary

Major results of this thesis are the derivations of expressions for the proper operators measuring the dwell time and the group delay in wave scattering. We show that a previously discussed operator [18] returns the dwell time as its expectation value for arbitrary systems, including systems featuring loss and gain. This fact has, to the best of our knowledge, previously been overseen. We also derive a general expression for the operator measuring the group delay, which, as we find, can be constructed solely based on the knowledge of the system's scattering matrix. We show that for systems where flux is conserved, this operator coincides with the well-known Wigner-Smith time delay matrix.

In this work, we show that the operators measuring group delay and dwell time may be used to create very special scattering states, featuring beam-like propagation patterns, following bundles of particle trajectories. These particle-like states form a unique subspace of the eigenspace of the time delay operators. We apply an operational protocol we presented in an earlier work [17] to create such states to both of these operators, and we discuss the outcome for systems featuring three different kinds of potential landscapes in the scattering region.

The first class of systems we investigate are flux-conserving systems, for which the potential is hermitian. For the presented geometry consisting of two wave guides attached to a quadratic cavity and the chosen scattering parameters, group delay and dwell time appear to be practically identical and both operators can be used to create beam-like states of high quality. We also discuss the conditions for a divergency of the two delay times.

The second class of systems we study features uniform absorption and is experimentally very important. We find that for systems with uniformly absorbing potentials, a very simple expression for the dwell time operator can be derived starting from the Schrödinger equation, which is based only on the scattering matrix of the system. This expression was found earlier by Savin and Sommers [25], but with our results we can put their findings on solid ground and give the proper physical interpretation. This dwell time operator involves only the scattering matrix at a single energy and gives beam-like states of excellent quality. The construction of the group delay operator, however, generally includes taking the energy derivative of the scattering matrix. Also the latter operator may be used to create beams of very good quality.

The third kind of systems we investigate are PT-symmetric systems. The term 'PT-symmetric' refers to the presence of a very special, spatially shaped potential including both loss and gain regions which are arranged in such a way, that these systems remain invariant under the combined action of spatial reflection and time inversion. Here, we find, that again both of the general expressions for the time delay operators yield highly

collimated scattering states, but we show that in the case of an intrinsic resonance of the system, the dwell time operator is preferable to the group delay operator. Unlike in the case of uniformly absorptive systems, it is not possible to express the dwell time operator in terms of the scattering matrix only. We derive the proper generalizations of the group delay and dwell time operator to PT-symmetric systems and find, that if the loss/gain-strength is not too high, these operators form a true alternative to the dwell time matrix, since for their construction, the knowledge of the scattering matrix is sufficient.

Summarizing, we can state, that for systems with an arbitrary distribution of gain and loss, the dwell time operator is preferable to the group delay operator with regard to the construction of highly collimated beams in wave scattering. Constructing the dwell time operator, however, in general requires more information about the internal dynamics of the specific system than stored in the scattering matrix .

In addition to the main results concerning delay times and beam-like scattering states, we also present in this thesis a very practical formulation of the coupling matrix for the investigated systems. The coupling matrix contains the information about the 'opening' of the system, e.g., the coupling of the closed resonator to the wave guides for the presented systems. Our approach can be used to construct the effective Hamiltonian, the scattering matrix and the dwell time operator. In contrast to previous expressions [10], our formulation enables a straight-forward numerical implementation and analytical usage.

In PT-symmetric systems, the Hamiltonian and the scattering matrix feature the remarkable property, that below certain thresholds depending on the strength of loss and gain, their eigenvalues are real and unimodular, respectively. We provide here the missing link between the thresholds in the spectra of the scattering matrix and the Hamiltonian of the corresponding closed system and thereby explain how open and closed PT-symmetric systems relate to each other.

A. Unitary systems

A.1. Derivation of Q_d

The surface term (3.27) for the system displayed in Fig. 2.1(a) has to be evaluated only at the lead openings $\partial\Omega_1$ and $\partial\Omega_2$, since the wave function at the hard-wall boundary of the cavity is strictly zero. We will split (3.27) into the parts corresponding to the left lead (1) and the right lead (2) respectively.

$$\tau_d = G_1 + G_2, \tag{A.1}$$

with

$$G_i = -\frac{\hbar^2}{2m}\int_{\partial\Omega_i} d\vec{A}\cdot\left[\psi_i^\star\vec{\nabla}\dot{\psi}_i - \dot{\psi}_i\vec{\nabla}\psi_i^\star\right]. \tag{A.2}$$

ψ_i, $i = 1, 2$ denotes the wave in the left and right lead. For ψ_1 we have

$$\psi_1(x,y) = \sum_{n=1}^{n_{in}} a_n \frac{1}{\sqrt{v_n}}\chi_n(y)\, e^{ik_{x,n}x} + \sum_{n=1}^{\infty} b_n \frac{1}{\sqrt{v_n}}\chi_n(y)\, e^{-ik_{x,n}x}. \tag{A.3}$$

The terms needed in the integrand in (A.2), taking into account $d\vec{A}\cdot\vec{\nabla} = -dy\frac{\partial}{\partial x}$ for $\vec{x}\epsilon\partial\Omega_1$, evaluate with $\dot{a}_n \equiv 0$ to

$$\psi_1^\star(0,y) = \sum_{n=1}^{n_{in}} a_n^\star \frac{1}{\sqrt{v_n}}\chi_n(y) + \sum_{n=1}^{\infty} b_n^\star \frac{1}{\sqrt{v_n}}\chi_n(y) \tag{A.4}$$

$$\frac{\partial\psi_1^\star(x,y)}{\partial x}\,|_{x=0} = \sum_{n=1}^{n_{in}} (-ik_n)\, a_n^\star \frac{1}{\sqrt{v_n}}\chi_n(y) + \sum_{n=1}^{\infty} (ik_n^\star)\, b_n^\star \frac{1}{\sqrt{v_n}}\chi_n(y) \tag{A.5}$$

$$\dot{\psi}_1(0,y) = \sum_{n=1}^{\infty} \dot{b}_n \frac{1}{\sqrt{v_n}}\chi_n(y) + \sum_{n=1}^{n_{in}} a_n \dot{\left(v_n^{-1/2}\right)}\chi_n(y) \tag{A.6}$$

$$+ \sum_{n=1}^{\infty} b_n \dot{\left(v_n^{-1/2}\right)}\chi_n(y) \tag{A.7}$$

$$\frac{\partial^2\psi(x,y)}{\partial x\partial E}\,|_{x=0} = \sum_{n=1}^{\infty} (-ik_n)\,\dot{b}_n \frac{1}{\sqrt{v_n}}\chi_n(y) + \sum_{n=1}^{n_{in}} \left(i\dot{k}_n\right) a_n \frac{1}{\sqrt{v_n}}\chi_n(y) \tag{A.8}$$

$$+ \sum_{n=1}^{\infty} \left(-i\dot{k}_n\right) b_n \frac{1}{\sqrt{v_n}}\chi_n(y) \tag{A.9}$$

$$+ \sum_{n=1}^{n_{in}} (ik_n)\, a_n \dot{\left(v_n^{-1/2}\right)}\chi_n(y) + \sum_{n=1}^{\infty} (-ik_n)\, b_n \dot{\left(v_n^{-1/2}\right)}\chi_n(y)\,. \tag{A.10}$$

We dropped the subscript x in $k_{x,n}$ for the sake of simplicity. For the unevaluated energy derivatives we get with

$$k_n = \sqrt{\frac{2mE}{\hbar^2} - \left(\frac{n\pi}{d}\right)^2} \tag{A.11}$$

$$\Rightarrow \dot{k}_n = \frac{m}{\hbar}\frac{1}{\hbar k_n}, \tag{A.12}$$

and with

$$v_n = \frac{\hbar k_n}{m} \tag{A.13}$$

$$\Rightarrow \dot{\left(v_n^{-1/2}\right)} = \left(\frac{m}{\hbar}\right)^{1/2}\left(-\frac{1}{2}\right)(k_n)^{-3/2}\dot{k}_n = -\frac{1}{2}\left(\frac{m}{\hbar}\right)^{3/2}\frac{1}{\hbar}(k_n)^{-5/2}. \tag{A.14}$$

For $n > n_{in}$ we have instead of (A.11) and (A.13)

$$\kappa_n = -ik_n = \sqrt{\left(\frac{n\pi}{d}\right)^2 - \frac{2mE}{\hbar^2}} \tag{A.15}$$

$$v_n = \frac{\hbar\kappa_n}{m}, \tag{A.16}$$

and therefore

$$\dot{\kappa}_n = -\frac{m}{\hbar}\frac{1}{\hbar\kappa_n} \tag{A.17}$$

and

$$\Rightarrow \dot{\left(v_n^{-1/2}\right)} = \frac{1}{2}\left(\frac{m}{\hbar}\right)^{3/2}\frac{1}{\hbar}(\kappa_n)^{-5/2}. \tag{A.18}$$

Inserting (A.4) - (A.6) and (A.8) into (A.2), we get with $\int_0^W dy\,\chi_m(y)\,\chi_n(y) = \delta_{mn}$,

$$\frac{2m}{\hbar^2}G_1 = -i\sum_{n=1}^{n_{in}} a_n^\star \dot{b}_n \frac{m}{\hbar} + i\sum_{n=1}^{n_{in}} a_n^\star a_n \frac{m^2}{\hbar^3}\frac{1}{k_n^2} - i\sum_{n=1}^{n_{in}} a_n^\star b_n \frac{m^2}{\hbar^3}\frac{1}{k_n^2} \tag{A.19}$$

$$-\frac{i}{2}\sum_{n=1}^{n_{in}} a_n^\star a_n \frac{m^2}{\hbar^3}\frac{1}{k_n^2} + \frac{i}{2}\sum_{n=1}^{n_{in}} a_n^\star b_n \frac{m^2}{\hbar^3}\frac{1}{k_n^2} - i\sum_{n=1}^{n_{in}} b_n^\star \dot{b}_n \frac{m}{\hbar} \tag{A.20}$$

$$+i\sum_{n=1}^{n_{in}} b_n^\star a_n \frac{m^2}{\hbar^3}\frac{1}{k_n^2} - i\sum_{n=1}^{n_{in}} b_n^\star b_n \frac{m^2}{\hbar^3}\frac{1}{k_n^2} - \frac{i}{2}\sum_{n=1}^{n_{in}} b_n^\star a_n \frac{m^2}{\hbar^3}\frac{1}{k_n^2} \tag{A.21}$$

$$+\frac{i}{2}\sum_{n=1}^{n_{in}} b_n^\star b_n \frac{m^2}{\hbar^3}\frac{1}{k_n^2} + \sum_{n=n_{in}+1}^{\infty} b_n^\star \dot{b}_n \frac{m}{\hbar} - \sum_{n=n_{in}+1}^{\infty} b_n^\star b_n \frac{m^2}{\hbar^3}\frac{1}{\kappa_n^2} \tag{A.22}$$

$$+\frac{1}{2}\sum_{n=n_{in}+1}^{\infty} b_n^\star b_n \frac{m^2}{\hbar^3}\frac{1}{\kappa_n^2} + i\sum_{n=1}^{n_{in}} a_n^\star \dot{b}_n \frac{m}{\hbar} - \frac{i}{2}\sum_{n=1}^{n_{in}} a_n^\star a_n \frac{m^2}{\hbar^3}\frac{1}{k_n^2} \tag{A.23}$$

$$-\frac{i}{2}\sum_{n=1}^{n_{in}} a_n^\star b_n \frac{m^2}{\hbar^3}\frac{1}{k_n^2} - i\sum_{n=1}^{n_{in}} b_n^\star \dot{b}_n \frac{m}{\hbar} + \frac{i}{2}\sum_{n=1}^{n_{in}} b_n^\star a_n \frac{m^2}{\hbar^3}\frac{1}{k_n^2} \tag{A.24}$$

$$+\frac{i}{2}\sum_{n=1}^{n_{in}} b_n^\star b_n \frac{m^2}{\hbar^3}\frac{1}{k_n^2} - \sum_{n=n_{in}+1}^{\infty} b_n^\star \dot{b}_n \frac{m}{\hbar} - \frac{1}{2}\sum_{n=n_{in}+1}^{\infty} b_n^\star b_n \frac{m^2}{\hbar^3}\frac{1}{\kappa_n^2}. \tag{A.25}$$

Elementary algebra leads to the following simplified expression for G_1,

$$G_1 = -i\hbar \sum_{n=1}^{n_{in}} b_n^\star \dot{b}_n + \frac{i}{2}\frac{m}{\hbar}\sum_{n=1}^{n_{in}} \frac{1}{k_n^2}\left(b_n^\star a_n - a_n^\star b_n\right) - \frac{1}{2}\frac{m}{\hbar}\sum_{n=n_{in}+1}^{\infty} b_n^\star \frac{1}{\kappa_n^2} b_n. \tag{A.26}$$

The analogous calculation for G_2 using $d\vec{A}\cdot\vec{\nabla} = dy\frac{\partial}{\partial x}$ for $\vec{x}\epsilon\partial\Omega_2$ gives

$$G_2 = -i\hbar \sum_{n=1}^{n_{out}} c_n^\star \dot{c}_n + \frac{i}{2}\frac{m}{\hbar}\sum_{n=1}^{n_{out}} \left(c_n^\star d_n - d_n^\star c_n\right) - \frac{1}{2}\frac{m}{\hbar}\sum_{n=n_{out}+1}^{\infty} c_n^\star \frac{1}{\kappa_n^2} c_n. \tag{A.27}$$

Inserting the expressions (3.29) and (3.30) for the expansion coefficients of the outgoing waves into (A.26) and (A.27) respectively, yields for $\tau_d = G_1 + G_2$ a sum of four terms

$$\tau_d = \int_\Omega dV\, \psi^\star\psi = -i\hbar T_1 + \frac{i}{2}\frac{m}{\hbar}\left(T_2 - T_3\right) - \frac{1}{2}\frac{m}{\hbar}T_4,$$

with

$$\begin{aligned}
T_1 &= a_n^\star \left(r_{nm}^\dagger \dot{r}_{ml} + t_{nm}^\dagger \dot{t}_{ml}\right) a_l && \text{(A.28)}\\
&+ a_n^\star \left(r_{nm}^\dagger \dot{t}'_{ml} + t_{nm}^\dagger \dot{r}'_{ml}\right) d_l && \text{(A.29)}\\
&+ d_n^\star \left(t'^\dagger_{nm} \dot{r}_{ml} + r'^\dagger_{nm} \dot{t}_{ml}\right) a_l && \text{(A.30)}\\
&+ d_n^\star \left(r'^\dagger_{nm} \dot{r}'_{ml} + t'^\dagger_{nm} \dot{t}'_{ml}\right) d_l, && \text{(A.31)}
\end{aligned}$$

$$\begin{aligned}
T_2 &= a_n^\star r_{nm}^\dagger \frac{1}{k_m^2} a_m && \text{(A.32)}\\
&+ a_n^\star t_{nm}^\dagger \frac{1}{k_m^2} d_m && \text{(A.33)}\\
&+ d_n^\star t'^\dagger_{nm} \frac{1}{k_m^2} a_m && \text{(A.34)}\\
&+ d_n^\star r'^\dagger_{nm} \frac{1}{k_m^2} d_m, && \text{(A.35)}
\end{aligned}$$

$$\begin{aligned}
T_3 &= a_n^\star \frac{1}{k_n^2} r_{nm} a_m && \text{(A.36)}\\
&+ a_n^\star \frac{1}{k_n^2} t'_{nm} d_m && \text{(A.37)}\\
&+ d_n^\star \frac{1}{k_n^2} t_{nm} a_m && \text{(A.38)}\\
&+ d_n^\star \frac{1}{k_n^2} r'_{nm} d_m && \text{(A.39)}
\end{aligned}$$

and

$$
\begin{aligned}
T_4 &= a_n^\star \left(\tilde{r}_{nm}^\dagger \frac{1}{\kappa_m^2} \tilde{r}_{ml} + \tilde{t}_{nm}^\dagger \frac{1}{\kappa_m^2} \tilde{t}_{ml} \right) a_l && \text{(A.40)} \\
&+ a_n^\star \left(\tilde{r}_{nm}^\dagger \frac{1}{\kappa_m^2} \tilde{t}'_{ml} + \tilde{t}_{nm}^\dagger \frac{1}{\kappa_m^2} \tilde{r}'_{ml} \right) d_l && \text{(A.41)} \\
&+ d_n^\star \left(\tilde{t}'^\dagger_{nm} \frac{1}{\kappa_m^2} \tilde{r}_{ml} + \tilde{r}'^\dagger_{nm} \frac{1}{\kappa_m^2} \tilde{t}_{ml} \right) a_l && \text{(A.42)} \\
&+ d_n^\star \left(\tilde{r}'^\dagger_{nm} \frac{1}{\kappa_m^2} \tilde{r}'_{ml} + \tilde{t}'^\dagger_{nm} \frac{1}{\kappa_m^2} \tilde{t}'_{ml} \right) d_l. && \text{(A.43)}
\end{aligned}
$$

In (A.28) - (A.43) the Einstein sum convention is used. Note however, that the sums run over different index-ranges, quantities in the left lead run from $1 \ldots n_{in}$ and from $n_{in} + 1 \ldots \infty$ for open and closed channels, respectively. Quantities in the right lead run from $1 \ldots n_{out}$ and $n_{out} + 1 \ldots \infty$.

The T_i are exactly the expectation values evaluated in the lead-mode basis appearing in (3.33) - (3.36).

A.2. Equivalence of the different expressions for Q_d

We will show the equivalence of the general expression for the dwell time operator

$$
Q_d = \hbar^2 V^\dagger G^\dagger G V, \tag{A.44}
$$

and the expression

$$
Q_d = -i\hbar S^\dagger \dot{S} + \frac{i}{2}\frac{m}{\hbar}\left(S^\dagger \frac{1}{k^2} - \frac{1}{k^2} S \right) - \frac{1}{2}\frac{m}{\hbar} \tilde{S}^\dagger \frac{1}{\kappa^2} \tilde{S} \tag{A.45}
$$

for unitary scattering systems on an abstract operator level. To this purpose we insert into (A.45) the expressions

$$
S = -\mathbb{I} + i\hbar V^\dagger G V \tag{A.46}
$$

$$
\tilde{S} = i\hbar \tilde{V}^\dagger G V \tag{A.47}
$$

for the scattering matrix and the scattering amplitudes into evanescent lead modes,

$$
\begin{aligned}
Q_d &= -i\hbar \left[\left(-\mathbb{I} - i\hbar V^\dagger G^\dagger V \right) \left(i\hbar \left\{ \dot{V}^\dagger G V + V^\dagger \dot{G} V + V^\dagger G \dot{V} \right\} \right) \right] && \text{(A.48)} \\
&+ \frac{i}{2}\frac{m}{\hbar} \left[\left(-\mathbb{I} - i\hbar V^\dagger G^\dagger V \right) \frac{1}{k^2} - \frac{1}{k^2} \left(-\mathbb{I} + i\hbar V^\dagger G V \right) \right] && \text{(A.49)} \\
&- \frac{1}{2}\frac{m}{\hbar} \left[\left(-i\hbar V^\dagger G^\dagger \tilde{V} \right) \frac{1}{\kappa^2} \left(i\hbar \tilde{V}^\dagger G V \right) \right]. && \text{(A.50)}
\end{aligned}
$$

In matrix analysis, a formula for the derivative of a function f of matrices A that depend on a parameter t is known [15],

$$
\frac{d}{dt} f\left(A(t)\right)|_{t=t_0} = \left[\begin{pmatrix} A(t_0) & \frac{d}{dt} A(t)|_{t=t_0} \\ 0 & A(t_0) \end{pmatrix} \right]_{12}. \tag{A.51}
$$

The notation $[\cdot]_{12}$ means that we take the upper right block of the corresponding matrix. With (A.51) we find for $f(A) \equiv G = (A)^{-1}$ with $A \equiv E - H_{\text{eff}}$ and $H_{\text{eff}} = H_D - \frac{\hbar}{2} W\sigma W^\dagger + \frac{\hbar}{2}\tilde{V}\tilde{V}^\dagger - \frac{i\hbar}{2} V V^\dagger$ the energy derivative of the Green's function to be

$$\dot{G} = G\left(\dot{H}_{\text{eff}} - \mathbb{I}\right) G \tag{A.52}$$

$$= G\left(\frac{\hbar}{2}\dot{\tilde{V}}\tilde{V}^\dagger + \frac{\hbar}{2}\tilde{V}\dot{\tilde{V}}^\dagger - \frac{i\hbar}{2}\dot{V}V^\dagger - \frac{i\hbar}{2}V\dot{V}^\dagger\right) G. \tag{A.53}$$

In the continuum limit, the term $-\frac{\hbar}{2} W\sigma W^\dagger$ just denotes Neumann boundary conditions, which are independent of the scattering energy. The only energy dependance of the coupling matrices V and $\tilde{V}$ comes via the factors $\sqrt{v_n}$, such that their derivatives with respect to the energy can therefore be written as

$$\dot{V} = V\,\frac{1}{2}\frac{m}{\hbar^2}\frac{1}{k^2} \tag{A.54}$$

and

$$\dot{\tilde{V}} = -\tilde{V}\,\frac{1}{2}\frac{m}{\hbar^2}\frac{1}{\kappa^2}, \tag{A.55}$$

since

$$(\dot{\sqrt{v_n}}) = \sqrt{\frac{\hbar}{m}}\left(\dot{\sqrt{k_n}}\right) = \frac{1}{2}\sqrt{\frac{m}{\hbar}}\frac{1}{\hbar}k_n^{-3/2} = \sqrt{v_n}\frac{m}{\hbar^2}\frac{1}{k_n^2} \tag{A.56}$$

for $n < n_{in}$ (or $n < n_{out}$ for the right lead) and

$$(\dot{\sqrt{v_n}}) = -\sqrt{v_n}\frac{m}{\hbar^2}\frac{1}{\kappa_n^2} \tag{A.57}$$

for $n > n_{in}$ (or $n > n_{out}$). Consider the scattering matrix $S = -\mathbb{I} + i\hbar V^\dagger G V$ and its hermitian conjugate $S^\dagger = -\mathbb{I} - i\hbar V^\dagger G^\dagger V$. From the unitarity of S, $S^\dagger S = \mathbb{I}$, it follows that

$$V^\dagger\left[i\left(G^\dagger - G\right)\right]V = -\hbar V^\dagger\left[G^\dagger V V^\dagger G\right]V. \tag{A.58}$$

Since $G = \left(E - H_h + \frac{i\hbar}{2}VV^\dagger\right)^{-1}$ and H_h contains the potential inside the scattering region, which needs to be hermitian, but can otherwise be completely arbitrary, also the following relation must be true

$$i\left(G^\dagger - G\right) = -\hbar G^\dagger V V^\dagger G. \tag{A.59}$$

(A.59) can also be obtained rigorously via a simple calculation using the defining property of the Green's function $G = (E - H_{\text{eff}})^{-1}$. It follows that

$$G^\dagger\left(E - H_{\text{eff}}\right)^\dagger = \mathbb{I}, \tag{A.60}$$

$$\left(E - H_{\text{eff}}\right)G = \mathbb{I}. \tag{A.61}$$

Therefore,

$$G^\dagger\left(-H_{\text{eff}} + H_{\text{eff}}^\dagger\right)G = G^\dagger - G. \tag{A.62}$$

Inserting for $H_{\text{eff}} = H_h - \frac{i\hbar}{2} VV^\dagger$ and taking into account the hermiticity of H_h, we get

$$i\hbar G^\dagger VV^\dagger G = G^\dagger - G, \tag{A.63}$$

which is perfectly equivalent to (A.59).

Inserting (A.52), (A.54) and (A.55) for the energy derivatives into (A.48) using (A.59), one finds that all the terms except $\hbar^2 V^\dagger G^\dagger G V$ cancel. This is exactly the general expression for Q_d and, therefore, the desired result.

B. Uniform loss systems

B.1. Derivation of Q_d

Since large parts of the derivation presented in this section work analogously to the derivation in appendix A.1, we will only sketch the concepts and present the result.

In order to evaluate the surface term on the left-hand side of (3.49), we decompose the wave function ψ according to (A.3). Inserting again the expressions (3.29) and (3.30) for the expansion coefficients of the outgoing waves finally gives

$$\tau_d = \frac{\hbar}{2\gamma}\left[T_1 - T_2\right], \tag{B.1}$$

with

$$\begin{aligned} T_1 &= a_m^\star a_m && \text{(B.2)} \\ &+ d_m^\star d_m && \text{(B.3)} \end{aligned}$$

and

$$\begin{aligned} T_2 &= a_m^\star \left(r_{mn}^\dagger r_{nl} + t_{mn}^\dagger t_{nl}\right) a_l && \text{(B.4)} \\ &+ a_m^\star \left(r_{mn}^\dagger t'_{nl} + t_{mn}^\dagger r'_{nl}\right) d_l && \text{(B.5)} \\ &+ d_m^\star \left(t'^\dagger_{mn} r_{nl} + r'^\dagger_{mn} t_{nl}\right) a_l && \text{(B.6)} \\ &+ d_m^\star \left(t'^\dagger_{mn} t'_{nl} + r'^\dagger_{mn} r'_{nl}\right) d_l. && \text{(B.7)} \end{aligned}$$

Einstein sum convention was used just as in appendix A.1. We can identify the terms T_1 and T_2 as the expectation values taken in the lead-mode basis appearing in (3.50).

B.2. Equivalence of the different expressions for Q_d

The derivation presented in this section goes back to Savin and Sommers [25] who found the expression for Q_d (3.51) in this way. For the (sub-unitary) scattering matrix $S = -\mathbb{I} + i\hbar V^\dagger G V$ we find

$$-\frac{\hbar}{2\gamma}\left(S^\dagger S - \mathbb{I}\right) = -\frac{\hbar}{2\gamma}\left(i\hbar V^\dagger \left(G^\dagger - G\right) V + \hbar^2 V^\dagger G^\dagger V V^\dagger G V\right). \tag{B.8}$$

This expression can be simplified using $G = \left(E - H^u_{eff} + i\gamma\right)^{-1}$ with $H^u_{eff} = H^u_h - \frac{i\hbar}{2}VV^\dagger$ denoting the Hamiltonian of the corresponding system without loss.

$$
\begin{aligned}
G^\dagger - G &= \frac{1}{E - H^{u\dagger}_{eff} - i\gamma} - \frac{1}{E - H^u_{eff} + i\gamma} && \text{(B.9)} \\
&= \frac{E - H^u_{eff} + i\gamma - E + H^{u\dagger}_{eff} + i\gamma}{\left(E - H^{u\dagger}_{eff} - i\gamma\right)\left(E - H^u_{eff} + i\gamma\right)} && \text{(B.10)} \\
&= G^\dagger \left(i\hbar VV^\dagger + 2i\gamma\right) G && \text{(B.11)}
\end{aligned}
$$

With (B.11), (B.8) becomes

$$
-\frac{\hbar}{2\gamma}\left(S^\dagger S - \mathbb{I}\right) = \hbar^2 V^\dagger G^\dagger G V = Q_d, \qquad \text{(B.12)}
$$

which is the desired result.

C. PT-symmetric systems

C.1. Correspondence between the eigenvalue problem of the scattering matrix and the boundary values

Consider the scattering system displayed in Fig. 2.2(a). We define the origin of the x-axis as follows

$$\psi_1 \equiv \psi(x=0) \tag{C.1}$$
$$\psi_N \equiv \psi(x=L), \tag{C.2}$$

such that the scattering region is located in $[0, L]$. If we choose the plane-wave basis to be the same on the left- (I) and on the right-hand (II) side of the cavity

$$\psi_{\mathrm{I}}(x) = ae^{ikx} + be^{-ikx} \tag{C.3}$$
$$\psi_{\mathrm{II}}(x) = ce^{ikx} + de^{-ikx} \tag{C.4}$$

and set $V_{pot}(x) = 0\,\forall x$, the scattering matrix becomes

$$S = \begin{pmatrix} 0 & 1 \\ 1 & 0 \end{pmatrix}. \tag{C.5}$$

(C.5) is of course a valid, unitary scattering matrix, but does not contain the proper, physical phase the wave accumulates traversing the scattering region. However, if we define the basis to be

$$\psi_{\mathrm{I}}(x) = ae^{ikx} + be^{-ikx} \tag{C.6}$$
$$\psi_{\mathrm{II}}(x) = ce^{ik(x-L)} + de^{-ik(x-L)}, \tag{C.7}$$

as we did in section 4.3, the scattering matrix for free propagation reads

$$S = \begin{pmatrix} 0 & e^{ikL} \\ e^{ikL} & 0 \end{pmatrix}, \tag{C.8}$$

containing the proper phase shifts. The way this basis is defined in (C.6) and (C.7) for the left and the right side of the cavity, the plane waves are set to have zero phase at the boundaries at $x = 0$ and $x = L$, respectively, leading to the general relation between the scattering eigenvalue σ and the boundary value parameter λ (4.46).

If the cavity is shifted along the x-axis to $[A, A+L]$, however, the phases of the waves at the boundaries are different from zero, $e^{\pm ikA}$. This leads to a modified relation $\sigma(\lambda)$. For ψ_{I} we find

$$\sigma = \frac{e^{-ik\Delta x} - \lambda}{\lambda - e^{ik\Delta x}} e^{2ikA}, \tag{C.9}$$

but for ψ_{II} we find

$$\sigma = \frac{e^{-ik\Delta x} - \lambda}{\lambda - e^{ik\Delta x}} e^{-2ikA}, \tag{C.10}$$

which is different from (C.10). In this shifted basis, the scattering eigenstates cannot be properly reproduced using the same λ for the boundary conditions on both sides of the cavity. Nevertheless, (C.9) and (C.10) can be valid simultaneously if we allow two different λ for both boundaries rather than choosing the ansatz (4.34).

Since the scattering matrix connects incoming and outgoing channels, shifting the origin of the basis on either one or both sides corresponds to a transformation of S of the form

$$S' = RSR. \tag{C.11}$$

This transformation preserves the absolute values of the eigenvalues of S, because R is a unitary matrix. Since (C.11) is, however, not a unitary transformation the eigenvalues of S will in general change their phases as a result of the transfer-motion.

The basis (C.6, C.7) for a cavity located between $x = 0$ and $x = L$ is preferable in a twofold way: It properly describes the phase shift due to the finite extension of the scattering region, and contains only the phases associated to the actual scattering process, not due to propagation to the boundaries.

C.2. Derivation of Q_d^{PT}

Large parts of the derivations presented in section 4.5 work in analogy to the calculations in subsection 3.3.1 and appendix A.1. For that reason we will restrict ourselves on sketching the concepts and presenting the results in this section.

Inserting the decomposition of the wave function ψ into the lead modes (3.28) into the surface term on the left-hand side of (4.55) using (3.29, 3.30) for the expansion coefficients and making use of (4.59) for the action of the parity operator eventually results in

$$\tau_d^{PT} = \int_\Omega dV\ [PT\psi]\,\psi = -i\hbar T_1 + \frac{i}{2}\frac{m}{\hbar}\left(T_2 - T_3\right) - \frac{1}{2}\frac{m}{\hbar}\,T_4, \tag{C.12}$$

with

$$\begin{aligned}
T_1 &= a_m^\star \left(t_{mn}^\dagger\,(-1)^{n-1}\,\dot{r}_{nl} + r_{mn}^\dagger\,(-1)^{n-1}\,\dot{t}_{nl}\right) a_l && \text{(C.13)}\\
&+ a_m^\star \left(t_{mn}^\dagger\,(-1)^{n-1}\,\dot{t}'_{no} + r_{mn}^\dagger\,(-1)^{n-1}\,\dot{r}'_{nl}\right) d_l && \text{(C.14)}\\
&+ d_m^\star \left(r_{mn}'^\dagger\,(-1)^{n-1}\,\dot{r}_{nl} + t_{mn}'^\dagger\,(-1)^{n-1}\,\dot{t}_{nl}\right) a_l && \text{(C.15)}\\
&+ d_m^\star \left(r_{mn}'^\dagger\,(-1)^{n-1}\,\dot{t}'_{nl} + t_{mn}'^\dagger\,(-1)^{n-1}\,\dot{r}'_{nl}\right) d_l, && \text{(C.16)}
\end{aligned}$$

$$
\begin{aligned}
T_2 &= a_m^\star \left(t_{mn}^\dagger (-1)^{n-1} \frac{1}{k_n^2} \right) a_n && \text{(C.17)} \\
&+ a_m^\star \left(r_{mn}^\dagger (-1)^{n-1} \frac{1}{k_n^2} \right) d_n && \text{(C.18)} \\
&+ d_m^\star \left(r_{mn}'^\dagger (-1)^{n-1} \frac{1}{k_n^2} \right) a_n && \text{(C.19)} \\
&+ d_m^\star \left(t_{mn}'^\dagger (-1)^{n-1} \frac{1}{k_n^2} \right) d_n, && \text{(C.20)}
\end{aligned}
$$

$$
\begin{aligned}
T_3 &= a_m^\star \left((-1)^{m-1} \frac{1}{k_m^2} t_{mn} \right) a_n && \text{(C.21)} \\
&+ a_m^\star \left((-1)^{m-1} \frac{1}{k_m^2} r'_{mn} \right) d_n && \text{(C.22)} \\
&+ d_m^\star \left((-1)^{m-1} \frac{1}{k_m^2} r_{mn} \right) a_n && \text{(C.23)} \\
&+ a_m^\star \left((-1)^{m-1} \frac{1}{k_m^2} t'_{mn} \right) d_n && \text{(C.24)}
\end{aligned}
$$

and

$$
\begin{aligned}
T_4 &= a_m^\star \left(\tilde{r}_{mn}^\dagger (-1)^{n-1} \frac{1}{\kappa_n^2} \tilde{t}_{nl} + \tilde{t}_{mn}^\dagger (-1)^{n-1} \frac{1}{\kappa_n^2} \tilde{r}_{nl} \right) a_l && \text{(C.25)} \\
&+ a_m^\star \left(\tilde{r}_{mn}^\dagger (-1)^{n-1} \frac{1}{\kappa_n^2} \tilde{r}'_{nl} + \tilde{t}_{mn}^\dagger (-1)^{n-1} \frac{1}{\kappa_n^2} \tilde{t}'_{nl} \right) d_l && \text{(C.26)} \\
&+ d_m^\star \left(\tilde{t}_{mn}'^\dagger (-1)^{n-1} \frac{1}{\kappa_n^2} \tilde{t}_{nl} + \tilde{r}_{mn}'^\dagger (-1)^{n-1} \frac{1}{\kappa_n^2} \tilde{r}_{nl} \right) a_l && \text{(C.27)} \\
&+ d_m^\star \left(\tilde{t}_{mn}'^\dagger (-1)^{n-1} \frac{1}{\kappa_n^2} \tilde{r}'_{nl} + \tilde{r}_{mn}'^\dagger (-1)^{n-1} \frac{1}{\kappa_n^2} \tilde{t}'_{nl} \right) d_l. && \text{(C.28)}
\end{aligned}
$$

The Einstein sum convention was used in the above expressions. Note that the summation indices in T_1, T_2, T_3 and the indices m and l in T_4 run from 1 to n_{in}, however, the index n in T_4 runs from $n_{in}+1$ to ∞. The tilded quantities are the scattering amplitudes connecting flux-carrying and evanescent modes according to (3.31, 3.32). From (C.13) - (C.28), we find that equation (C.12) is the expectation value for the vector of incoming coefficients $\vec{u} = \left(\vec{a}^T, \vec{d}^T \right)^T$ of an operator A,

$$
\tau_d^{PT} = \langle u | A | u \rangle = \langle u | PPA | u \rangle = \langle Pu | PA | u \rangle . \qquad \text{(C.29)}
$$

The last two equal signs are valid because $P^2 = \mathbb{I}$ and $P^\dagger = P$, respectively. So (C.12) can also be interpreted as the PT-expectation value of the operator PA. This operator is a sum of four terms; the T_i in (C.12) are exactly the PT-expectation values in the expressions (4.62) - (4.65), the operator PA is equal to Q_d^{PT} (4.67).

Acknowledgements

Eventually, I would like to acknowledge the support, encouragement, advice and help of the following people:

- My thesis advisor Prof. Dr. Stefan Rotter always took the time for questions and discussions, trying at all times to deepen my physical understanding, but also with the appropriate amusement.
- Dr. Florian Libisch granted me full access to his computer code, improved my coding, and was an indispensible aid in all sorts of coding and cluster troubles.
- Dipl.-Ing. Adrian Girschik and Rafael Reiter BSc helped me to translate my computer codes from FORTRAN to C++.
- I would like to thank the colleagues at the Institute for Theoretical Physics, especially Adrian Girschik, Fabian Lackner, Matthias Liertzer, Rafael Reiter and Roman Voglauer for useful discussions, but also for the many useless discussions we had.

I am grateful and would finally like to thank my mother and grandmother for their moral and financial support.

Bibliography

[1] C.E. Rüter, K.G. Makris, R. El-Ganainy, D.N. Christodoulides, M. Segev, D. Kip, Nature Physics **6,** pp. 192-195 (2010).

[2] Y.D. Chong, L. Ge, A.D. Stone, Phys. Rev. Lett. **106**, 093902 (2011).

[3] C.M. Bender, D.C. Brody, H.F. Jones, B.K. Meister, Phys. Rev. Lett. **98**, 040403 (2007).

[4] M. Liertzer, L. Ge, H.E. Türeci, S. Rotter, arXiv:1109.0454v1.

[5] I. M. Vellekoop, A.P. Mosk, Phys. Rev. Lett. **101,** 120601 (2008).

[6] S.M. Popoff, G. Lerosey, R. Carminati, M. Fink, A.C. Boccara, S. Gigan, Phys. Rev. Lett. **104,** 100601 (2010).

[7] O. Dietz, U. Kuhl, H.-J. Stöckmann, N.M. Makarov, F.M. Izrailev, Phys. Rev. B **83**, 134203 (2011).

[8] P.G. Silvestrov, M.C. Goorden, C.W.J. Beenakker, Phys. Rev. B **67**, 241301 (2003).

[9] C. M. Bender, Rep. Prog. Phys. **70** (2007) 947–1018.

[10] L. E. Reichl, The Transition to Chaos, Springer Verlag, New York (2004).

[11] H. E. Türeci, A. D. Stone, B. Collier, Phys. Rev. A **74**, 043822 (2006).

[12] S. Rotter, A Modular Recursive Green's Function Method for Quantum Transport, diploma thesis (1999).

[13] H.-J. Stöckmann, Quantum Chaos - An Introduction, Cambridge University Press, Cambridge (1999).

[14] M. Büttiker, Phys. Rev. B **33**, 3020 (1986).

[15] R. Mathias, SIAM. J. Matrix Anal. & Appl. **17**, pp. 610-620 (1996).

[16] S. Rotter, F. Aigner, J. Burgdörfer, Phys. Rev. B **75**, 125312 (2007).

[17] S. Rotter, P. A., F. Libisch, Phys. Rev. Lett. **106**, 120602 (2011) (see also suppl. material at http://link.aps.org/ supplemental/10.1103/PhysRevLett.106.120602).

[18] V. V. Sokolov, V. Zelevinsky, Phys. Rev. C **56,** pp. 311–323 (1997).

[19] D. Bohm, Quantum Theory, Prentice-Hall, New York (1951).

[20] M. Büttiker, Phys. Rev. B **27**, 6178 (1983).

[21] A. Goldberg, H. M. Schey, J. L. Schwartz, Am. J. Phys. **35**, 177 (1967).

[22] E. H. Hauge, J. P. Falck, T. A. Fjeldly, Phys. Rev. B **36**, 4203 (1987).

[23] E. H. Hauge, J. A. Støvneng, Rev. Mod. Phys. **61**, 917 (1989).

[24] I. Ilić, P. P. Belicev, V. Milanović, J. Radovanović Phys. Scr. **T135**, 014040 (2009).

[25] D. V. Savin, H.-J. Sommers, Phys. Rev. E **68**, 036211 (2003).

[26] F. T. Smith, Phys. Rev. **118**, 349 (1960).

[27] E. P. Wigner, Phys. Rev. **98**, 145 (1955).

[28] H.G. Winful, Phys. Rev. Lett. **91**, 260401 (2003).

[29] H. G. Winful, Phys. Rev. E **68**, 016615 (2003).